Departamento de Informática de Sistemas y Computadores

An urban traffic management framework integrating pollution criteria

By

José Daniel Padrón Pérez

Advisor:
Prof. Dr. Carlos Tavares Calafate

UNIVERSITAT POLITÈCNICA DE VALÈNCIA

Valencia, España

November 2024

"*Success is the result of perfection, hard work, learning from failure, loyalty, and persistence.*"

Colin Powell

Acknowledgements

Thanks to my advisor, Carlos, for always guiding and advising me in the best way. Without that interview in which you convinced me to join the GRC, I probably would not have done my PhD and I would not be here right now. I would also like to thank the GRC and all the professors in the group for welcoming me like a family. Moreover, thank you to all the wonderful people I have met over the years during my PhD and my stay. Thank you for taking me out of the routine and enjoying good times away from work. Finalmente, quisiera agradecer a toda mi familia. A mi novia por quererme y apoyarme en los buenos y malos momentos. A mi madre por siempre estar ahí y apoyar todas mis decisiones. A mis abuelos, los que están y los que no, por criarme cuando era un niño y ayudarme a sentar las bases de lo que soy hoy como persona.

José Daniel Padrón Pérez
Valencia, November 18, 2024

Abstract

Urban air pollution, primarily generated by vehicular emissions in densely populated cities, poses a significant threat to public health and environmental sustainability. Traditional traffic management strategies have historically focused on reducing congestion, neglecting the environmental impacts of vehicular traffic. This thesis addresses this issue by developing a framework for urban traffic management that integrates pollution criteria, particularly by incorporating real-time air quality data into traffic re-routing decisions. Using the city of Valencia as a case study, the framework combines realistic traffic modelling, emissions analysis, and new static and dynamic re-routing strategies based on environmental criteria.

Our journey begins with the innovative challenge of generating accurate traffic demand data without compromising privacy. Leveraging data from induction loop detectors, we propose an approach that utilises reverse engineering to create a realistic traffic demand model. This method significantly improves the accuracy in representing traffic volume, the spatial distribution of origin points, and route lengths compared to current solutions, providing a more reliable foundation for further analysis.

Building on this foundation, we use the Simulation of Urban MObility (SUMO) tool and the Handbook Emission Factors for Road Transport (HBEFA) emissions model to simulate vehicle traffic flow and emissions. SUMO provides detailed traffic simulation capabilities, while HBEFA offers comprehensive emission factors for road transport, making them ideal for our modelling needs. We then develop SUMO2GRAL, a custom tool that integrates SUMO results with the Graz Lagrangian Model (GRAL) to perform detailed pollutant dispersion modelling and translate emissions expressed in mass into concentration. This integration considers factors such as urban orography and meteorological conditions, thereby improving

the accuracy of air quality assessments in urban environments.

Next, we explore traffic re-routing strategies aimed at mitigating air pollution. First, we present a static re-routing approach that adjusts traffic weights on street segments based on fixed environmental parameters. By applying this method in Valencia, we demonstrate its effectiveness in reducing pollutant concentrations, especially in critical areas such as green spaces or parks, providing practical implications for urban policy and planning.

Recognising the limitations of static methods in adapting to dynamic conditions, we develop a novel dynamic traffic re-routing algorithm that adjusts vehicle routes based on street-level air quality data and specific vehicle emissions profiles. By introducing an emission sensitivity factor, our algorithm modulates routing decisions in response to environmental conditions. Simulations in Valencia of environmental crises, such as building fires and smog episodes, reveal that the dynamic approach significantly reduces pollutant concentrations in affected areas without severely impacting traffic efficiency, effectively balancing air quality and mobility levels. This provides valuable insights for urban planners and policymakers in designing responsive traffic management systems prioritising public health.

Finally, we extend our analysis to future urban traffic scenarios by examining the expected evolution of the vehicle fleet in Valencia, particularly the increase in electric vehicle adoption. Based on vehicle fleet evolution models from similar European cities, we simulate scenarios that consider technological advancements and social trends. Our findings suggest that a gradual transition to electric vehicles can substantially improve air quality over time, highlighting the importance of promoting cleaner technologies alongside effective traffic management.

Overall, this PhD thesis presents several strategies to alleviate urban air pollution through intelligent traffic management strategies. Integrating pollution criteria into urban traffic frameworks provides valuable insights and tools for policymakers and urban planners to create healthier, more sustainable urban environments to address this global challenge.

Resumen

La contaminación atmosférica urbana, generada en gran medida por las emisiones vehiculares en ciudades densamente pobladas, representa una amenaza significativa para la salud pública y la sostenibilidad ambiental. Las estrategias tradicionales de gestión del tráfico se han centrado históricamente en reducir la congestión, desatendiendo los impactos ambientales del tráfico vehicular. Esta tesis aborda este problema mediante el desarrollo de un marco de gestión del tráfico urbano que integra criterios de contaminación, particularmente a través de la incorporación innovadora de datos en tiempo real sobre la calidad del aire en las decisiones de reencaminamiento del tráfico. Utilizando la ciudad de Valencia como estudio de caso, el marco combina la modelización realista del tráfico, el análisis de emisiones y nuevas estrategias de reencaminamiento estático y dinámico basadas en criterios medioambientales.

Nuestro recorrido comienza con el innovador desafío de generar datos de demanda de tráfico precisos, sin comprometer la privacidad. Aprovechando los datos de detectores de bucles de inducción, proponemos un enfoque que se aprovecha del uso de la ingeniería inversa para crear un modelo de demanda de tráfico realista. Este método mejora significativamente la precisión en la representación del volumen de tráfico, la distribución espacial de los puntos de origen, y la longitud de las rutas en comparación con las soluciones actuales, proporcionando una base más fiable para análisis posteriores.

Sobre esta base, empleamos la herramienta SUMO, junto con el modelo de emisiones HBEFA, para simular el flujo de tráfico y las emisiones de los vehículos. SUMO proporciona capacidades detalladas de simulación de tráfico, mientras que HBEFA ofrece factores de emisión completos para el transporte por carretera, lo que los hace ideales para nuestras necesidades de modelización. A continuación

desarrollamos SUMO2GRAL, una herramienta personalizada que integra los resultados de SUMO con GRAL para realizar un modelado detallado de la dispersión de contaminantes, y traducir estas emisiones expresadas en masa a concentración. Esta integración tiene en cuenta factores como la orografía urbana y las condiciones meteorológicas, mejorando así la precisión de las evaluaciones de la calidad del aire en entornos urbanos.

A continuación, exploramos estrategias de reencaminamiento del tráfico dirigidas a mitigar la contaminación del aire. Primero, presentamos un enfoque de reencaminamiento estático que ajusta los pesos del tráfico en segmentos de calles según parámetros ambientales fijos. Al aplicar este método en Valencia, demostramos su efectividad en la reducción de las concentraciones de contaminantes, especialmente en áreas críticas como espacios verdes o parques, proporcionando implicaciones prácticas para la política y planificación urbanas.

Reconociendo las limitaciones de los métodos estáticos para adaptarse a condiciones dinámicas, desarrollamos un algoritmo dinámico de reencaminamiento del tráfico que ajusta las rutas de los vehículos basándose en los datos de calidad del aire de las calles, y en los perfiles específicos de emisiones de los vehículos. Al introducir un factor de sensibilidad de emisiones, nuestro algoritmo modula las decisiones de encaminamiento en respuesta a las condiciones ambientales. Las simulaciones de situaciones de crisis ambiental, como incendios de edificios, y episodios de niebla producida por la contaminación (*smog*), revelan que el enfoque dinámico reduce significativamente las concentraciones de contaminantes en las áreas afectadas sin afectar gravemente la eficiencia del tráfico, equilibrando eficazmente los niveles de calidad del aire y de movilidad. Esto proporciona valiosas ideas para urbanistas y responsables políticos en el diseño de sistemas de gestión del tráfico que prioricen la salud pública.

Finalmente, extendemos nuestro análisis a escenarios futuros de tráfico urbano al examinar la evolución esperada del parque vehicular de Valencia, en particular el aumento en la adopción de vehículos eléctricos. Basándonos en modelos de evolución de parques vehiculares de ciudades europeas similares, simulamos escenarios que consideran los avances tecnológicos y las tendencias sociales. Nuestros hallazgos sugieren que una transición gradual hacia los vehículos eléctricos puede mejorar sustancialmente la calidad del aire con el tiempo, subrayando la importancia de promover tecnologías más limpias junto con una gestión eficaz del tráfico.

En general, esta tesis doctoral presenta varias estrategias para paliar la contaminación atmosférica urbana mediante estrategias inteligentes de gestión del tráfico. La integración de criterios de contaminación en los marcos de tráfico urbano proporciona ideas y herramientas valiosas para que los responsables políticos y los planificadores urbanos creen entornos urbanos más saludables y sostenibles para hacer frente a este desafío global.

Resum

La contaminació atmosfèrica urbana, generada en gran part per les emissions de vehicles en ciutats densament poblades, representa una amenaça significativa per a la salut pública i la sostenibilitat ambiental. Les estratègies tradicionals de gestió del trànsit s'han centrat històricament en reduir la congestió, deixant de costat els impactes ambientals del trànsit vehicular. Esta tesi aborda este problema a través del desenroll d'un marc de gestió del trànsit urbà que integra criteris de contaminació, particularment mitjançant la incorporació innovadora de dades en temps real sobre la qualitat de l'aire en les decisions de reencaminament del trànsit. Utilisant la ciutat de Valéncia com a cas d'estudi, el marc combina la modelació realista del trànsit, l'anàlisi d'emissions i noves estratègies de reencaminament estàtic i dinàmic basades en criteris mediambientals.

El nostre recorregut comença amb el repte innovador de generar dades de demanda de trànsit precises sense comprometre la privacitat. Aprovisionant-se de les dades de detectors de bucles d'inducció, proponem un enfocament que es beneficia de l'ingenieria inversa per a crear un model de demanda de trànsit realista. Este métode millora significativament la precisió en la representació del volum de trànsit, la distribució espacial dels punts d'orige i la longitud de les rutes en comparació en les solucions actuals, proporcionant una base més fiable per a anàlisis posteriors.

Sobre esta base, usem l'eina SUMO, junt en el model d'emissions HBEFA, per a simular el flux de trànsit i les emissions dels vehicles. SUMO oferix capacitats detallades de simulació de trànsit, mentres que HBEFA proporciona factors d'emissió complets per al transport per carretera, lo que els fa ideals per a les nostres necessitats de modelació. A continuació, desenrollem SUMO2GRAL, una ferramenta personalisada que integra els resultats de SUMO en GRAL per a realisar

una modelació detallada de la dispersió de contaminants, i traduir estes emissions expressades en massa a concentració. Esta integració té en compte factors com l'orografia urbana i les condicions meteorològiques, millorant així la precisió de les evaluacions de la qualitat de l'aire en entorns urbans.

A continuació, explorem estratègies de reencaminament del trànsit dirigides a mitigar la contaminació de l'aire. Primer, presentem un enfocament de reencaminament estàtic que ajusta els pesos del trànsit en segments de carrers segons paràmetres ambientals fixos. En aplicar este mètode en Valéncia, demostrem la seua efectivitat en la reducció de les concentracions de contaminants, especialment en àrees crítiques com espais verds o parcs, proporcionant implicacions pràctiques per a la política i la planificació urbana.

Reconeguent les limitacions dels mètodes estàtics per a adaptar-se a condicions dinàmiques, desenrollem un algoritme dinàmic de reencaminament del trànsit que ajusta les rutes dels vehicles basant-se en les dades de qualitat de l'aire dels carrers i en els perfils específics d'emissions dels vehicles. Al introduir un factor de sensibilitat d'emissions, el nostre algoritme modula les decisions d'encaminament en resposta a les condicions ambientals. Les simulacions de situacions de crisi ambiental, com incendis d'edificis i episodis de boira produïda per la contaminació (*smog*), revelen que l'enfocament dinàmic reduïx significativament les concentracions de contaminants en les àrees afectades sense afectar greument l'eficiència del trànsit, equilibrant eficaçment els nivells de qualitat de l'aire i de mobilitat. Això proporciona valuoses idees per a urbanistes i responsables polítics en el disseny de sistemes de gestió del trànsit que prioritzen la salut pública.

Finalment, ampliem el nostre anàlisi a escenaris futurs de trànsit urbà examinant l'evolució esperada del parc vehicular de Valéncia, en particular l'augment en l'adopció de vehicles elèctrics. Basant-nos en models d'evolució de parcs vehiculars de ciutats europees similars, simulem escenaris que consideren els avanços tecnològics i les tendències socials. Els nostres resultats suggerixen que una transició gradual cap als vehicles elèctrics pot millorar substancialment la qualitat de l'aire en el temps, subratllant la importància de promoure tecnologies més netes junt en una gestió eficaç del trànsit.

En general, esta tesi doctoral presenta diverses estratègies per a pal·liar la contaminació atmosfèrica urbana a través d'estratègies intel·ligents de gestió del trànsit. La integració de criteris de contaminació en els marcs de trànsit urbà oferix idees i ferramentes valuoses per a que els responsables polítics i els planificadors urbans creen entorns urbans més saludables i sostenibles per a enfrontar este repte global.

Contents

List of Figures

List of Tables

Chapter 1

Introduction

The rapid urbanisation of societies worldwide has led to the appearance of complex and densely populated cities. With this growth, the concept of the smart city has gained prominence, envisioning urban areas that leverage technology and data to enhance the quality of life for their inhabitants. Central to this vision is the development of efficient, sustainable, and intelligent transportation systems that can address the challenges posed by increasing urban mobility demands [1, 2].

Historically, cities have evolved alongside advancements in transportation. From horse-drawn carriages to the widespread adoption of automobiles in the 20th century, each era has introduced new opportunities and challenges. Today, we are on the verge of another transformation due to Intelligent Transportation System (ITS) and autonomous vehicles. These technologies promise not only to revolutionise how we travel, but also to mitigate the negative effects of traditional transportation methods, such as congestion and pollution [3].

One of the most pressing concerns in urban environments is air pollution, primarily caused by vehicular emissions. Pollutants such as Nitrogen Oxides (NO_x) and Particulate Matter (PM_x) have serious implications for both public health and the environment. Despite advancements in vehicle technology and stricter emission standards, the sheer volume of urban traffic continues to pose significant environmental challenges [4]. Traditional traffic management strategies have focused on reducing congestion and improving traffic flow, but they have not sufficiently addressed the environmental impact of vehicular emissions.

In recent years, there has been a growing recognition of the need to incorporate environmental considerations into traffic management strategies [5]. However, existing approaches often rely on static measures or administrative decisions, lacking the flexibility to adapt to real-time conditions. Furthermore, while some research has explored re-routing traffic based on environmental data, there remains a gap in developing systems that can effectively improve air quality without significantly compromising traffic efficiency.

1.1 Motivation

Urban air quality remains a significant public health concern, particularly in cities with severe traffic congestion. Traffic-related air pollution has been linked to various adverse health effects, including respiratory diseases, cardiovascular problems, and increased mortality rates [6]. In economic terms, the European Environmental Agency (EEA) estimates that air pollution costs the European Union between 268 and 428 billion euros annually due to health expenses and lost productivity [7]. Moreover, traffic jams cause personal stress and contribute significantly to air pollution, as vehicles idling in stop-and-go traffic emit higher levels of pollutants than when the traffic is fluid. According to the Spanish Society of Pneumology and Thoracic Surgery (SEPAR), air pollution is responsible for 10,000 deaths annually in Spain [8], underscoring the urgent need for effective traffic management and environmental solutions.

Despite these severe impacts, existing traffic management strategies often prioritise congestion reduction over environmental considerations, leaving a critical gap in addressing the full spectrum of issues caused by vehicular traffic [9]. A paradigm shift in urban mobility is expected with the widespread adoption of electric and autonomous vehicles and advancements in Vehicle to Everything (V2X) communication [10]. These intelligent vehicles will be capable of interacting with both the urban infrastructure and other vehicles, providing opportunities for cities to implement centralised traffic management systems that make real-time, data-driven decisions. Such systems can optimise traffic flow from the perspective of individual vehicles and by considering the overall impact on air quality and public health. For example, a central traffic management platform could reroute vehicles dynamically to reduce congestion and lower pollutant emissions in heavily trafficked areas.

However, to fully leverage these technologies, several challenges must be addressed:

1. Realistic traffic models must be developed to simulate the interactions between intelligent vehicles and urban infrastructure.

2. Accurate and real-time air quality data and emissions profiles of different vehicle types must be integrated into traffic management systems.

3. A context-aware routing framework that optimises traffic flow while prioritising environmental considerations needs to be developed.

4. Evaluating the environmental impacts of these traffic management strategies is essential, ensuring they lead to sustainable improvements in urban air quality.

Motivated by these challenges and opportunities, this thesis aims to contribute to developing sustainable urban environments where technology and data are used to address real-world problems. By integrating environmental considerations into traffic management systems, we can improve public health and pave the way for more intelligent, cleaner transportation networks that adapt to the evolving needs of modern cities. Ultimately, this thesis seeks to lay the groundwork for the next generation of traffic management solutions benefiting society and the environment.

1.2 Objectives

The main objective of this PhD thesis is to develop a comprehensive vehicular traffic management framework that effectively reduces urban air pollution. This is achieved by integrating realistic traffic modelling, dynamic re-routing algorithms based on environmental criteria, and a detailed analysis of the environmental impact of traffic restrictions. The framework aims to improve urban air quality without compromising traffic efficiency, contributing to the advancement of ITS within the context of smart cities.

To achieve this overall goal, several sub-objectives must be defined. These are the following:

1. **Develop a Realistic Traffic Simulation Framework**: Create a simulation environment capable of modelling realistic traffic conditions based on actual traffic flow data. The framework should manage vehicle routes during simulations and accurately assess the pollutant emissions of each vehicle.

2. **Define Realistic Urban Traffic Scenarios**: Establish simulation scenarios that accurately represent urban vehicular environments. This scenario includes accounting for various vehicle types and behaviours and modelling their interactions with road networks, congestion patterns, and traffic flow dynamics to reflect realistic conditions within Valencia.

3. **Design and Implement Dynamic Re-routing Algorithms**: Develop algorithms that assign optimal traffic routes by considering traffic flow optimisation and pollution levels across the city. These algorithms should dynamically adjust routes based on air quality data and vehicle emission profiles.

4. **Characterise Air Quality and Vehicle Emissions**: Perform an in-depth analysis of air quality impacts by integrating emission models with traffic simulations. This analysis will assess how different vehicle engine types and routes contribute to pollutant levels, enabling the identification of major emission sources and their environmental effects in urban settings.

5. **Evaluate the Environmental Impact of Traffic Management Strategies**: Investigate the effects of various traffic restrictions and management decisions on actual traffic patterns and pollutant emissions. This research includes analysing the trade-offs between reducing pollution in specific areas and maintaining acceptable congestion levels city-wide.

6. **Develop a Context-Aware Routing Framework**: Propose a routing system that adapts to environmental contexts, such as pollution hotspots and environmental crises. This system should integrate air quality data to provide adaptive routing solutions that mitigate air pollution while ensuring efficient traffic flow.

7. **Evaluate Air Quality in Future Urban Scenarios**: Simulate and analyse the air quality in Valencia under different future vehicle distribution scenarios. This objective focuses on predicting the air quality improvements that can be achieved as we gradually reduce the share of combustion engine vehicles, increasing the proportion of electric cars accordingly. The goal is determining the expected impact of such changes from an air quality perspective with a high level of detail.

1.3 Structure of the Thesis

The thesis dissertation is organised in nine chapters. Below is a brief overview of each chapter:

- **Chapter 2, Air Pollution**, provides a foundation in the basics of air pollution. It discusses the pollutants contributing to poor air quality, methods for measuring these pollutants, the concept of Air Quality Index (AQI), and the computational techniques used to estimate pollution concentrations. This

chapter lays the groundwork for understanding the environmental pollutants relevant to vehicular emissions.

- **Chapter 3, Vehicular Traffic and Re-routing Solutions**, explores methods of traffic data collection, reviews vehicular traffic simulators and emission models, and examines existing re-routing solutions. The chapter discusses the challenges of reducing urban pollution through traffic management, surveying state-of-the-art technologies and strategies for mitigating air pollution via traffic re-routing.

- **Chapter 4, Proposed Vehicular Traffic Management Framework**, introduces our comprehensive framework for managing vehicular traffic to reduce air pollution. It explains the use of the SUMO tool, outlines methodologies for pollutant concentration calculations, and discusses the calibration of pollution concentrations. This framework forms the basis for testing and implementing the proposed traffic management strategies.

- **Chapter 5, Generating Traffic Demand in a Realistic Way**, focuses on creating realistic traffic demand models for simulation. It provides an overview of Valencia's traffic conditions and identifies unresolved issues in current traffic demand generation methods. A novel solution is proposed and validated through experiments by comparing results against DFROUTER, and demonstrating the effectiveness of our method in generating realistic traffic patterns.

- **Chapter 6, Traffic Re-routing Based on Air Pollution: A Static Approach**, presents a static traffic re-routing strategy aimed at reducing air pollution. The chapter details the proposed solution, which adjusts traffic flows based on predefined environmental constraints. Experiments conducted using Valencia as a case study are analysed to assess the impact of the static re-routing on pollutant concentrations and traffic efficiency.

- **Chapter 7, Traffic Re-routing Based on Air Pollution: A Dynamic Approach**, expands on the static approach by introducing a dynamic traffic re-routing algorithm. This method adjusts vehicle routes based on current air quality data and vehicle emission profiles. The chapter describes the development of the dynamic algorithm, simulates various environmental crisis scenarios, and evaluates the results, focusing on reducing pollutant concentrations while maintaining traffic efficiency.

- **Chapter 8, Predicting Air Quality for Current and Future Urban Traffic**, examines the evolution of Valencia's vehicular fleet and its impact

on future air quality. It analyses trends such as the increasing adoption of electric vehicles, and predicts how these changes might affect urban pollution. The chapter presents experiments that offer insights into the long-term impact of evolving traffic compositions on air quality.

- **Chapter 9, Conclusions, Future Work, and Publications**, summarises the key findings of the research, and reflects on its contributions to urban traffic management and air quality improvement. It discusses future research directions, such as incorporating advanced emission models or exploring further dynamic re-routing strategies. The chapter also lists the publications resulting from this research, showcasing the dissemination of the work within the scientific community.

Chapter 2

Air Pollution

Urban air pollution is a critical environmental and public health issue, with vehicular emissions being a major contributor in cities worldwide. This chapter covers the key aspects of air pollution caused by road transport, emphasising the primary pollutants emitted by vehicles, and their significant impacts on human health and the environment. First, we analyse the major pollutants regulated by international organisations such as the EEA and the United States Environmental Protection Agency (USEPA). Each pollutant is discussed in terms of its primary sources, health implications, and environmental effects, with a focus on vehicular emissions. The chapter also explores the methods used to measure these pollutants, categorising them into fixed, mobile, and remote sensing techniques, all essential for accurate air quality monitoring. Additionally, we introduce the concept of the AQI, explaining how pollutant concentrations are converted into standardised indices that reflect air quality levels. Finally, we cover the methods for calculating pollution concentrations from vehicular emissions, focusing on modelling techniques such as the "Fixed Box Model" and the GRAL. These models are vital for translating emission data into concentration levels, allowing us to assess the impact of traffic emissions on urban air quality. This comprehensive understanding of air pollution provides the foundation for developing effective strategies to mitigate vehicular emissions in urban environments, which will be explored in the following chapters.

2.1 Pollutants

This section analyses the urban pollutants emitted by road transport, which are regulated by international organisations such as the EEA and the USEPA. These pollutants present significant risks to both human health and the environment. Each pollutant is analysed in terms of its sources, primarily vehicular emissions, its impact on human health, and its broader environmental effects. The primary pollutants discussed include NO_x, PM_x, and Carbon Monoxide (CO), along with others such as Carbon Dioxide (CO_2), Ozone (O_3), Sulphur Dioxide (SO_2), and Volatile Organic Compounds (VOCs) [11, 12, 13].

2.1.1 NO_x

NO_x are a group of highly reactive gases containing varying amounts of nitrogen and oxygen, with the most significant forms in air pollution being Nitric Oxide (NO) and Nitrogen Dioxide (NO_2) [14]. These gases are generated during high-temperature combustion processes, such as those in vehicle engines. Specifically, in vehicular emissions, NO_x is primarily released from motor vehicle exhaust as a result of the reaction between nitrogen and oxygen during fuel combustion. Diesel engines, in particular, emit higher levels of NO_x compared to petrol engines, due to their higher combustion temperatures and pressures [15].

Regarding health impacts, exposure to elevated levels of NO_x can cause a variety of adverse effects. In the short term, it can irritate the respiratory system, leading to symptoms such as coughing, wheezing, and difficulty breathing. Moreover, it can exacerbate asthma and increase vulnerability to respiratory infections [16]. Prolonged exposure is associated with the development of asthma and an increased risk of cardiovascular diseases [17].

In addition to health concerns, NO_x has significant environmental effects. It plays a critical role in atmospheric reactions that produce ground-level O_3 and fine particulate matter ($PM_{2.5}$), both of which have additional health implications. Furthermore, NO_x contributes to the formation of acid rain and nutrient pollution in coastal waters, causing imbalances in ecosystems [18].

2.1.2 PM_x

PM_x refers to a complex mixture of tiny particles suspended in the air. The "x" denotes the particle's diameter in micrometers, with PM_{10} (particles with diameters of 10 micrometers or less) and $PM_{2.5}$ (2.5 micrometers or less) being the most commonly monitored sizes due to their ability to penetrate the respiratory system.

Regarding vehicular emissions, PM_x is generated from several sources. Exhaust emissions, particularly from diesel engines, are significant contributors to $PM_{2.5}$ [19]. Additionally, non-exhaust emissions such as brake wear, tire wear, and road dust resuspension contribute to both PM_{10} and $PM_{2.5}$ levels in urban environments.

Regarding health impacts, exposure to particulate matter poses serious risks. $PM_{2.5}$ can penetrate deep into the lungs and even enter the bloodstream, leading to respiratory and cardiovascular diseases, aggravated asthma, decreased lung function, and premature death in individuals with heart or lung diseases [20]. There is evidence that both short-term and long-term exposures can have significant health effects, and no safe threshold has been identified.

Environmentally, PM_x contributes to reduced visibility (haze) and can settle on soil and water bodies, leading to environmental degradation [21]. Particulate matter can also affect climate by influencing the Earth's radiation balance, either by absorbing or reflecting sunlight [22]. This can have further implications for climate change and weather patterns.

2.1.3 CO

Carbon monoxide is a colourless, odourless gas produced by the incomplete combustion of carbon-containing fuels.

In terms of vehicular emissions, CO is primarily emitted from motor vehicle exhaust when the combustion process is inefficient, such as during cold starts, or when engines are not properly tuned [23]. Older vehicles and those in poor mechanical condition tend to emit higher levels of CO.

Concerning health impacts, CO can lead to cardiovascular and neurological effects, especially in individuals with pre-existing heart conditions [24]. Symptoms of CO exposure include headaches, dizziness, weakness, nausea, confusion, and at very high levels, it can be fatal.

From an environmental perspective, while CO does not have significant direct environmental effects, it plays a role in the formation of ground-level ozone by reacting with other pollutants in the presence of sunlight. This indirect contribution to O_3 formation can have further environmental and health implications.

2.1.4 Other Relevant Pollutants

In addition to primary pollutants, several other substances emitted by vehicles significantly impact health and the environment.

SO_2, a colourless gas, results from burning sulphur-containing fuels, such as diesel. Although SO_2 emissions from vehicles have decreased due to low-sulphur

fuel regulations, they remain a concern where higher sulphur fuels are used. Short-term exposure to SO_2 irritates the respiratory system, exacerbating asthma and bronchitis, while, environmentally, it contributes to acid rain, damaging ecosystems and infrastructure [25].

CO_2, a primary greenhouse gas, is a major contributor to climate change. It is produced as a by product of fossil fuel combustion in vehicles and leads to global warming, resulting in rising sea levels, extreme weather, and biodiversity loss. Though CO_2 itself is not harmful at typical ambient concentrations, the broader effects of climate change severely impact human health [26].

VOCs, organic chemicals that easily evaporate at room temperature, are released through fuel evaporation and incomplete combustion in vehicles [27]. Exposure to VOCs can irritate the eyes, nose, and throat, and some are carcinogenic [28]. Additionally, VOCs react with NO_x in sunlight to form ground-level ozone, contributing to smog, and further damaging air quality and ecosystems.

Ground-level O_3, a secondary pollutant formed from NO_x and VOCs, is a key component of urban smog. It causes respiratory issues, reduces lung function, and worsens asthma. O_3 also damages vegetation, reducing crop yields and forest growth, which harms ecosystems and biodiversity [29].

Ultimately, understanding these pollutants is crucial for developing effective strategies to reduce vehicular emissions. Table 2.1 provides a summary of the primary pollutants discussed, highlighting their sources, health effects, and environmental impacts.

2.2 Methods of Measuring Pollutants

Accurate measurement of air pollutants is critical for monitoring air quality, ensuring compliance with environmental regulations, and informing effective pollution control strategies. Methods for measuring pollutants can be broadly categorised into fixed sensing, mobile sensing, and remote sensing.

2.2.1 Fixed Sensing

Air quality monitoring stations are fixed installations equipped with instruments that continuously measure concentrations of key pollutants such as NO_x, PM_x, SO_2, CO, and O_3 [30]. These stations are strategically placed in urban, suburban, and rural areas to provide comprehensive coverage of air quality across different regions. The instruments used in these stations include:

Table 2.1: Summary of primary pollutants from vehicular emissions.

Pollutant	**Sources**	**Health Effects**	**Environmental Effects**
NO_x	Vehicle exhaust	Respiratory irritation, asthma, increased infection risk	Ground-level ozone, acid rain, nutrient pollution
PM_x	Exhaust emissions, brake and tire wear, road dust	Respiratory and cardiovascular diseases, reduced lung function	Reduced visibility, climate effects
CO	Incomplete combustion in engines	Reduced oxygen delivery, cardiovascular and neurological effects	Contributes to ground-level ozone
SO_2	Sulphur-containing fuel combustion	Respiratory irritation, asthma	Acid rain formation, ecosystem damage
CO_2	Fuel combustion	Indirect health impacts via climate change	Greenhouse gas, global warming
VOCs	Fuel evaporation, incomplete combustion	Respiratory irritation, organ damage, some carcinogenic	Ground-level ozone, photochemical smog
O_3	Formed from NO_x and VOCs	Respiratory problems, reduced lung function	Vegetation damage, reduced crop yields

- **Gas Analysers**: Devices that measure gaseous pollutants using techniques such as chemiluminescence for NO_x, fluorescence for SO_2, and infrared absorption for CO [31].
- **Particulate Matter Monitors**: Instruments such as Beta Attenuation Monitors (BAMs) and Tapered Element Oscillating Microbalances (TEOMs) measure the mass concentration of particulate matter in the air [32].
- **Meteorological Sensors**: Equipment that measures wind speed, wind direction, temperature, and humidity, which are essential for interpreting pollutant dispersion patterns [33].

To illustrate, Figure 2.1 presents an example of an air quality monitoring station.

Figure 2.1: Example of an air quality monitoring station [34].

2.2.2 Mobile Sensing

Advances in technology have led to the development of portable and low-cost sensors capable of measuring air pollutants [35]. These devices include:

- **Electrochemical Sensors**: These are used to detect gases like NO_2, SO_2, and CO by measuring the current produced by the chemical reaction of the target gas at an electrode [36].
- **Optical Sensors**: These sensors use light scattering or absorption to detect PM_x concentrations [37].
- **Photoionisation Detectors**: These devices measure VOCs by ionising organic compounds with ultraviolet light, and then measuring the resulting current [38].

Such sensors are increasingly used in networks to provide high-resolution spatial data on air quality, complementing data from fixed monitoring stations. Their portability and affordability make them suitable for community-based monitoring and personal exposure assessments.

2.2.3 Remote Sensing

Remote sensing involves the use of satellites, aircraft, or ground-based remote sensors to detect and measure pollutants in the atmosphere [39]. The main techniques include:

- **Satellite Observations**: Instruments onboard satellites measure the Earth's reflected and emitted radiation, allowing for the estimation of atmospheric concentrations of pollutants such as NO_2, SO_2, and O_3 [40].
- **Light Detection and Ranging (LiDAR) Systems**: LiDAR technology uses laser pulses to measure PM_x aerosols in vertical profiles of the atmosphere [41].
- **Aerial Measurements**: Aircraft equipped with sensors provide high-resolution data over specific areas, useful for validating satellite data and capturing localised pollution events [42].

Ultimately, remote sensing provides valuable data over large spatial scales, contributing to global air quality monitoring, climate research, and the validation of ground-based measurements.

Figure 2.2 provides a graphical overview of the various methods and techniques discussed in this section, highlighting the main advantages and disadvantages of each.

	Fixed Sensing	Mobile Sensing	Remote Sensing
Advantages	Accurate	Flexible	Inexpensive
Disadvantages	Expensive	User-Dependent	Inaccurate
Gases	Gas Analysers	Electrochemical Sensors	Satellite Observations
PMx	PMx Monitors	Optical Sensors	LiDAR Systems
Other	Meteorological Sensors	Photoionization Detectors	Aerial Measurements

Figure 2.2: Comparison of pollutant measurement methods.

In summary, accurate measurement of air pollutants is essential for effective air quality management. Fixed sensing provides continuous, high-accuracy data at specific locations, which is vital for regulatory compliance and long-term monitoring. Mobile sensing enhances spatial coverage and offers flexibility, making it valuable for exposure assessments and identifying pollution hotspots. Remote sensing extends the monitoring capabilities to regional and global scales, contributing to comprehensive environmental assessments and supporting climate change research. Combining these methods allows for a more complete understanding of air pollution patterns, and supports the development of effective mitigation strategies.

2.3 Air Quality

Air quality is a crucial factor in urban health and environmental sustainability, particularly in areas with heavy vehicular traffic. Pollutants emitted from vehicles significantly affect air quality, posing serious health risks, especially for vulnerable populations such as children, the elderly, and those with pre-existing respiratory conditions. To monitor and manage air quality, indices like the AQI are commonly used. These indices offer a standardised assessment of air quality by measuring the concentration of key pollutants, enabling comparisons across regions and time periods. In this section, we examine the concept of the AQI, and the standards established by regulatory bodies such as the EEA and the USEPA.

2.3.1 AQI

The AQI is a numerical scale designed to communicate air pollution levels to the public. It is calculated based on the concentrations of key pollutants, including NO_x, PM_{10}, $PM_{2.5}$, SO_2, and O_3. Although the specific pollutants used to calculate the AQI may vary slightly across countries and organisations, the primary goal is to provide an easily interpretable index that reflects the potential health risks associated with current air quality conditions.

In this thesis, we focus on NO_x and PM_{10}, as these are key pollutants covered by the EEA's air quality guidelines [43]. Although traffic simulators also provide data on pollutants like CO as we will see in the Chapter 3, it is not included in our analysis because it is not considered by the EEA for AQI calculations [44]. However, CO is included in the USEPA framework [45]. To maintain relevance, our pollutant selection aligns with the EEA standards, while also incorporating the USEPA methodology for converting pollutant concentrations into AQI values.

The AQI for each pollutant is calculated using Equation 2.1, which converts pollutant concentrations into an index value based on predefined concentration breakpoints. This formula ensures consistency when comparing pollutant levels against health impact thresholds.

$$I_p = \frac{I_{Hi} - I_{Lo}}{BP_{Hi} - BP_{Lo}} \cdot (C_p - BP_{Lo}) + I_{Lo} \tag{2.1}$$

where:

- I_p is the index for pollutant p,
- C_p is the truncated concentration of pollutant p,
- BP_{Hi} is the concentration breakpoint that is greater than or equal to C_p,

- BP_{Lo} is the concentration breakpoint that is less than or equal to C_p,
- I_{Hi} is the AQI value corresponding to BP_{Hi},
- I_{Lo} is the AQI value corresponding to BP_{Lo}.

After calculating the AQI for each pollutant, the overall AQI for a given area is determined by taking the maximum index value from the pollutants under consideration, as shown in Equation 2.2:

$$I = max(I_{PMx}, I_{NOx}) \tag{2.2}$$

This approach ensures that the most critical pollutant at any given time dictates the overall air quality rating, thereby informing the public of the highest potential health risk.

2.3.2 Air Quality Standards

The AQI is derived from pollutant concentration thresholds established by organisations such as the EEA and the USEPA. These thresholds represent varying levels of air quality concern, ranging from "Good" air quality, which poses no risk, to "Extremely Poor" air quality, which poses significant health risks to the general population. Although the standards set by these agencies differ slightly due to regional variations in air quality regulations, both aim to protect public health and reduce environmental harm. The thresholds defined by both agencies for key pollutants can be observed in Tables 2.2 and 2.3.

Table 2.2: USEPA thresholds for PM_{10} and NO_x.

Level of Concern	**AQI Range**	**PM_{10} (µg/m^3)**	**NO_x (µg/m^3)**
Good	0-50	0-54	0-100
Fair	51-100	55-154	101-188
Moderate	101-150	155-254	189-283
Poor	151-200	255-354	284-376
Very Poor	201-300	355-424	377-565
Extremely Poor	301 and higher	425 and higher	566 and higher

As can be observed, the EEA standards are generally stricter at lower pollutant concentrations than the USEPA standards. For example, the EEA defines "Good" air quality for PM_{10} as concentrations up to 20 µg/m^3, while the USEPA considers concentrations up to 54 µg/m^3 as "Good". Similarly, for NO_x, the EEA's "Good"

Table 2.3: EEA thresholds for PM_{10} and NO_x.

Level of Concern	**PM_{10} (µg/m³)**	**NO_x (µg/m³)**
Good	0-20	0-40
Fair	20-40	40-90
Moderate	40-50	90-120
Poor	50-100	120-230
Very Poor	100-150	230-340
Extremely Poor	150-1200	340-1000

threshold is up to 40 µg/m^3, whereas the USEPA sets it at up to 100 µg/m^3. These differences highlight how regional health assessments and policy priorities influence air quality regulations.

In this thesis, we adopt a combination of standards from both the EEA and USEPA, with a focus on two primary pollutants: PM_{10} and NO_x. Table 2.4 presents the threshold values for each pollutant and their corresponding AQI levels, offering a consistent framework for evaluating air quality across different urban areas.

Table 2.4: AQI thresholds for PM_{10} and NO_x used in this thesis.

Level of Concern	**AQI Range**	**PM_{10} (µg/m³)**	**NO_x (µg/m³)**
Good	0-50	0-20	0-40
Fair	51-100	20-40	40-90
Moderate	101-150	40-50	90-120
Poor	151-200	50-100	120-230
Very Poor	201-300	100-150	230-340
Extremely Poor	301 and higher	150-1200	340-1000

These standards ensure that our analysis of vehicular emissions adheres to internationally recognised guidelines, providing a solid foundation for assessing urban air quality and its associated health impacts. In particular, it facilitates meaningful comparisons within the European context and underscores our commitment to rigorous environmental assessment.

2.4 Pollution Concentration Computation

Road transport emissions are a significant source of urban air pollution, accounting for 37% of NO_x, and for 18% of CO emissions in the European Union [46]. However, to fully assess their impact on air quality and associated health risks, emission quantities must be converted into pollutant concentration levels, which represent the amount of pollution in a given volume of air. This conversion is crucial for determining whether pollutant levels exceed the thresholds established by air quality standards, such as the AQI.

To achieve this, mathematical models are used to simulate the dispersion of pollutants in the atmosphere. These models take into account factors such as emission rates, meteorological conditions, and urban environmental characteristics to estimate how pollutants spread and concentrate in different areas [47]. This section reviews the main modelling techniques used for pollutant dispersion, and specifically focuses on the two approaches applied in this thesis for calculating pollution concentrations: the "Fixed Box Model" and the GRAL. While both are atmospheric dispersion models, they differ in complexity and application, offering complementary advantages based on the specific needs of the study.

The following subsections outline the principles behind these models, explaining how they convert emission data into concentration values, and examining their strengths and limitations for urban air quality assessments.

2.4.1 Overview of Modelling Techniques

Several techniques are available to model the concentration and dispersion of pollutants in the atmosphere, each varying in complexity, required input data, and suitability for different environmental conditions. They can be grouped into three main categories:

- **Dispersion Models**: These models simulate how pollutants disperse in the atmosphere from point or area sources. Gaussian plume models, or the "Fixed Box Model", are often used for quick, preliminary assessments. In contrast, more advanced tools like GRAL [48] offer higher accuracy, particularly in complex urban environments.

- **Chemical Transport Models**: These models simulate the physical and chemical transformations that pollutants undergo as they travel through the atmosphere. They account for processes such as chemical reactions, wet and dry deposition, and large-scale transport of pollutants [49].

- **Computational Fluid Dynamics (CFD) Models**: CFD models provide high-resolution simulations of pollutant dispersion, making them particularly valuable in detailed studies of urban environments. However, they are computationally intensive and require extensive data on pollutant sources, meteorology, and urban layout [50].

For the purposes of this thesis, two primary models, the "Fixed Box Model", and GRAL, were selected for their ability to convert emissions data into concentration levels, evaluate pollution impacts, and provide valuable insights into urban air quality.

2.4.2 Fixed Box Model

The "Fixed Box Model" is a simple and yet widely used atmospheric dispersion model that estimates pollutant concentrations by assuming uniform mixing of pollutants within a defined volume, or "box" [51, 52]. The dimensions of the box are set according to the characteristics of the study area, and the model assumes that pollutants remain within this volume over a specified time, typically one hour. The model is particularly useful for quick, preliminary assessments of air quality.

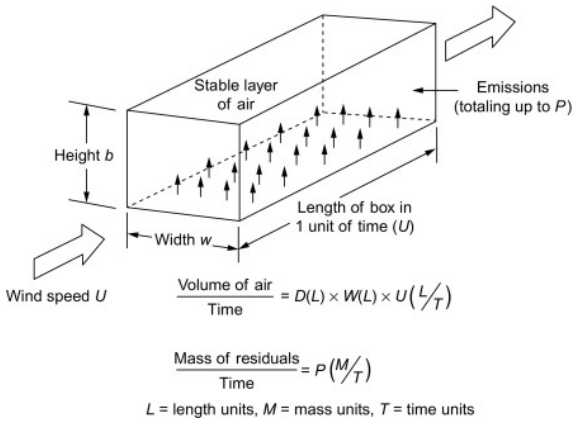

Figure 2.3: Air available for dilution in a "Fixed Box Model" [51].

In this thesis, the "Fixed Box Model" is applied to convert emission data generated by the traffic simulator, which is expressed in mass, into pollutant concentrations that can be compared with AQI standards. The concentration of pollutants, C, is calculated using the following equation:

$$C = \frac{Q \cdot t}{x \cdot y \cdot z} \tag{2.3}$$

where:

- Q is the release rate of the pollutant (mass per unit time),
- t is the time period for which mixing occurs,
- x and y are the horizontal dimensions of the box (downwind and crosswind), z is the vertical dimension of the box.

The "Fixed Box Model" is straightforward and requires minimal input data, making it a valuable tool for estimating pollutant concentrations over short time frames. However, its simplicity also presents limitations. It assumes constant emissions, stationary meteorological conditions, and a uniform pollutant mix, which may not always reflect real-world scenarios. Additionally, it does not account for the complex interactions between buildings, terrain, and local meteorology. Despite these drawbacks, its low computational cost and ease of use make it ideal for initial assessments.

2.4.3 GRAL

GRAL is a more advanced dispersion model designed to simulate pollutant dispersion in complex urban environments. It takes into account factors like terrain, building geometry, vegetation, and internal wind flows, making it highly accurate for studies requiring detailed modelling of pollution dispersion. Developed by the Austrian Technical University of Graz, GRAL is widely used in urban air quality studies, offering a more sophisticated alternative to simpler models like the "Fixed Box Model".

Unlike the "Fixed Box Model", GRAL accounts for the three-dimensional structure of urban areas, which significantly affects the way pollutants disperse. This makes it especially useful for cities like Valencia, where interactions between buildings, traffic, and meteorological conditions create complex pollution patterns.

For this thesis, GRAL is used to convert emissions data from SUMO into concentration levels, similar to the "Fixed Box Model" but with greater precision. Its advanced algorithms enable the modelling of dynamic urban environments, where factors like wind turbulence, street canyons, and local meteorology play a significant role in determining pollution levels. Additionally, GRAL has been validated in multiple studies, including those conducted by Austrian regulatory bodies and international research projects [53, 54]. This strong validation and its open-source nature make GRAL a reliable and valuable tool for this research study.

2.4.4 Comparison of Fixed Box Model and GRAL

While both the "Fixed Box Model" and GRAL are effective tools for estimating pollutant concentrations, they serve different purposes and are suited for different scales of analysis. The "Fixed Box Model" is ideal for rapid, low-cost assessments, where the primary concern is to gain a general understanding of pollution impacts. In contrast, GRAL provides a more detailed and accurate representation of pollutant dispersion in complex urban environments. A comparison of the main features can be observed in Table 2.5.

Table 2.5: Comparison between "Fixed Box Model" and GRAL.

Feature	**Fixed Box Model**	**GRAL**
Complexity	Low	High
Data Requirements	Minimal	Extensive (topography, meteorology)
Computation Time	Fast	Slower due to higher precision
Suitable Applications	Preliminary assessments	Detailed urban air quality studies
Real-World Accuracy	Limited	High, especially in urban areas
Use in Thesis	Quick emission estimates	Accurate modelling of urban pollution

In summary, both models are essential in this thesis. The "Fixed Box Model" provides a simple, computationally efficient method for initial assessments of pollution concentration, while GRAL allows for more complex, detailed simulations that account for the intricacies of urban environments. Together, these models enable a comprehensive understanding of the relationship between vehicle emissions and air quality, providing a robust framework for assessing the environmental impact of traffic management strategies.

Chapter 3

Vehicular Traffic and Re-routing Solutions

In the previous chapter, we explored the fundamental aspects of air pollution, focusing on key pollutants, measurement methods, and the calculation of pollution concentrations. We highlighted the critical impact of air quality on public health and the environment, underscoring the need for effective monitoring and reduction strategies. Building upon this foundation, the current chapter examines the significant role of vehicular traffic in urban air pollution, and explores re-routing solutions to mitigate its effects. Vehicular emissions, including CO_2, NO_x, and PM_x, are major contributors to city pollution, making efficient traffic management essential for reducing emissions and improving air quality. We begin by discussing various traffic data collection methods, emphasising on their unique benefits and challenges in terms of accuracy, privacy, and infrastructure. The chapter then reviews vehicular traffic simulators and emission models, assessing their effectiveness and integration for emission estimation. Finally, we critically evaluate existing re-routing solutions, highlighting their limitations in addressing congestion, pollution, and real-time air quality data integration. This analysis sets the stage for proposing new strategies in the following chapters to address these challenges, thereby enhancing urban sustainability.

3.1 Traffic Data Collection

Traffic data can be obtained from various sources such as Global Positioning System (GPS), cellular networks, inductive loops, video image processors, and others, as studied by Leduc [55] and Jain *et al.* [56]. These data collection methods can be broadly categorised into Floating Car Data (FCD) and conventional "*in-situ*" technologies. FCD approaches collect traffic data by tracking individual vehicles, primarily through two methods: GPS-based and cellular phone-based approaches. On the other hand, "*in-situ*" technologies collect data from detectors placed along the road, such as induction loops and video image processors.

To enhance understanding, Figure 3.1 provides a comparative overview of FCD and "*in-situ*" data collection methods, highlighting their examples of data sources, advantages, and limitations.

	FCD	"*In-situ*"
Advantages	Real traffic demand data	More privacy
	Comprehensive coverage	Controlled by public authorities
Disadvantages	Privacy concerns	Custom solutions for traffic demand
	Data accessibility issues	Limited coverage
Examples	GPS data	Induction loops
	Cellphone data	Cameras

Figure 3.1: Comparison of FCD and "*in-situ*" traffic data collection methods.

As depicted, FCD methods offer comprehensive and detailed data by tracking individual vehicles, providing high-resolution temporal and spatial information. However, they face challenges such as privacy concerns, data accessibility issues, and often high costs due to reliance on private companies for data access. In contrast, "*in-situ*" methods like induction loops and cameras are less intrusive, provide more privacy and are controlled by public administrations. They offer reliable and continuous data collection but may require custom solutions to create traffic demand and provide less coverage compared to FCD methods.

3.1.1 FCD Methods

In recent years, the affordability and widespread use of GPS systems have led to their increased integration in vehicles. This growth, coupled with the proliferation of smartphones, has made it possible to analyse vehicles that lack built-in GPS systems. Herrera *et al.* [57] leveraged this source to create a system that retrieves GPS data directly from smartphones. Their system comprises four layers: (i) GPS-enabled smartphones inside vehicles, (ii) a cellular network provider, (iii) a data collection infrastructure, and (iv) an information display system. The smartphones sent their location (latitude, longitude, altitude) every 3 seconds, which allowed for the calculation of the car's speed and trajectory. Building on this, Ge and Fukade [58] further developed a solution to create Origin-Destination (OD) traffic matrices by aggregating GPS traces and applying spatial interaction models. Despite its advantages, acquiring GPS data is often challenging due to privacy concerns, and the difficulty of accessing data owned by private companies.

An alternative to GPS for traffic data collection is the use of cellular networks. With advancements in technologies like Long Term Evolution (LTE) and 5G, tracking vehicles through cellular networks has become more feasible. Cáceres *et al.* [59] evaluated six different models to estimate vehicle movement between cells using anonymous phone call data, selecting a physical model that correlates call activity with traffic mobility. This model assumes that a cell phone is in motion when it either initiates a call in two different cells within a short period, or has an active call while switching from one cell to another. The results showed a reasonable estimation of traffic flow. Similarly, Iqbal *et al.* [60] developed a method to create OD matrices based on cell phone Call Detail Records (CDR). Their approach involves three steps: (i) generating an initial OD matrix from tower-to-tower transit data, (ii) converting it to a node-to-node transient OD matrix, and (iii) applying a scaling factor to obtain the final OD matrix. Despite its potential, this method is also limited by data accessibility issues, as it relies on telecommunication companies, making it costly and difficult for public administrations to deploy.

3.1.2 "*In-situ*" Methods

Video image processors are among the most widely used "*in-situ*" methods for traffic data collection. Recent advancements in artificial intelligence have made it easier to monitor traffic mobility through video cameras. For instance, Mallikarjuna *et al.* [61] developed a system that uses video image processing for traffic data collection, involving two key methodologies: data collection and traffic estimation. Cameras are placed to cover substantial portions of the road, and a multistep AI process (learning, detection, classification, filtering, tracking, and feature extraction) enables

both macroscopic and microscopic traffic data collection. Savrasovs and Pticina [62] proposed a method to generate OD matrices using video data, following a five-step process involving data collection, OD matrix generation, manual validation, calibration, and regression analysis. While video image processing is effective for traffic monitoring, it requires a significant investment in infrastructure, making it more suitable for smaller cities or specific high-traffic areas, rather than extensive urban coverage.

Among "*in-situ*" methods, induction loops are one of city administrations' most reliable and widely used technologies to monitor traffic volume across large urban areas. These sensors create an electromagnetic field that detects the presence of metallic objects, such as vehicles, as they pass over or near the loop embedded in the road surface. When a vehicle passes over the induction loop, it disturbs the electromagnetic field, triggering a change in inductance detected by the loop's connected hardware. This allows the system to count vehicles and measure traffic density in real-time.

In Valencia, 720 induction loops have been strategically placed across the city's road network to monitor traffic volume and gather essential data for traffic analysis and management. These sensors are connected to a central data repository, with traffic information stored in a database accessible through an Application Programming Interface (API) for research and public use [63]. The data collected includes timestamps, vehicle counts, and traffic density, providing high temporal resolution for ongoing analysis. One notable tool that uses induction loop data is DFROUTER [64], which generates traffic demand based on such data. DFROUTER operates through four key steps: importing the road network and induction loop data, classifying detectors into source, middle, and sink types, calculating vehicle flow between consecutive detectors, and generating demand based on route usage probabilities. Our research builds upon this foundation, addressing DFROUTER's limitations in generating realistic traffic volumes and route lengths with a refined solution, as discussed in chapter 5.

3.2 Vehicular Traffic Simulators and Emission Models

Efficiently managing urban traffic while minimising its environmental impact requires the use of advanced modelling tools, particularly vehicular traffic simulators and emission models. Traffic simulators are essential for modelling vehicle movements and traffic flow on road networks, enabling the analysis of congestion patterns, and assessing the effectiveness of various traffic management strategies. Emission models complement these tools by estimating the pollutant emissions from vehicles, which is vital for determining the environmental impact of different

traffic scenarios.

Vehicular traffic simulators are generally categorised into three types: microscopic, mesoscopic, and macroscopic models [65]. Microscopic models provide detailed simulations of individual vehicle behaviour, capturing interactions such as lane changes and accelerations. Mesoscopic models strike a balance by representing vehicle groups with simplified dynamics, while macroscopic models treat traffic as a continuous flow, focusing on aggregated metrics like speed and density. Integrating emission models with these simulators allows for the assessment of pollutants such as CO_2, CO, NO_x, and PM_x, offering a comprehensive understanding of both traffic dynamics and their environmental consequences.

This section provides a detailed overview of various traffic simulators and emission models, and presents a comparative evaluation of their strengths and limitations in supporting effective traffic management and pollution mitigation in urban environments.

3.2.1 Vehicular Traffic Simulators: Classification and Overview

Vehicular traffic simulators are essential for analysing, predicting, and managing traffic flow in urban and suburban areas. They allow transportation planners and engineers to assess the impact of infrastructure changes, traffic management strategies, and policy decisions without the costs and disruptions associated with real-world experiments. As stated above, traffic simulators are often classified into three categories based on their modelling approach and level of detail: macroscopic, mesoscopic, and microscopic. Each type has specific strengths and is suited to different types of traffic studies, from large-scale strategic planning to detailed operational analysis. Below we provide a more detailed overview of each category, highlighting state-of-the-art simulators used in each of them.

Macroscopic Traffic Simulators

Macroscopic traffic simulators model traffic flow using aggregated variables such as flow rates, average speeds, and vehicle densities, treating traffic as a continuous fluid. This approach emphasises on overall traffic patterns and system-level behaviours, rather than individual vehicle interactions [66]. Macroscopic models are particularly useful for strategic planning, long-term infrastructure development, and policy analysis, where large-scale impacts are of primary interest. They are computationally efficient, allowing for the simulation of extensive road networks over long time horizons. This makes them ideal for assessing scenarios like urban expansion, regional transportation policies, and large-scale traffic management systems.

One notable macroscopic simulator is TRAffic Network StudY Tool (TRANSYT) [67], developed by TRL Software in the UK. TRANSYT focuses on optimising traffic signal timings across extensive networks. Utilising traffic flow theory, it calculates queue lengths, delays, and stops, enabling urban planners to enhance signal coordination across multiple intersections rather than optimising them individually. This holistic approach reduces overall congestion and improves traffic flow efficiency on a network-wide scale.

Another prominent macroscopic tool is VISUM [68], developed by the PTV Group. VISUM excels in transport demand modelling and strategic planning. It integrates seamlessly with other PTV tools like VISSIM to facilitate multi-resolution modelling, combining macroscopic, mesoscopic, and microscopic simulation capabilities within a single framework. VISUM is extensively used by transportation agencies for long-term planning, public transport analysis, and infrastructure investment decisions, providing comprehensive insights into future transportation needs and the effects of various policy interventions.

Mesoscopic Traffic Simulators

Mesoscopic traffic simulators strike a balance between the detailed vehicle-level modelling of microscopic simulators, and the aggregated flow-based approach of macroscopic models [69]. They simulate traffic at an intermediate level of detail, typically representing groups of vehicles or traffic streams, rather than individual vehicles. This approach offers a compromise between computational efficiency and the ability to capture essential interactions within traffic flows. Mesoscopic simulators are well-suited for corridor-level studies, medium-sized urban networks, and scenarios requiring moderate detail without the high computational demands of microscopic models.

A leading mesoscopic simulator is DynaMIT [70], developed by the Massachusetts Institute of Technology. DynaMIT is designed for real-time traffic management applications, integrating traffic assignment models with dynamic traffic prediction. It provides real-time information to travellers and traffic managers, making it valuable for evaluating Advanced Traveller Information Systems (ATIS) and dynamic traffic management strategies. By enabling the assessment of real-time interventions such as dynamic routing, variable message signs, and adaptive signal control, DynaMIT helps enhance traffic flow and reduce congestion.

Similarly, TransModeler [71], developed by Caliper Corporation, offers versatility by operating in microscopic and macroscopic modes as well. This flexibility allows TransModeler to handle a wide range of traffic simulation scenarios, from corridor studies and congestion management to evacuation planning. Its ability to switch between different levels of granularity makes it a powerful tool for comprehensive

traffic analysis, accommodating diverse study requirements, and providing detailed insights into traffic dynamics across various contexts.

Microscopic Traffic Simulators

Microscopic traffic simulators provide the highest level of detail by modelling the behaviour and interactions of individual vehicles within a road network. These simulators incorporate car-following models, lane-changing algorithms, and gap acceptance rules to replicate realistic traffic behaviour at the level of individual drivers and vehicles. This granular approach allows for detailed analysis of traffic phenomena such as queue formation, intersection conflicts, and the impact of specific traffic control measures. Microscopic models are essential for operational studies, detailed traffic impact assessments, and the design and evaluation of ITS.

A widely-used microscopic simulator is VISSIM [72], developed by PTV Group. VISSIM is celebrated for its flexibility and detailed modelling capabilities, allowing for comprehensive urban traffic analysis, intersection design, public transport simulation, and pedestrian flow modelling. Its rich set of APIs facilitates extensive customisation and integration with external systems, making VISSIM a preferred choice for detailed traffic studies, traffic signal optimisation, and the simulation of complex traffic scenarios involving multiple modes of transportation.

Finally, SUMO [73], an open-source simulator developed by the German Aerospace Centre (DLR), is renowned for its extensibility and versatility. SUMO is particularly popular in academic research due to its open-source nature, which allows users to modify and extend its functionalities to suit specific research needs. It supports multi-modal traffic simulation, including vehicles, public transport, and pedestrians, making it ideal for studies on traffic emissions, traffic control algorithms, and smart city applications. SUMO's comprehensive suite of tools and active user community contribute to its widespread adoption and continuous development.

To sum up, Figure 3.2 provides a visual comparison of these simulation types, illustrating the scale and detail of macroscopic, mesoscopic, and microscopic simulators, ranging from more aggregated to more detailed levels.

3.2.2 Emission Models in Traffic Simulations: an Overview

Emission models are indispensable tools in traffic simulations, enabling researchers and policymakers to evaluate the environmental impact of vehicular traffic. According to Boulter *et al.* [75], these models are classified into five main types based on their approach and level of detail: aggregated emission factor models, average speed models, traffic situation models, multiple linear regression models, and modal

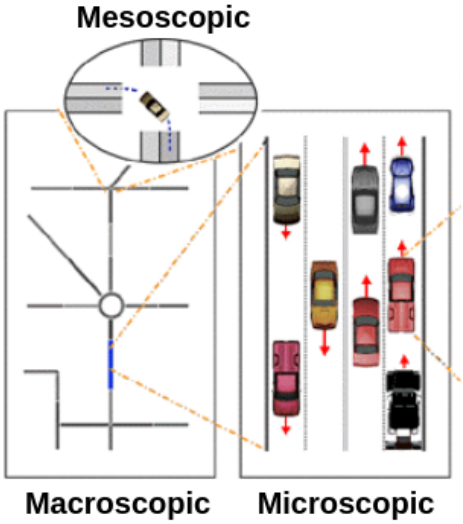

Figure 3.2: Comparison of traffic simulators: from macroscopic to microscopic [74].

models. Typically, emission models estimate pollutants such as CO_2, CO, NO_x, and PM_x. Despite sharing common objectives, these models differ significantly in their methodologies, level of detail, and data requirements. This section provides a comprehensive overview of the primary emission models used in traffic simulations, highlighting their features, strengths, limitations, and typical applications.

Aggregated Emission Factor Models

Aggregated emission factor models represent the most basic category of emission estimation tools. They adopt a single emission factor to characterise the emissions from a particular type of vehicle on a specific type of road (e.g., urban, rural, highway) [76]. However, their simplistic approach often lacks the granularity needed for detailed, local-level studies, as they do not account for variations in driving behaviour or traffic conditions [77].

Examples of aggregated emission factor models include those developed during projects like Coordination Information AIR (CORINAIR) [78].

Average Speed Models

Average speed models estimate emissions based on the average speed of vehicles, using emission factors typically expressed in grams per kilometre (g/km) [79]. Adjusted average speed models enhance this approach by including correction factors that account for different driving modes such as acceleration, cruising, and idling, thereby providing more refined emission estimates [80].

Prominent examples of average speed models include Computer Programme to Calculate Emissions from Road Transport (COPERT), extensively used in Europe for national emission inventories [81], and Motor Vehicle Emission Simulator (MOVES), developed by the U.S. Environmental Protection Agency [82]. Additionally, the HBEFA model is widely adopted in several European countries. HBEFA provides emission factors based on average speeds, and includes a comprehensive database for different vehicle categories and traffic situations, enhancing the accuracy of emission estimations [83].

Traffic Situation Models

Traffic situation models improve emission estimations by integrating speed and driving cycle dynamics to model emissions under specific traffic conditions [84]. These models consider factors such as speed variability, traffic density, and signal timing, offering a more accurate representation of real-world driving conditions [85]. By capturing the nuances of different traffic situations, they provide enhanced emission estimates over average speed models. An example is the Traffic Energy and Emissions Model (TEE), developed by the Italian National Agency for New Technologies, Energy and Sustainable Economic Development [86].

Multiple Linear Regression Models

Multiple linear regression models employ statistical techniques to predict emissions based on various driving cycle variables, including idle time and positive kinetic energy [87]. By considering a broader range of influencing factors, these models offer improved accuracy in emission estimations [88]. However, they require detailed driving pattern data, which may limit their applicability in scenarios lacking such information [89]. VERSIT+, developed by the Netherlands Organisation for Applied Scientific Research, is an example of such a model. It predicts emission factors for different vehicle fleets and traffic situations by analysing extensive empirical data [90].

Modal Models

Modal models, also known as instantaneous emission models, are based on detailed vehicle operating modes such as idling, cruising, acceleration, and deceleration [91]. These models provide high-resolution emission estimates, often on a second-by-second basis, making them suitable for detailed studies where specific operating conditions are known [92]. While more complex to develop and implement, they offer greater accuracy, especially for analyses involving dynamic driving conditions [93].

Examples of modal models include Passenger Car and Heavy-duty Emission Model (PHEM), which estimates emissions based on instantaneous engine power demand, and that can simulate a wide range of vehicles under various driving conditions [94]. Similarly, Comprehensive Modal Emissions Model (CMEM) models emissions as a function of vehicle operating modes, being applicable to diverse vehicle types and technologies [95]. Vehicle Transient Emissions Simulation Software (VeTESS) calculates emissions for individual vehicles over specific driving cycles, allowing for detailed analysis of transient emission behaviour [96].

Finally, Table 3.1 summarises the different emission models, highlighting their key characteristics, applications, and levels of detail. This comparative overview shows that, while each model type offers different advantages, they vary considerably in terms of both approach taken and granularity.

3.2.3 Comparative Evaluation of Traffic Simulators and Emission Models

In this subsection we present a comparative evaluation of various traffic simulators and emission models, aiming to identify the most suitable tools for our research. The analysis considers several key factors, including the level of detail, computational efficiency, data requirements, cost, and suitability for emission estimation.

Traffic Simulators

Table 3.2 outlines the key features of macroscopic, mesoscopic, and microscopic traffic simulators, emphasising their relevance for emission modelling.

Since this thesis requires detailed vehicle behaviour modelling to accurately assess emissions, microscopic simulators are the most appropriate choice. Among these, VISSIM and SUMO stand out.

VISSIM is a commercial software that offers extensive features and customisation options; however, it comes with high licensing costs, which may not be feasible for all projects. In contrast, SUMO, being open-source, provides similar functionalities at

Table 3.1: Summary of Emission Models in Traffic Simulations.

Model Type	Level of Detail	Key Features	Typical Applications
Aggregated Emission Factor Models	Low	Use single emission factors for vehicle-road type combinations; minimal data requirements	Large-scale emission inventories; strategic assessments
Average Speed Models	Low to Medium	Estimate emissions based on average vehicle speeds; can include correction factors for driving modes; examples include COPERT, MOVES, and HBEFA	National emission inventories; policy analysis
Traffic Situation Models	Medium	Integrate speed and driving cycle dynamics; consider traffic conditions like speed variability	Localised emission studies; urban planning
Multiple Linear Regression Models	Medium to High	Use statistical methods to predict emissions based on driving variables; require detailed data; example includes VERSIT+	Detailed emission estimations; research applications
Modal Models	High	Provide second-by-second emission estimates based on vehicle operating modes; highly detailed; examples include PHEM, CMEM, and VeTESS	Micro-scale studies; dynamic traffic simulations

Table 3.2: Comparison of Traffic Simulators

Simulator Type	Level of Detail	Advantages	Disadvantages	Examples
Macroscopic	Low	Computationally efficient; suitable for large-scale planning	Lacks detail for individual vehicle behavior; inadequate for emission modeling	TRANSYT, VISUM
Mesoscopic	Medium	Balances detail and efficiency; appropriate for medium-scale studies	Insufficient for micro-level emission analysis	DynaMIT, TransModeler
Microscopic	High	Detailed vehicle modeling; suitable for emission estimation	Computationally intensive; requires more data	VISSIM, SUMO

no cost, and allows for extensive customisation, making it more suitable for academic research. Thus, SUMO is selected due to its adaptability, cost-effectiveness, and flexibility.

Emission Models

Table 3.3 compares the different emission models described before, examining factors such as the level of detail, data requirements, availability, and suitability for integration with traffic simulators.

Table 3.3: Comparison of Emission Models.

Model Type	Level of Detail	Advantages	Disadvantages	Examples
Aggregated Emission Factor Models	Low	Simple; minimal data needs	Inadequate for detailed analysis; lacks granularity	CORINAIR
Average Speed Models	Low to Medium	Widely used; suitable for large-scale inventories	Insufficient for micro-level analysis; limited driving dynamics	COPERT, MOVES, HBEFA
Traffic Situation Models	Medium	Accounts for traffic conditions; more accurate than average speed models	Requires more data; limited for high-resolution studies	TEE
Multiple Linear Regression Models	Medium to High	Improved accuracy; considers driving variables	Requires detailed data; complex	VERSIT+
Modal Models	High	High-resolution estimates; captures dynamic conditions	Complex; may require proprietary software; high data demands	PHEM, CMEM, VeTESS

Given that our thesis focuses on detailed emission modelling, modal models are therefore the preferred option as they offer high resolution, and they can capture instantaneous emission variations. Among the modal models, PHEM provides detailed emission estimations, but its proprietary nature and associated licensing fees, approximately €16,000 [97], make it less accessible.

Within the SUMO simulator, there are two main emission modelling options: PHEMLight, which is a simplified version of PHEM, and also HBEFA. While PHEMLight's free version is limited to two emission classes, HBEFA provides a comprehensive database of emission factors for various vehicle categories and standards, at no cost. Moreover, HBEFA is widely used in Europe, and it integrates seamlessly with SUMO, making it the most suitable choice for our research despite being an average speed model.

In conclusion, combining SUMO with HBEFA allows us to conduct detailed traffic and emission simulations without incurring in prohibitive costs, while still meeting the required level of detail and accuracy for the thesis.

3.3 Re-routing Solutions and Challenges for Reducing Urban Pollution

Recent years have seen extensive exploration of re-routing solutions aimed at mitigating the environmental impact of urban traffic by reducing vehicular emissions. Various approaches have been proposed, each with distinct methods and objectives. These solutions generally focus on optimising traffic flow to decrease congestion and to reduce vehicular emissions, primarily targeting greenhouse gases like CO_2, or pollutants such as NO_x and PM_x.

One notable contribution is EcoTrec, a vehicle routing solution introduced by Doolan and Muntean [98]. EcoTrec aims to reduce CO_2 emissions while minimising impacts on travel time. It uses a Vehicular Ad-Hoc Network (VANET) where vehicles exchange messages about traffic and road conditions to build a fuel efficiency model. The routing engine calculates the most fuel-efficient route by evaluating road segments based on factors such as road and traffic conditions. While EcoTrec shows promise in reducing fuel consumption, it has limitations in handling congestion, and it does not account for pollutants beyond CO_2. Moreover, it lacks a model for measuring air pollutant concentrations and AQI levels.

Similarly, Akabane *et al.* proposed *i*MOB, an intelligent urban mobility management system that uses Vehicular Social Networks (VSN) and Social Network Analysis (SNA) to manage traffic flow [99]. The system uses a collaborative, three-layered architecture that enables vehicles to reroute altruistically to avoid congestion. The results demonstrate a reduction in average travel time and CO_2 emissions. However, the study focuses only on CO_2, failing to address other pollutants or air pollutant concentrations, which are crucial for a comprehensive assessment of urban air quality.

Another approach, SmartFlow, proposed by Khan and Koubaa [100], is designed for Vehicle to Infrastructure (V2I) communications to minimise delays at traffic signals by suggesting optimal speeds to vehicles. It uses frequent beacon messages to communicate with other vehicles and Road Side Units (RSUs). Although effective in reducing waiting times, SmartFlow relies entirely on autonomous vehicles and lacks AQI measurement capabilities, limiting its applicability in current urban environments.

Gomides *et al.* introduced REACT, a traffic management solution aimed at minimising congestion in smart cities through a Vehicle to Vehicle (V2V) network architecture where vehicles act as intelligent agents [101]. While REACT reduces communication overhead and travel time effectively, it remains largely conceptual and lacks validation with real-world traffic data. Also, it does not analyse pollutant emissions or concentrations, thereby having limited applicability in environmental

impact assessments.

Another relevant study by Akabane *et al.* is the distributed traffic management system called dEASY [102]. This infrastructure-less system relies on a three-layer architecture to gather, process, and distribute traffic data for route suggestions. The system performs well in reducing travel time and CO_2 emissions. However, it only considers CO_2, and does not account for other pollutants like NO_x or PM_x, nor does it measure pollutant concentrations and their corresponding AQI values.

Managing urban air quality becomes especially challenging during environmental crises like wildfires, smog, and dust storms, which rapidly deteriorate air quality [103, 104, 105]. These situations underscore the need for advanced traffic management systems that dynamically respond to changes in air quality. For instance, during smog episodes, pollutants can increase by 10 $\mu g/m^3$, leading to a 3% increase in mortality [106]. Current Low Emission Zones (LEZ) implemented in cities like Berlin, Amsterdam, Paris, London, and Madrid have proven effective [107]. However, these strategies often fail to dynamically incorporate real-time air quality data and diverse vehicle emission profiles, despite the rapidly changing nature of these emissions [108, 109].

Previous studies have also explored various methods for air quality monitoring and traffic management, but often lack the granularity needed to respond to sudden changes in air quality during environmental crises [110, 111, 112, 113, 114]. These traditional methods provide valuable data, but often do not integrate real-time air quality data with dynamic traffic management, which is crucial for mitigating health impacts during crises. The increasing frequency and intensity of environmental disasters, such as wildfires in California in 2020, and dust storms in the Middle East in 2022, further highlight the need for systems that integrate real-time environmental data with urban traffic management [115, 116, 117, 118, 119].

In contrast to previous published works, the solution proposed in this PhD thesis, and which will be detailed in the following chapters, addresses these research challenges by dynamically integrating AQI data with detailed vehicle emissions profiles so as to minimise pollution in critically affected areas. Unlike existing solutions, we adopt a holistic approach targeting multiple pollutants, including, NO_x, and PM_x, while also incorporating pollutant concentration modelling to calculate AQI levels. This comprehensive approach aims to provide a more effective response to urban air quality crises, balancing both environmental and traffic management needs. Additionally, our solution is designed to adapt dynamically to changes in environmental conditions and vehicle emissions profiles, which is often lacking in current systems.

Chapter 4

Proposed Vehicular Traffic Management Framework

In this chapter, we present our proposed vehicular traffic management framework designed to assess and mitigate urban air pollution caused by vehicular emissions. The framework integrates several components to simulate realistic traffic flow, calculate vehicle emissions, and compute pollutant concentrations in urban environments. Starting with traffic data collected from induction loop detectors, we generate realistic traffic demand using an algorithm that processes these data, and manages vehicle routes within the network. The SUMO tool is then used to simulate the traffic demand, incorporating detailed network configurations and vehicle types to accurately reflect real-world scenarios. By integrating the HBEFA emission model, SUMO generates detailed outputs on vehicle emissions and traffic measures, including edge-based emissions, which are critical for pollution analysis. We then focus on how these emissions are translated into pollutant concentrations within our framework, using the two options outlined in Figure 4.1 and discussed in chapter 2: the "Fixed Box Model" and GRAL. For GRAL, we use SUMO2GRAL, a tool we have developed to automate the conversion of SUMO outputs, and thay incorporates additional data, such as building geometries and meteorological conditions. By integrating these components, our framework provides a comprehensive approach to modelling vehicular traffic, estimating emissions, and assessing air quality impacts in urban environments.

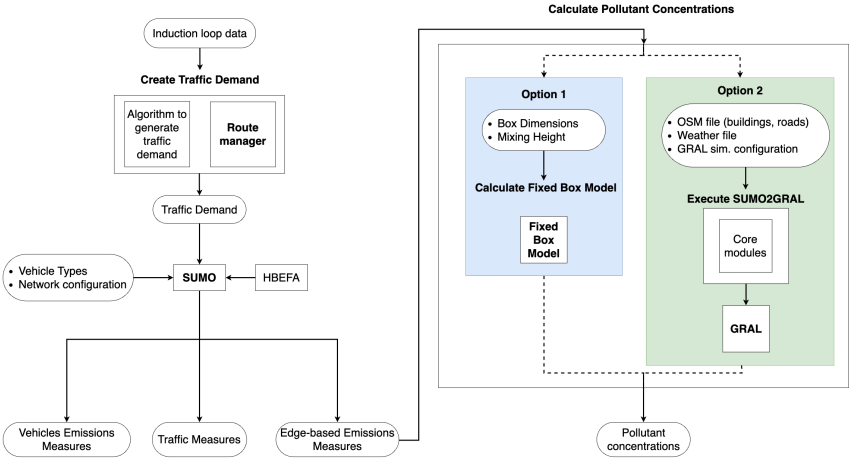

Figure 4.1: Proposed vehicular traffic management framework.

4.1 SUMO

As stated in chapter 3, SUMO is an open-source microscopic traffic simulator recognised for its accuracy and versatility in modelling various traffic environments, including urban areas and highways. Its open-source framework and detailed simulation capabilities make it particularly suitable for our traffic management framework. In this section, we focus on key SUMO tools that are essential to the proposed framework, specifically network editing, traffic demand generation, vehicle emissions modelling, and emissions measurement. By integrating these tools, we create realistic traffic scenarios and assess their impacts on urban air quality.

Furthermore, this section explains how SUMO generates crucial outputs for analysis. These outputs include vehicle emissions measures, which quantify emissions from individual vehicles; traffic measures, which provide data on vehicle flow and speeds across the network; and edge-based emissions measures, which capture emissions along specific road segments (edges). These outputs form the basis for pollutant concentration calculations and subsequent air quality assessments.

In the following subsections, we detail the processes of network creation, traffic demand generation, vehicle type configuration, and emission calculations. Additionally, we discuss the specific outputs produced by the simulation.

4.1.1 Network Creation

The first step in setting up a simulation in SUMO is the creation of a realistic traffic network, for which two essential tools are used: NETCONVERT [120] and NETEDIT [121].

NETCONVERT converts external map data, such as OpenStreetMap (OSM) files, into SUMO's network format (.net.xml). OSM files provide valuable real-world geographic and road data, but the conversion process often introduces errors, such as incorrect lane directions or missing traffic lights. Thus, while this initial conversion step is fundamental for building the traffic network, further refinements are necessary to ensure accuracy.

To address these issues, NETEDIT is employed to correct inaccuracies introduced during the network conversion. This tool enables manual adjustments to lane directions, turn restrictions, traffic lights, speed limits, and other critical components, ensuring the network more accurately reflects real-world conditions. Figure 4.2 illustrates a comparison between the raw network generated by NETCONVERT, the refined version created using NETEDIT, and the actual intersection as seen on Google Maps.

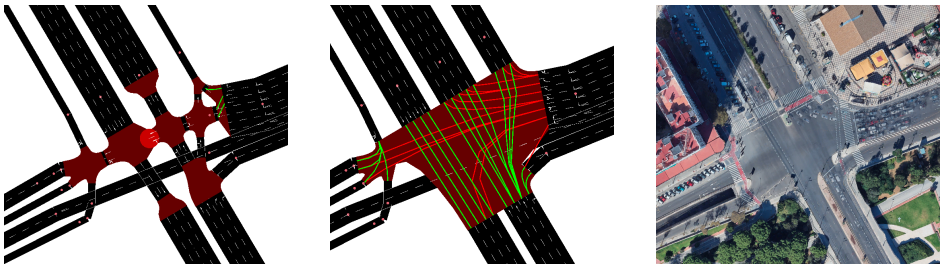

(a) Raw network generated by NETCONVERT.

(b) Edited network using NETEDIT.

(c) Real intersection from Google Maps.

Figure 4.2: Comparison of a traffic intersection.

In the raw network (Figure 4.2a), generated with NETCONVERT, several small intersections display incorrect lane directions and turnarounds. In contrast, the refined version produced using NETEDIT (Figure 4.2b) closely mirrors the real intersection (Figure 4.2c), combining multiple smaller intersections into a larger one with correct lane assignments and turn restrictions. This refinement process is critical, as it significantly enhances the accuracy of the traffic simulation, and ensures that the simulated environment accurately reflects real-world traffic behaviour.

4.1.2 Traffic Demand Generation

After refining the network, the next step in the simulation process is generating realistic traffic demand. In SUMO, traffic demand refers to the movement of vehicles through the network, which can be described either as trips or routes. A trip defines a starting point (source edge), an endpoint (destination edge), and a departure time. In particular, a trip can follow different alternative routes between the two points. In contrast, a route includes all the edges a vehicle will travel along between the source and destination.

To generate traffic demand in our framework, we rely on several SUMO tools, with one of the primary tools being DFROUTER [64]. DFROUTER creates routes based on detector data collected from sources such as induction loops. These loops, commonly used by traffic authorities, provide valuable data on vehicle flow and traffic patterns. DFROUTER processes this data to create routes that mirror real-world traffic demand by using observed vehicle counts. However, as discussed in chapter 5, DFROUTER has certain limitations, including producing unrealistic route lengths and traffic volumes when applied to large or complex networks. To address these challenges, we implemented adjustments and optimisations, ensuring that the generated traffic demand more accurately reflects actual traffic conditions.

For input data, we used a Comma Separated Values (CSV) file format containing geolocated vehicle counts, which capture the number of vehicles passing by specific points in the network over a given period. The CSV file structure includes data such as vehicle count, location (latitude and longitude), and the way ID from OSM. For DFROUTER, only the vehicle count and geolocation are required, while our proposed solution uses additional information like population and district data, which are not necessary for this method. An example of the CSV columns definition is provided in chapter 5, Table 5.3.

The output of the traffic demand generation process is an .rou.xml file, which contains both route definitions and vehicles assigned to those routes. Each route is identified by a unique route ID and consists of a sequence of edges that the vehicle will traverse. The vehicle entries specify the vehicle type, which will be discussed in more detail in the next subsection, linking each vehicle to specific emission profiles. Additionally, the vehicle entries include the route ID, departure time, departure speed, departure lane, among others. An example of the content of a .rou.xml file, illustrating both the route (see Figure 4.3a) and vehicle structure (see Figure 4.3b), is shown in Figure 4.3.

```
<routes xmlns:xsi="http://www.w3.org/2001/XMLSchema-instance" xsi:noNamespaceSchemaLocation="http://
sumo.dlr.de/xsd/routes_file.xsd">
        <vType id="gas_oil_b" emissionClass="HBEFA4/PC_diesel_Euro-4"/>
        <route id="150637612#2_to_118695379_gas_oil_b" edges="150637612#2 150637612#3 -39740019#0 643436578
39739010#0 39739010#1 39739010#2 554575392 39740023 441631994 23588334#0 23588334#1 23588334#2 23588337
383622104 469051365 469051364 12874097 12874131#1 12874131#2 12874131#3 36950239#0 100777802 428944465
428944459 428944489 428944483 428944463 428944460 428944473 428944469 468909192 428944476 12874085 12874085-
AddedOffRampEdge 23614665 721236853#0 730406938 -23365114#5 -23365114#2 23614672#0 107310438#0 142732694
142732696#5 142732696#6 142732696#7 103267574 -100790794 107833143#0 107833143#1 107833143#2 107833143#3
-708302800 -708302799 23576254 95512926#2 23576250 -128213266 144049340 128213283#1 128213268 118695379"/>
        <route id="36968738#2_to_11945183#2_gas_oil_b" edges="36968738#2 36968738#3 -36968734#1 36968743#1
36968743#2 36968689#0 36968689#3 820897795#0 820897795#1 -166181719#2 -166181719#1 166181723 36968726#7
```

(a) Route structure.

```
        <vehicle id="emitter_dd_468909207_571_gas_oil_b" type="gas_oil_b" depart="0" departLane="best"
departPos="last" departSpeed="avg" route="468909207_to_21096577_gas_oil_b"/>

        <vehicle id="emitter_dd_172463205#0_1_gas_oil_b" type="gas_oil_b" depart="1" departLane="best"
departPos="last" departSpeed="avg" route="172463205#0_to_-13075721#0_gas_oil_b"/>

        <vehicle id="emitter_dd_23565098#0_572_gas_oil_b" type="gas_oil_b" depart="1" departLane="best"
departPos="last" departSpeed="avg" route="23565098#0_to_11853824#0_gas_oil_b"/>

        <vehicle id="emitter_dd_143277287#0_2_gas_oil_b" type="gas_oil_b" depart="2" departLane="best"
departPos="last" departSpeed="avg" route="143277287#0_to_-23016506#2_gas_oil_b"/>
```

(b) Vehicle structure.

Figure 4.3: Example of a .rou.xml file structure.

4.1.3 Vehicle Types Configuration

In order to accurately assess emissions within our proposed framework, it is essential to define different vehicle types and their corresponding emission profiles. SUMO, combined with the HBEFA emission model, allows us to assign various vehicle categories based on fuel type, engine specifications, and emission standards. By doing so, we can simulate realistic vehicle behaviour and quantify emissions for different types of vehicles on the road.

In our framework, vehicles are categorised according to the HBEFA emission classes, which provide detailed information on emission factors based on vehicle type, engine type, and the European emission standard (EURO class) to which they belong. HBEFA allows for the classification of vehicles into multiple categories, including petrol and diesel cars, trucks, buses, hybrid vehicles, and electric vehicles, each with different emissions profiles.

Table 4.1 outlines the key HBEFA passenger vehicle classes used in this thesis, along with their corresponding EURO standards and engine types. For the purposes of this thesis, we focus solely on passenger vehicles, as will be explained later in chapter 5. This categorisation ensures that our simulations align with real-world traffic scenarios, where vehicles of various engine types and emission standards exist.

The vehicle types and their configurations are defined within the SUMO route file (.rou.xml) through a set of parameters, which include the vehicle ID, type,

Table 4.1: HBEFA passenger vehicle classes and corresponding EURO norms.

HBEFA class	EURO norm	Engine type
PC_petrol_Euro-3	Euro 3	Petrol
PC_petrol_Euro-6ab	Euro 6	Petrol
PC_diesel_Euro-4	Euro 4	Diesel
PC_diesel_Euro-6ab	Euro 6	Diesel
PC_CNG_petrol_Euro-6_(CNG)	Euro 6	Hybrid (Petrol CNG)
PC_BEV	Euro 6	Battery Electric

route, and departure attributes (time, lane, speed). The vehicle type is specified using the "vType" tag, where parameters such as emission class can be defined. Figure 4.4 provides an example of a vehicle type definition within the .rou.xml file.

```
<vType id="gas_oil_b" emissionClass="HBEFA4/PC_diesel_Euro-4"/>
    <vehicle id="veh0" type="gas_oil_b" route="route0" depart="0"
        departLane="best" departSpeed="max"/>
```

Figure 4.4: Example of vehicle type definition in SUMO .rou file.

In this example, the vehicle type "gas_oil_b" is linked to the HBEFA emission class for Euro 4 diesel passenger cars. The "vType" tag defines the vehicle's physical properties, such as the emissions profile, while the "vehicle" tag assigns this type to a specific vehicle with its departure time, route, and other driving behaviour parameters.

By configuring vehicle types, we are able to make that each vehicle in the simulation adheres to real-world emissions profiles, making the emission calculations more accurate, and allowing us to better understand the contribution of different vehicle types to overall urban emissions.

4.1.4 Emission Calculation

In our proposed framework, vehicle emissions are calculated using the HBEFA emission model integrated within SUMO, as described in chapter 3. SUMO computes emissions for each vehicle at every simulation time step, accounting for factors such as engine type, and fuel consumption. The emissions are saved in eXtensible Markup Language (XML) files and provide detailed data on pollutants, including CO_2, NO_x, and PM_x, as emitted by each vehicle.

4.1.5 Vehicles Emissions Measures

In SUMO, emissions data for each vehicle are saved in the tripinfo XML output file [122], which combines both traffic and emissions data for individual vehicles. The emissions tracked during each trip include key pollutants, such as CO, CO_2, Hydrocarbon (HC), PM_x, and NO_x, as well as total fuel consumption, all expressed in milligrams. This data is summarised at the end of each trip, providing a comprehensive overview of the vehicle's environmental impact throughout its journey.

Although this data is valuable for analysing emissions at the individual vehicle level, our framework does not directly use the tripinfo file for pollutant concentration calculations. Instead, we rely on edge-based emissions data, which aggregates emissions by edges. This aggregated data is more suitable for calculating pollution concentrations, and is essential for estimating urban air quality across the entire network. Further details on edge-based emissions are discussed in the following subsection.

An example of the emissions section from the tripinfo output file is shown in Figure 4.5.

```
<emissions CO_abs="116.963373" CO2_abs="271948.875074" HC_abs="29.300938"
PMx_abs="22.583611" NOx_abs="539.353814" fuel_abs="87396.776677"
electricity_abs="0"/>
```

Figure 4.5: Example of vehicle emissions output in the tripinfo XML file.

4.1.6 Traffic Measures

In SUMO, traffic measures are essential for understanding the flow and performance of both individual vehicles and the entire traffic network. Traffic data is captured in two primary ways: one file provides vehicle-level information (using the tripinfo XML file), while another file contains network-wide traffic statistics based on edges, stored in the edge-based traffic XML file [123].

For each vehicle, SUMO generates a tripinfo file that contains detailed traffic metrics such as departure time, arrival time, travel duration, route length, and average speed. These metrics are critical for assessing vehicle-level performance. In our framework, tripinfo data is primarily used to evaluate the impact of traffic management strategies on congestion, travel time, and route length. These measures help identify trade-offs between emissions reduction and potential increases in travel time or route length. Figure 4.6 provides an example of vehicle traffic data stored in the tripinfo file.

```
<tripinfo id="emitter_dd_41056268#0_576_hybrid" depart="5.00" departLane="41056268#0_1" departPos="79.72"
departSpeed="13.89" departDelay="0.00" arrival="158.00" arrivalLane="-52391667_0" arrivalPos="105.52"
arrivalSpeed="7.84" duration="153.00" routeLength="1576.61" waitingTime="9.00" waitingCount="1" stopTime="0.00"
timeLoss="25.46" rerouteNo="0" devices="vehroute_emitter_dd_41056268#0_576_hybrid
tripinfo_emitter_dd_41056268#0_576_hybrid emissions_emitter_dd_41056268#0_576_hybrid" vType="hybrid"
speedFactor="1.03" vaporized="">
```

Figure 4.6: Example of vehicle-level traffic data in the tripinfo XML file.

On the other hand, SUMO also generates traffic measures for each edge within the network. Such data are stored in a separate edge-based traffic file, which contains metrics such as time loss, average speed, and traffic density for each edge. This file provides a broader perspective of network performance, helping us assess congestion and traffic patterns across the entire simulated area. Figure 4.7 shows an example of edge-level traffic data stored in the edge-based traffic file.

```
        <edge id="-100790794" sampledSeconds="44.89" traveltime="9.94"
overlapTraveltime="11.22" density="0.22" laneDensity="0.22" occupancy="0.10"
waitingTime="4.00" timeLoss="14.29" speed="5.56" speedRelative="0.67" departed="0"
arrived="0" entered="4" left="4" laneChangedFrom="0" laneChangedTo="0"/>
        <edge id="-1021891675#0" sampledSeconds="45.92" traveltime="11.08"
overlapTraveltime="11.48" density="0.09" laneDensity="0.09" occupancy="0.04"
waitingTime="0.00" timeLoss="2.31" speed="13.00" speedRelative="0.94" departed="0"
arrived="0" entered="4" left="4" laneChangedFrom="0" laneChangedTo="0"/>
```

Figure 4.7: Example of edge-level traffic data in the edge-based traffic XML file.

4.1.7 Edge-based Emission Measures

In our framework, edge-based emission measures are critical for estimating pollution concentrations across the city. These data capture emissions from all vehicles on each edge. The output is structured in XML format and includes detailed information on both traffic flow and emissions for each edge. Unlike vehicle-specific emissions in the tripinfo file, edge-based emissions aggregate pollution data, providing a comprehensive view of emissions over time and space.

The output file records several key metrics, including absolute pollutant emissions and traffic-related data. These absolute values, expressed in milligrams (mg), represent the total amount of pollutants emitted during a specified period (e.g., one hour). The primary fields include CO_abs, CO2_abs, HC_abs, PMx_abs, NOx_abs, fuel_abs, and electricity_abs, which correspond to the total emissions or consumption on a particular edge or lane. For example, CO_abs refers to the total CO emitted by all vehicles on a specific edge. Similar fields are used for CO_2, HC, PM_x, NO_x, fuel consumption (fuel_abs), and electricity consumption (electricity_abs). These absolute emission measures form the basis of our analysis, allowing us to estimate the concentration of pollutants in the city through the models described in chapter 2.

```
<meandata xmlns:xsi="http://www.w3.org/2001/XMLSchema-instance"
xsi:noNamespaceSchemaLocation="http://sumo.dlr.de/xsd/meandata_file.xsd">
    <interval begin="0.00" end="3600.00" id="edges_emissions_data_gasoline_c">
        <edge id="-100011394#2" sampledSeconds="3.55" CO_abs="8.646946" CO2_abs="6975.893363"
HC_abs="0.151517" PMx_abs="0.688554" NOx_abs="2.169048" fuel_abs="2261.640114" electricity_abs="0"
            CO_normed="0.318371" CO2_normed="256.844380" HC_normed="0.005579" PMx_normed="0.025352"
NOx_normed="0.079862" fuel_normed="83.270991" electricity_normed="0"
            traveltime="3.55" CO_perVeh="8.646946" CO2_perVeh="6975.893363" HC_perVeh="0.151517"
PMx_perVeh="0.688554" NOx_perVeh="2.169048" fuel_perVeh="2261.640114" electricity_perVeh="0"/>
```

Figure 4.8: Example of edge-level emissions data in the edge-based emissions XML file.

Additionally, the output provides other useful fields such as “sampledSeconds”, which indicates the total time vehicles were measured on the edge or lane. Likewise, the “traveltime” field estimates the average time vehicles take to travel across an edge, based on mean speed.

In the output, data is saved for each edge (edge_id) or lane (lane_id), and aggregated over specified time intervals, marked by begin and end times in seconds. Figure 4.8 shows an example of the edge-based emissions output in XML format.

As shown, the output also includes normalised emission values (e.g., CO_normed, NOx_normed) in grams per kilometre per hour (g/km/h), normalised by time and road length. These values allow comparisons across different road segments, regardless of their length or the duration of the simulation. However, in our framework, we prioritise absolute emission values, as they directly represent total pollutant output, making them more suitable for calculating pollution concentrations.

By using edge-based emissions, our framework aggregates emissions data across the entire traffic network, providing the base for calculating pollution concentrations in urban areas.

4.2 Pollutant Concentration Calculation

In our proposed framework, we provide two options for calculating pollutant concentrations from the vehicle emissions data generated by SUMO. As detailed in chapter 2, both methods are dispersion models that convert vehicle emissions into pollutant concentration levels, allowing us to assess the impact of vehicular traffic on air quality.

The first option uses the “Fixed Box Model”, a fast and straightforward method for estimating pollutant concentrations. This approach is ideal for preliminary assessments where computational efficiency is important. However, its simplicity results in less accuracy compared to more complex models.

The second option employs GRAL, a more sophisticated model that simulates pollutant dispersion in complex urban environments. GRAL incorporates factors such as meteorology and building configurations, making it suitable for studies that

require high precision. Despite its accuracy, the setup and configuration process for GRAL can be time-consuming and requires significant detail.

To streamline the use of GRAL in our framework, we developed a tool called SUMO2GRAL [124]. This tool automates the conversion of SUMO emissions data into the format required by GRAL, eliminating the need for external software like Geographic Information System (GIS) software or the GRAL GUI. SUMO2GRAL is cross-platform, ensuring that users can perform the workflow efficiently without manually converting their emissions output into the CSV format, or relying on other tools, simplifying what would otherwise be a tedious process. We now proceed to describe it more in detail.

4.2.1 Proposed SUMO2GRAL tool

This section details the architecture of SUMO2GRAL, highlighting its key components, modules, and their interactions within the context of our traffic management framework. SUMO2GRAL plays a key role in preparing SUMO-generated emissions data for pollution dispersion modelling in GRAL.

SUMO2GRAL operates in both online and offline modes. In online mode, if users do not have an OSM file or specific meteorological data, SUMO2GRAL can automatically generate default geographic and weather files. However, in this thesis, we focus on the offline mode, where it is assumed that all necessary files, such as OSM and meteorological data, are already available.

Developed in Python 3.10, SUMO2GRAL is cross-platform compatible, enabling its use across various operating systems. Its modular architecture ensures an efficient workflow, with four main modules executed sequentially and independently. The following subsection describes each module in detail.

Modules

The SUMO2GRAL tool consists of six primary modules: (i) Buildings, (ii) Weather, (iii) Line Emission Sources, (iv) Local Files Processor, (v) GRAL Processor, and (vi) Display. Below is an overview of their functions:

- **Buildings**: This module processes geographic data about buildings from the OSM file and converts it into a Shapefile. The process ensures clean and consistent building data, free from anomalies, to avoid errors during the pollutant dispersion simulation.
- **Weather**: This module manages weather data to ensure compatibility with GRAL's input requirements. It processes parameters such as wind speed, wind direction, and atmospheric stability classes. If specific weather data is

unavailable, SUMO2GRAL generates a default weather file to proceed with the simulation.

- **Line Emission Sources**: This module combines road data from the OSM file with SUMO's edge-based emissions data, generating a Shapefile that integrates the road network and emissions for GRAL simulation. It also identifies and corrects inconsistencies in the road data.
- **Local Files Processor**: This module processes local OSM and SUMO XML files. Using libraries like osmium and XML parsing tools, it reads OSM and SUMO data, and passes relevant information to the Buildings and Line Emission Sources modules for further processing.
- **GRAL Processor**: This module generates the input files required for GRAL. It compiles outputs from the Buildings, Line Emission Sources, and Weather modules, while allowing users to specify GRAL parameters such as pollutant types, dispersion time, and particle count.
- **Display**: This optional module allows to visualise GRAL simulation results, offering an intuitive display of pollutant concentrations for a quick assessment of the simulation's accuracy and outcomes.

Workflow

Having described the individual modules, we now explore how these components interconnect to form a workflow.

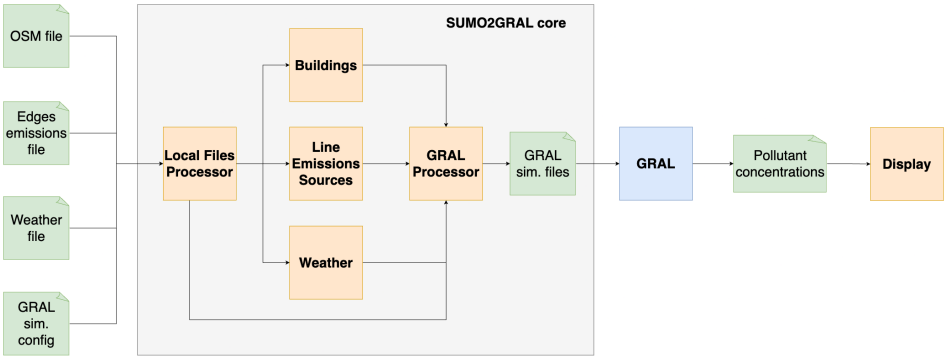

Figure 4.9: SUMO2GRAL workflow.

As illustrated in Figure 4.9, the workflow begins with input files such as the OSM file, the edge-based emissions file, the weather data, and the GRAL configuration

file. These files are processed sequentially by their respective modules to ensure compatibility with GRAL.

The workflow starts with the Local Files Processor, which reads OSM and SUMO data, and converts it into suitable formats. Then, the Buildings, Line Emission Sources, and Weather modules process their respective data, ensuring it meets the required standards for GRAL.

Once all data is prepared, the GRAL Processor compiles the inputs and generates the final files for the GRAL simulation. The GRAL simulation is then executed, producing pollutant dispersion data based on these inputs.

Finally, the Display module can be used to visualise the simulation results, offering an intuitive representation of pollutant concentrations in the study area. This allows users to assess the realism of the simulation and make adjustments if necessary.

4.3 Pollutant Concentration Calibration

While two methods for calculating pollutant concentrations were outlined earlier, the "Fixed Box Model" and GRAL, only the latter requires calibration. The "Fixed Box Model" is a simplified approach that assumes uniform pollutant dispersion, making it useful for quick assessments, but less accurate for real-world applications; hence, there is little use in calibrating it, reason why we discarded such option. In contrast, GRAL provides a more detailed simulation of pollutant dispersion, especially in urban environments where factors such as buildings, wind patterns, and multiple pollution sources must be considered. To enhance the accuracy of GRAL outputs, calibration with real-world data is recommendable.

Our model uses GRAL to simulate pollutant dispersion based on vehicular emissions alone. However, real-world pollution levels are generally higher, as vehicles represent just one of many pollution sources in urban areas. To address this discrepancy, we calibrate the simulated pollutant concentrations with actual air quality monitoring data, bringing the simulation in line with real-world conditions.

The calibration process begins by collecting real-world air quality data for NO_x and PM_{10} from monitoring stations in Valencia [125]. This data corresponds to the same date and time as the simulated scenario, and it is geographically aligned with the simulation for accurate location-specific comparisons. Once the data is prepared, outliers are removed by capping values outside the 1st and 99th percentiles, ensuring that extreme values do not distort the calibration process.

Next, adjustment factors are calculated for each monitoring station by comparing the real NO_x and PM_{10} levels with the simulated values at each station. These factors are applied to the simulated pollutant concentrations based on proximity

to the monitoring stations. For locations within 200 meters of a station, the specific adjustment factor for that station is used. Beyond this radius, an average adjustment factor from all stations is applied. This method ensures comprehensive calibration across the simulation area, including locations where direct monitoring data is unavailable.

For future environmental scenarios, such as those discussed in chapter 7, the adjustment process involves scaling the future scenario's GRAL output by the percentage difference between the calibrated current scenario and its simulation output. This allows for more accurate predictions of future air quality conditions based on the calibration of the current scenario.

4.4 Summary

In this chapter, we introduced a comprehensive vehicular traffic management framework designed to assess and reduce urban air pollution caused by vehicular emissions. The framework starts with the collection of traffic data from induction loop detectors, which is processed through an algorithm to generate realistic traffic demand (discussed in the next chapter) and manage vehicle routes within the network. Using SUMO, we simulated traffic flow with detailed network configurations and vehicle types, while using the HBEFA emission model. SUMO provided valuable outputs, including vehicle emissions, traffic measures, and edge-based emissions, essential for analysing pollution levels across the network.

To compute pollutant concentrations from the emissions data, we employed the two methods introduced in chapter 2. The first is the "Fixed Box Model". The second method uses SUMO2GRAL, a tool we developed to integrate SUMO with GRAL, enabling detailed and accurate pollutant dispersion modelling in urban environments. SUMO2GRAL automates the conversion of SUMO outputs and incorporates additional data, such as building geometries from OSM and meteorological conditions, to improve the accuracy of the simulations.

Additionally, we addressed the calibration of pollutant concentrations using real-world air quality data, specifically for GRAL simulations. This calibration adjusts the simulated pollutant concentrations to align with observed data from air quality monitoring stations, accounting for factors not included in the simulation, such as background emissions, or other transport emissions.

In conclusion, this chapter established a robust framework that integrates traffic simulation, emission modelling, and pollutant dispersion analysis. By combining these components, the framework provides a solid foundation for evaluating the impact of traffic management strategies on urban air quality, setting the way for developing effective pollution mitigation measures in the chapters that follow.

Chapter 5

Generating Traffic Demand in a Realistic Way

In the previous chapters, we have discussed the different vehicle traffic simulators, and the reason we have selected SUMO as our simulator. We have also examined traffic emissions and outlined the process of obtaining these emissions from SUMO. In this sense, to be able to perform those simulations, we need to have some accurately modelled traffic demand data, and to do so, having a reliable traffic dataset is fundamental. Usually, it is difficult to obtain reliable traffic demand if they are not obtained through GPS traces. However, the use of GPS traces is a challenging task due to the difficulty of accessing GPS data from personal vehicles or drivers' smartphones, which raises significant privacy concerns. In general, the solution to the aforementioned problem lies in the use of induction loop detectors or cameras in the cities. Along this chapter, we will focus on the first ones, which count the number of vehicles passing over them. Such data help to identify areas with varying congestion levels. However, this is not enough to generate traffic demand, and so external tools are necessary to compute this demand accurately. In this chapter, we will analyse existing state-of-the-art solutions to this problem, highlighting their shortcomings. Furthermore, we will introduce our proposed solution, demonstrating how it addresses these issues, and surpasses the performance of current methods.

5.1 Overview of Valencia's Traffic Conditions

Understanding the different traffic intensities can help city administrations to better plan different scenarios. This can avoid unnecessary congestion and discomfort for people living in the city. Traffic intensity, which is the number of vehicles passing over an induction loop, is a key metric in analysing traffic flow and congestion in cities. By examining this data, we can identify patterns in traffic behaviour over time and space, which is crucial for developing ITS and traffic management strategies.

In this regard, we retrieve the data from the Open Data portal of the City Council of Valencia [63]. The portal provides access to different sources of data. In particular, we gather the traffic intensity data for the year 2022 from 720 induction loops placed all over the city. These induction loops are embedded within road surfaces, and employ electromagnetic fields to detect passing vehicles, logging each instance to provide continuous traffic information, such as vehicle count, density, and timestamp.

The placement of these induction loops throughout Valencia ensures extensive coverage of major roads, secondary streets, and residential areas, providing a detailed and representative picture of traffic flow across different types of roads. Such data helps identify peak congestion times and specific locations with high traffic volumes, allowing for a more targeted analysis of urban traffic behaviour, as well as informed decision-making for future traffic management solutions.

To gain an overall view of Valencia's traffic, we start by analysing the average monthly traffic intensity, which is depicted in Figure 5.1. As observed, traffic is lower in August and December, likely due to people going on holiday and leaving the city. Conversely, months like May, June, October, and November have the highest traffic intensity. For our study, we choose November, as Calafate *et al.* [126] did, because it is a month without major holiday periods, and it has traffic values similar to other high-traffic months like May.

Following the analysis of monthly traffic intensity, Figure 5.2 shows the traffic pattern throughout the week. As seen, traffic intensity is higher on weekdays (around 45,000 vehicles) than on weekends (around 33,000 vehicles). Monday and Tuesday have the highest intensity, with approximately 50,000 vehicles each day. Thus, for a detailed hourly analysis, we choose Monday as the representative day.

Figure 5.3 illustrates the hourly evolution of average traffic intensity for a typical Monday. Peak hours are from 7 a.m. to 9 a.m., and from 5 p.m. to 7 p.m., with a smaller peak around 2 p.m. The morning and evening peaks correspond to people commuting to and from work, while the midday peak likely results from people leaving work for lunch or picking up their children from school. For our study, we focus on the time slot between 8 a.m. and 9 a.m., as it exhibits the

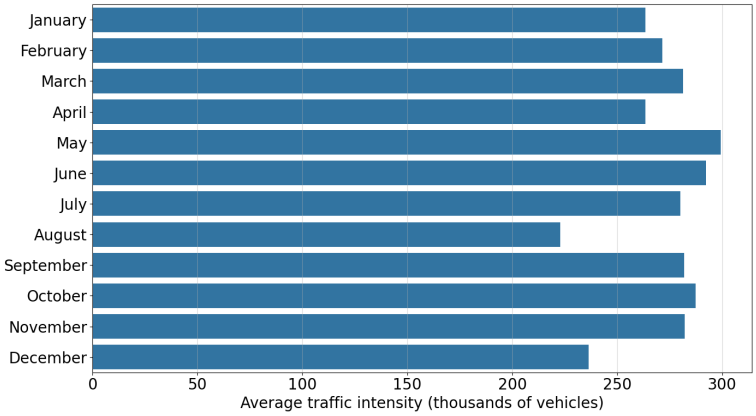

Figure 5.1: Average traffic intensity in Valencia per month.

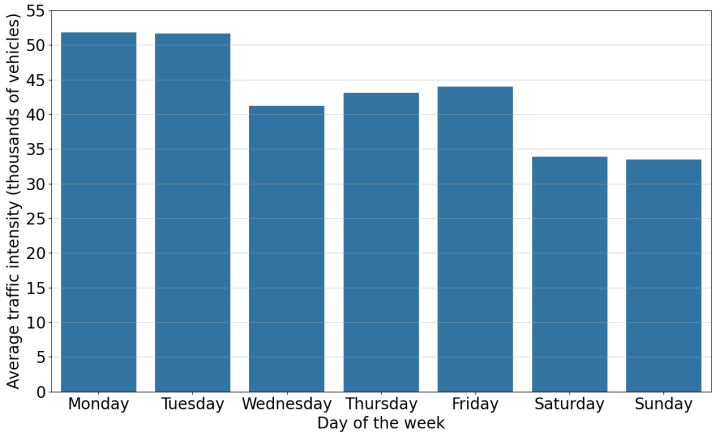

Figure 5.2: Average traffic intensity in Valencia per day of the week.

highest traffic intensity during the day.

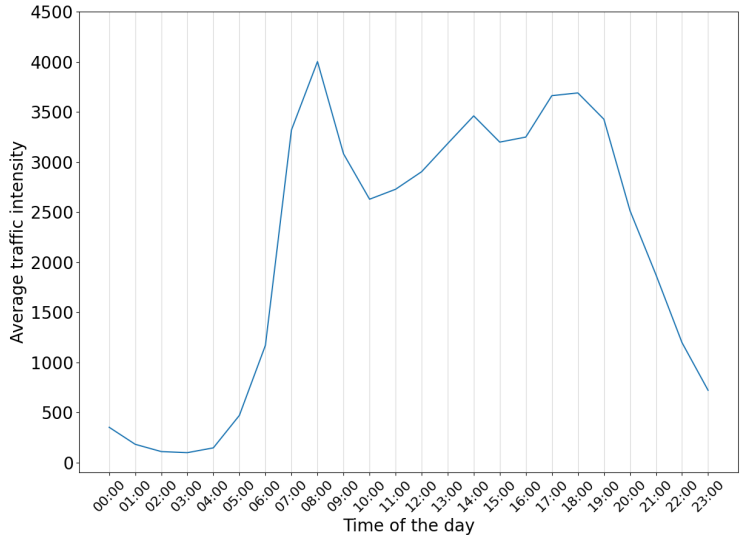

Figure 5.3: Daily behaviour in a typical weekday (Monday).

5.2 State-of-the-Art Unresolved Issues

In this section, we will focus on DFROUTER due to its capability of generating vehicle routes from induction loop count data. In particular, we want to address some of the limitations of it, specifically in regard to determining actual traffic injected into a network, and analysing the lengths of generated routes, particularly in urban environments. Notice that DFROUTER was designed primarily for highways and not city streets or avenues, as its authors state in [127]: "The idea behind this router is that nowadays, most highways are well-equipped with induction loops, measuring each of the highways' entering and leaving flows." This means that its usefulness in generating a traffic demand in a city is limited.

5.2.1 DFROUTER Traffic Injected Issue

In [128], Zambrano *et al.* discussed a problem for DFROUTER, which is related to the number of vehicles that pass over the different induction loops in the output that is generated. In particular, the authors found that it has a large deviation compared to the real data. Furthermore, this deviation is also reflected in the

number of vehicles injected. This means that DFROUTER injects a number of vehicles that is greater than expected, being that the overall difference obtained was +238% when compared to real data. Due to this issue, the traffic demand generated was not representative of the actual traffic conditions in the city.

For evaluating and analysing our proposed new methodology, we have recreated their experiments to obtain the reliability of the DFROUTER data. Specifically, we have also used DFROUTER and the city induction loop real data, although such data was retrieved much more recently using web tools, and so correspond to current traffic patterns, as opposed to the former ones. As a result, we have obtained via DFROUTER the traffic distribution throughout the city (traffic demand). Then, applying reverse engineering, we obtained the distribution of vehicles per induction loop. This allowed us to compare, side by side, the percentage error between the real data and the data provided by DFROUTER.

Analysing the induction loop data distribution in more depth, we can look at the Empirical Cumulative Distribution Function (ECDF) presented in Figure 5.4. This figure shows the number of vehicles that pass over each induction loop, sorted by size. In it, we can observe that there is a great difference between both functions, evidencing that DFROUTER is not generating realistic traffic routes. Specifically, for the real data function, we observe a linear function with a small slope, and with a parable at around 600 induction loops, with a maximum value of about 2,5k vehicles. In contrast, the DFROUTER function has a maximum value of 17k vehicles, and it is 0 for the first 270 detectors. Then, it behaves like a linear function with a big slope until 650, a value beyond which it starts to make a parable. This leads us to think that the difference between the detector data for DFROUTER, and the actual traffic, will be somewhat high.

Table 5.1 complements the data shown in Figure 5.4. In particular, Table 5.1 presents different statistical measures that provide a complete overview of the differences between the real and the DFROUTER induction loop data. Notice that such difference is calculated for each detector. We can see that the minimum values absolute difference between the data of induction loops and DFROUTER is -4, while the maximum values' difference goes up to 530% more in DFROUTER. In terms of quartiles, we observe that the first half of the values (Q2) already experience an increase of +314%, but, for the Q3 threshold, this number increases to +554%. Due to these numbers, the average percentage difference between real and DFROUTER induction loop data is 516%.

All in all, considering both the analysis of Zambrano *et al.*, and our own analysis, we can state that DFROUTER has an issue when distributing and injecting the traffic in a city when having induction loop data as input. In particular, we observe that the variation remains with an overestimation tendency: 238% in the former work, and 516% in our work. This led us to think that the error DFROUTER

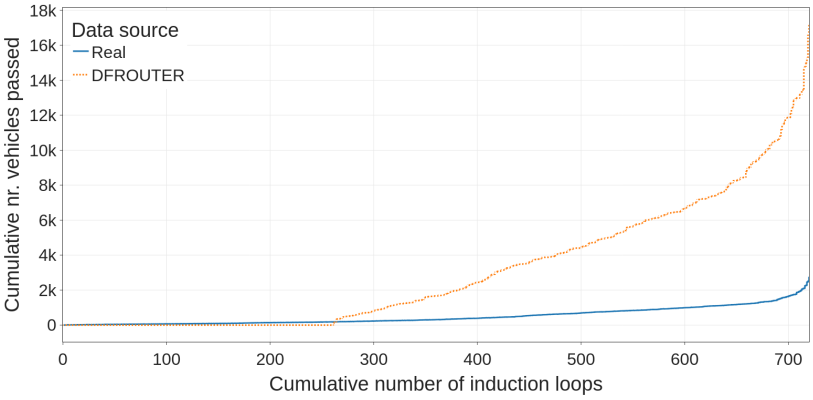

Figure 5.4: ECDF of induction loop real and DFROUTER data.

Table 5.1: Induction loop data difference stats (Real vs. DFROUTER).

	Real	DFROUTER	Abs. Difference	Rel. Difference
Avg.	504	3,108	2,604	+516%
Std. Dev.	481	4,000	3,519	+732%
Q1	125	0	-125	N.A.
Q2	313	1,670	1,357	+314%
Q3	815	5,330	4,515	+554%
Min.	4	0	-4	N.A.
Max.	2,728	17,204	14,476	+530%

introduces is consistent, and repetitive. Specifically, in the next subsection, we focus on evaluating the length of routes.

5.2.2 DFROUTER Routes Length Issue

As previously stated, DFROUTER is more oriented toward generating routes for highways than for streets or avenues. Since there is a clear difference between a highway environment and a city environment, the resulting lengths of the routes are prone to have little representativeness in urban environments. In order to check the validity of this statement, we have generated the routes for the city of Valencia. To contextualise, in terms of population, Valencia is the 3rd city in Spain, and

the 23rd in the European Union, with 800,215 inhabitants. Regarding size, the analysed area has a size of 127.89 square kilometres (approx.: 12.6 km W-E; 10.1 km N-S). Likewise, the city has around 4,000 streets and avenues, with major roads such as the "*Calle San Vicente Mártir*" with a length of approximately 4 km, and minor roads such as the "*Calle Doctor Serrano*", with a length of approximately 180 m.

The route length distribution is presented in Figure 5.5. As we can see, most of the routes are concentrated in the range from 1,000 m to 2,500 m. In addition, we can observe that there is a large number of routes with a length of less than 1,000 m, and even as low as 500 m in some cases. These short lengths are not representative of a city such as Valencia, with very limited parking availability, meaning that most people will make such trips on foot or using public transport like the underground.

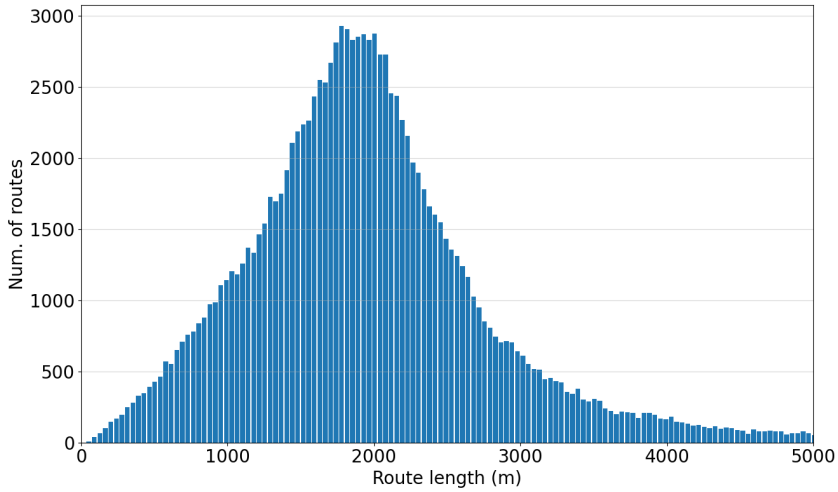

Figure 5.5: Route length distribution for DFROUTER.

To make a more complete analysis of the results generated by DFROUTER, we can observe the routes statistics from DFROUTER on Table 5.2. In particular, the minimum length of a route is 34 m, which is very small and is not close to real situations. On the contrary, the maximum length is 17,401 m., which is a large route, and representative of someone who lives on the outskirts of the city. Additionally, for the median and average length, we have 1,897 and 2,035 meters,

respectively. These lengths, as we said before, are too short considering the actual citizen experience. In fact, 75% of the routes can be considered not representative as they are below 2,385 m.

Table 5.2: Routes statistics from the DFROUTER route output file.

Statistic	**Value**
Num. of routes	123,958
Avg.	2,035 m.
Std. Dev.	1,068 m.
Q1	1,448 m.
Q2	1,897 m.
Q3	2,385 m.
Min.	34 m.
Max.	17,401 m.

Finally, to summarise, considering that 75% of the routes are below 2,385 m, we can state that the length of most of the routes clearly does not represent the traffic in this city considering its size. To sum up, it has been demonstrated that DFROUTER has an issue with the length of the routes when generating them in the context of a city.

5.3 Proposed Solution

In traffic simulators, there is a constant problem when trying to generate representative traffic for a city based on data from induction loops. As detailed in the previous section, the problem is generated by DFROUTER. Specifically, DFROUTER faces two main problems when generating traffic within a city; (i) the amount of traffic injected is excessive, and (ii) the length of the routes remains too short. In this section, we detail how to solve these issues by proposing a novel traffic route generator using the library of SUMO, sumolib [129]. Since DFROUTER generates the routes, along with the traffic distribution in time and space, we divide our algorithm in 4 parts for the sake of clarity. These are: (i) data collection and curation, (ii) routing core, (iii) data expansion, and (iv) time distribution. In addition, we will explain how data is prepared in order to apply our algorithm effectively. The complete workflow of the proposed solution can be observed in Figure 5.6.

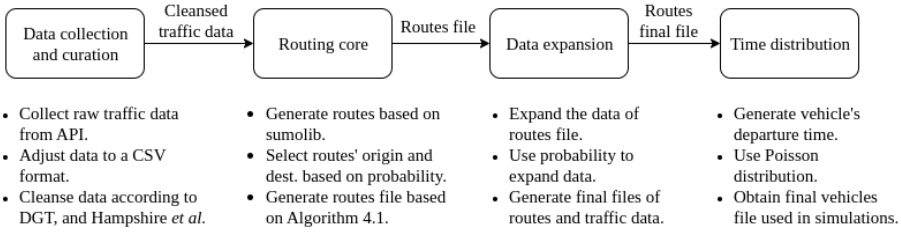

Figure 5.6: Workflow of the proposed solution.

5.3.1 Data Collection and Curation

As we discussed previously in section 5.1, we start by gathering data from the Valencia City Council through a public API [63]. Then, based on our study, we focus on the data from the year 2022 obtained from the 720 induction loops in the city between 8am and 9am on an ordinary Monday. To clarify, all sensors are of the same type, and were deployed in different sections of the main streets and avenues of the city. Afterwards, we converted the data from a JSON file to a CSV file in order to better deal with such data.

Secondly, we add to the CSV: (i) the ID of the street, based on the information provided by OpenStreetMap [130], (ii) the district code where the detector is placed, and (iii) the population of each district based on the information gathered from the City Hall. Then, since data is split into 5-minute slots, we combine all the data for the same induction loop to be more efficient. Having done that, the CSV columns will resemble the structure presented in Table 5.3. The "ATA" column corresponds to the ID of the induction loop as provided by the City Hall, and it adopts a string format. The "n_vehicles" column is the aggregated number of vehicles that pass over the induction loop between 8 and 9 am. Then, the "way_id" column correspond to the associated ID of the way(s) for the induction loop. Finally, the district_code and population columns correspond to the district and population of the district on where the detector is placed.

Thirdly, we cleansed the data based on two main factors: the number of passenger cars, and the number of vehicles cruising to find a parking spot.

Concerning the first one, we have obtained the number of passenger cars for Valencia from the Spanish Department of Traffic (DGT) (*Dirección General de Tráfico*) on their 2022 annual table statistics [131]. According to this, the number of passenger cars is 72% of the total. So, because our goal is to analyse the routes of passenger cars in particular, we reduce the number of vehicles corresponding to each induction loop by 28%.

Table 5.3: CSV columns structure

ATA	n_vehicles	way_id	district_code	population
1	65	429492850	18	14546
1001	1408	770904161	4	39164
1003	131	13945413	4	39164
...	...	...	...	...

Regarding the second one, the number of passenger cars cruising for parking is 15%. This value is estimated according to Hampshire *et al.* [132], considering that in Stuttgart (207.4 km^2, and 634,830 inhabitants), a city similar to Valencia (134.6 km^2, and 791,413 inhabitants), that is the percentage of vehicles cruising for parking. Since we only want vehicles that do a specific route instead of a cruise for parking, we now subtract a 15% from the 72% of the previous step. To sum up, we have reduced the data of the vehicles that pass through the induction loop by 38.8% so as to achieve more representative route data in terms of traffic that actually requires management and/or improvement.

Finally, with the use of NETCONVERT [120], we add the edges (ID of the road given by SUMO) and their associated nodes, and the nodes with their associated coordinates in a database. Likewise, we include in the database the cleansed data of the CSV, in order to have all the parameters in the same file.

At the conclusion of this process, we have the necessary data to operate the "Routing core" part.

5.3.2 Routing Core

Having obtained the required data by following the procedures detailed above, we now proceed to describe the core part of our solution. As stated above, the route generator of our routing algorithm will be the sumolib package. In particular, the function getOptimalPath() from the Net class. This is a function that finds the optimal (shortest or fastest) path from source edge to destination edge by using Dijkstra's algorithm. Afterwards, along with sumolib, our implementation consists of the combination of various steps. These can be observed in Algorithm 5.1, and with them, it will be able to generate more representative routes.

As can be seen in Algorithm 5.1, the inputs consist on: (i) the edges of SUMO and their relation to nodes; (ii) the nodes and their relation to coordinates; and (iii) the traffic data provided by the induction loops. Furthermore, the outputs are two CSV files: one with the routes created, and the other one with the updated traffic data. The idea of the algorithm is to iteratively obtain the routes, selecting the

Algorithm 5.1: Proposed routing algorithm.

Input: Edges, Nodes, Traffic data
Output: CSV with routes, CSV with updated traffic data

$\boldsymbol{d} \leftarrow$ Num. of detectors, $\boldsymbol{\beta} \leftarrow$ reduction coefficient;
$\boldsymbol{n} \leftarrow$ Num. of vehicles for a detector, $\sum_{\boldsymbol{i=1}}^{\boldsymbol{d}} \boldsymbol{n_i} \leftarrow$ Total num. of vehicles;
$\boldsymbol{\delta_{o,des,mid}} \leftarrow$ tolerated error for origin, destination and intermediate point;
$endCondition \leftarrow (\sum_{\boldsymbol{i=1}}^{\boldsymbol{d}} \boldsymbol{n_i}) \times (\boldsymbol{1-\beta})$, $currentVehicles \leftarrow$ Current $\sum_{\boldsymbol{i=1}}^{\boldsymbol{d}} \boldsymbol{n_i}$;
$routesGenerated \leftarrow 0$;
$SUMORt$, $NodesRt \leftarrow \{\}$;
Filter suitable edges;
Interpolate Traffic data;
while $currentVehicles \geq endCondition$ **do**
    $originPoint$ = getMostProbablePoint(Interpolated traffic data);
    Filter possible destination points → min. distance 1,25km;
    $destinationPoint$ = getMostProbablePoint(Filtered interpolated traffic data);
    $SUMORoute$ = getOptimalPath($originPoint$, $destinationPoint$);
    $NodesRoute$ = SUMOtoNodesFormat($SUMORoute$);
    $ATAList \leftarrow \{\}$;
    if $\boldsymbol{n_o \leq \delta_o}$ ***and*** $\boldsymbol{n_{des} \leq \delta_{des}}$ **then**
        Add origin and destination ATA to $ATAList$;
        for $node$ ***in*** $NodesRoute$ **do**
            ATA = getATAFromNode($node$);
            if $\boldsymbol{n_{mid} \leq \delta_{mid}}$ **then**
                Add the ATA to $ATAList$ if is not present yet;
                if $node == lastNode$ **then**
                    Update $currentVehicles \leftarrow$ Decrease n by 1 for each detector present in the $ATAList$;
                    AddRouteToCorresponding Set($SUMORoute$,$NodesRoute$);
                    if $routesGenerated$ % 1000 == 0 **then**
                        Interpolate Traffic data;
                    end
                end
            else
                break;
            end
        end
    end
end
CSV with routes ← generateCSV($SUMORt$,$NodesRt$) ;
Return (CSV with routes, CSV with updated traffic data);

origin and destination based on the number of vehicles that pass over the induction loops.

We now proceed to explain in detail the four key parts of our algorithm. Firstly, in lines 7 and 8, we prepare the data to adjust it to our needs. In particular, in line 7 we filter the edges in order to get only the suitable ones. The condition to be suitable is that the edge must be a secondary, tertiary, or residential street, and its length must be greater than 50 meters. This way we can ensure that no route will start in the middle of an intersection or roundabout, nor on a primary or highway road where no parking is available. In line 8, we interpolate the input traffic data to get more points from where the routes can start or finish. In this way, we can have a better granularity rather than using only the detector's location as source or destination.

Secondly, the loop condition present on line 9. This condition is fundamental because the algorithm iterates up to a certain value, which affects the accuracy of the results. This is because the process of obtaining routes is costly in terms of execution time because, by placing constraints on the allowed error, the difficulty of obtaining a route gradually increases. Therefore, we have chosen to obtain the routes for a percentage of the vehicles through the use of a reduction factor β. These routes will be expanded in the next module "Data expansion". If we now analyse the values of the condition, these are: the total number of vehicles that pass over the induction loops, and a reduction factor β. This reduction factor will be $0 \leq \beta \leq 1$. As an example, if we want to iterate over 50% of the data, β needs to be 0.50. It is important to mention that the $\sum_{i=1}^{d} n_i$ on the left on the condition decreases according to line 23, while the $\sum_{i=1}^{d} n_i$ on the right is a copy, and remains unchanged.

Thirdly, the block between lines 10 and 14 includes two main functions: one that gets the most probable point, and one that retrieves the route from sumolib's function *getOptimalPath()*. Regarding the first one, it works in a way where an interpolated point is selected based on the number of vehicles associated with it, and the number of people living in its associated district. Then, its associated edge is selected, in order to obtain the specific source edge of the route. This mechanism is applied to select origin and destination points, which results in a more accurate and comprehensive estimation. The only difference between them is that the destination point must be at least 1.25 km away in a straight line from the origin point. In this sense, this minimum distance seems reasonable because it corresponds to a 15-minute walk, or a 6-minute trip by bike. With regard to the second function, it calls the *getOptimalPath()* function to obtain the route path in the SUMO format. This route covers the streets without induction loops because sumolib adopts the full map to create paths, and not only the streets with

induction loop detectors. Since routes are long and traverse many points of the city, roads without induction loops are mainly covered. At the end, this route is converted into a sequence of nodes. This is done in order to be able to run the next part of this algorithm.

Finally, with regard to the rest of the lines, notice that the conditions present on lines 16 and 20, and the update step on line 23, are critical. With respect to the condition on line 16, the tolerated error $\delta_{o,des}$ is the ratio of vehicles exceeded (compared to the reference value), which we do not want to surpass to avoid high error values. Specifically, for the origin and destination points, the tolerated error is 0, and so the counter of that detector must not be less than 0. On the contrary, the δ_{mid} in the condition shown on line 20 must not exceed a certain percentage of the initial value of the detector. This percentage will vary depending on the chosen β value. This is because, when a higher β is chosen, the execution time will be longer, and so a very restrictive δ_{mid} will be counterproductive. Regarding line 23, this is where we update the data in order to be able to execute the algorithm correctly. In particular, we subtract 1 from the counter of each induction loop present in the route. This will lead to the variation of $currentVehicles$, and, consequently, to the variation of the selected origin and destination points. This is because, as we have already mentioned, both points are selected based on probability, and the change in the number of vehicles will modify this probability. To conclude, each time 1,000 routes are generated, the updated traffic data is interpolated to obtain a newer version of the interpolated traffic data.

5.3.3 Data Expansion

In the previous subsection, we discussed that the total amount of vehicles is not generated by our solution due to an excessive execution time. This is the reason why we need to implement another algorithm that expands the generated data so that a reduced dataset can mimic the results of the full dataset. This process is accomplished by Algorithm 5.2.

As can be seen, the algorithm is mainly based on the variance (σ^2) and mean (μ) values, for both real traffic data and the generated traffic data in Algorithm 5.1. The algorithm begins with an iteration that satisfies the condition $\frac{\mu_{gen.}}{\mu_{real}} < 1.1$. This is in order to ensure that the ratio between both means is acceptable (just a 10% higher) to generate representative data. Then, the rate between both σ^2_{real} and $\sigma^2_{gen.}$ must be less than 1, in order to generate a more accurate result. Afterwards, if the condition is satisfied, it will choose a route from the *Generated routes file* with probability p_{route}. Then, it updates by adding 1 to the values corresponding to those detectors present in the route. Finally, since detector data are changed, a recalculation of $\sigma^2_{gen.}$ and $\mu_{gen.}$ is needed.

Algorithm 5.2: Data expansion algorithm.

Input: Real traffic data, Generated traffic data, CSV routes file
Output: CSV with all the routes, CSV with the total traffic data

$\boldsymbol{\sigma}^2_{real,gen.} \leftarrow$ Variance of real traffic and generated traffic;
$\boldsymbol{\mu}_{real,gen.} \leftarrow$ Mean of real traffic and generated traffic;
$\boldsymbol{n} \leftarrow$ Detector count;
$\boldsymbol{p_{route}} \leftarrow$ Probability to choose a route;
RoutesCopy $\leftarrow$ copy of the data in the CSV routes file;
while $\frac{\mu_{gen.}}{\mu_{real}} < 1.1$ **do**
    if ***not*** $\frac{\sigma^2_{gen.}}{\sigma^2_{real}} > 1$ **then**
        Choose a route based on $\boldsymbol{p_{route}}$;
        Add the route to *RoutesCopy*;
        Update generated traffic data $\leftarrow +1$ to all $\boldsymbol{n}$ present in the route;
        Recalculate $\boldsymbol{\mu}_{gen.}$ and $\boldsymbol{\sigma}^2_{gen.}$;
    else
        Generate CSV $\leftarrow$ *RoutesCopy*;
        Generate CSV with the total generated traffic data;
        break;
    end
end
Return (CSV with all the routes, CSV with the total traffic data);

On the contrary, if the variance condition is not satisfied, it means that the iteration process needs to stop. Before this, the algorithm will generate the output CSV including all the routes generated, and the traffic data generated.

5.3.4 Time Distribution

In order to have the same outputs as DFROUTER we need to create a vehicles file. Specifically, what differentiates this file from the route file generated in Algorithm 5.2 is that our routes (from now on referred to as vehicles) have no depart time. These vehicles are generated by counting the number of routes and the number of repetitions of each of them. The number of repetitions will be the number of vehicles that travel through the route. Therefore, we generate all the routes, and then we count the number of repetitions of each route to assign the number of vehicles that travel through that route. Having made this clear, in order to satisfy the DFROUTER requirement, we need to assign to all vehicles a specific departure

time. This is done by applying a Poisson Distribution for the vehicles that take the same route. The complete behaviour of this function can be observed in Algorithm 5.3.

Algorithm 5.3: Time distribution algorithm.

Input: CSV with all the routes
Output: CSV with vehicles traffic information
$\boldsymbol{T} \leftarrow$ simulation period;
$\boldsymbol{\lambda_{route}} \leftarrow$ mean number of vehicles for a certain route during T;
Routes $\leftarrow$ New set with routes ID and num. of vehicles associated to it;
for $route, vehicles_{route}$ ***in*** *Routes* **do**
    $A \leftarrow$ Empty set of size T;
    $\frac{vehicles_{route}}{T} \leftarrow$ Calculate $\boldsymbol{\lambda}_{route}$;
    for k=0:T **do**
        Draw a sample from $P(x = k) = \frac{e^{-\lambda_{route}} \lambda_{route}^{k}}{k!}$ and add it to A;
    end
    for *element* ***in*** A **do**
        if *element* != 0 **then**
            Add vehicle to the CSV vehicles file;
        end
    end
end
Generate CSV with vehicles traffic information;
Optimise for simulation the CSV with vehicles traffic information;
Return (CSV with vehicles traffic information);

As stated above, the key functionality of the algorithm is the use of the Poisson Distribution Function. We have chosen Poisson, and not Gaussian or other alternatives, since Poisson processes are widely accepted as being adequate for generating the number of vehicles passing through a given route segment during a specific time interval [133, 134, 135]. Regarding the algorithm structure, we can observe that it iterates over the routes and vehicles per route. Then, in order to be able to draw samples from the Poisson distribution, an empty set of size T is created for each route. At the same time, the λ_{route} is calculated. Afterwards, we draw a sample from the execution of the Poisson Distribution Function, and add it to A at position k. This position refers to the simulation time at which the vehicle will depart. Then, we add each vehicle in a particular route to the CSV file of vehicles' traffic information and, once the iteration over all the routes is completed,

we generate the CSV. To conclude, and to avoid future simulation warm-up issues, we optimise it and return the result.

Algorithm 5.4: Optimisation of vehicle departure time.

Input: CSV with vehicles traffic information
Output: CSV with vehicles traffic information optimised

$\boldsymbol{\sigma_{veh}} \leftarrow$ Standard deviation of vehicles per second;
$\boldsymbol{\mu_{veh}} \leftarrow$ Mean of vehicles per second;
$\boldsymbol{\epsilon} \leftarrow$ Value that changes depending on the method used;
$\boldsymbol{\mu_{duration}} \leftarrow$ Mean of vehicles trip duration;
$\boldsymbol{\Gamma(\mu_{veh}, \epsilon)} \leftarrow$ Optimisation function;
$Vehicles \leftarrow$ Set of vehicles traffic information from the CSV;
$vehicleCounter$, $departureTime \rightarrow 0$;
for *vehicle* ***in*** $Vehicles$ ***where*** $vehicle_{departTime} \geq \boldsymbol{\mu_{duration}}$ **do**
    if $vehicle_{departTime} \neq departureTime$ **then**
        $vehicle_{departTime} = vehicle_{departTime}$ - $\boldsymbol{\mu_{duration}}$;
        $vehicleCounter = 1$;
    else
        if ***not*** $vehicleCounter \geq \boldsymbol{\Gamma(\mu_{veh}, \epsilon)}$ **then**
            $vehicle_{departTime} = vehicle_{departTime}$ - $\boldsymbol{\mu_{duration}}$;
            $vehicleCounter = vehicleCounter + 1$;
        end
    end
end
Return (CSV with vehicles traffic information optimised);

Elaborating on the optimisation algorithm (see Algorithm 5.4), this consists of an iteration over the CSV file containing vehicles' traffic information. The iteration starts over the last vehicle with a departure time equal to or greater than the $\boldsymbol{\mu_{duration}}$. Afterwards, the departure time of a certain number of vehicles is updated. This number is calculated by an optimisation function $\boldsymbol{\Gamma(\mu_{veh}, \epsilon)}$ which is established before running the iteration. This function is described as:

$$\boldsymbol{\Gamma(\mu_{veh}, \epsilon)} = \boldsymbol{\mu_{veh}} + \boldsymbol{\epsilon} \tag{5.1}$$

where $\boldsymbol{\epsilon}$ can be equal to 0, $\boldsymbol{\sigma_{veh}}$, -$\boldsymbol{\sigma_{veh}}$, or a random integer in the range {-$\boldsymbol{\sigma_{veh}}$,$\boldsymbol{\sigma_{veh}}$}. Finally, it returns the optimised CSV with the vehicles' traffic information.

5.4 Validation and Comparison Against DFROUTER

Having analysed the details of our proposed solution, we will now detail how the experiments used to validate our proposal were defined, and which performance metrics have been used. Afterwards, we discuss the quality of our solution by analysing the results for each experiment.

It is important to mention that all experiments have been done using as reference the data from the induction loops, and comparing the results using either the traffic demand produced by DFROUTER, or our traffic demand generated through the combination of Algorithms 5.1, 5.2, and 5.3. Likewise, the hardware used for these experiments consists of a PC with an Intel i7-12700 3.6 GHz CPU, 32 GB DDR4 2400 MHz RAM, and an M.2 SSD storage with a reading speed of 3300 MB/s, and a writing speed of 1200 MB/s.

5.4.1 Tuning Our Algorithm

To adequately tune our algorithm we first need to select an optimal β that achieves an acceptable performance in terms of Mean Squared Error (MSE), while avoiding excessive execution times when compared to other solutions.

In particular, we have tested different reduction factors to find the one offering the best trade-off: $\beta = \{0.01; 0.05; 0.10; 0.15; 0.20; 0.25;$
$0.30; 0.35; 0.40; 0.45; 0.50; 0.60; 0.75\}$. In the same way, the intermediate tolerated error used (normalised value) is $\boldsymbol{\delta_{mid}} = 1.1$, and so the value for each detector cannot exceed 10% of its reference value. Having this in mind, we will divide our experiments into two groups: the traffic distribution analysis along with the algorithm validation, and the characterisation of generated routes in terms of quality and representativeness.

In order to show the different trade-offs between our proposed solution and DFROUTER, we calculate the MSE with respect to the real data using the following equation:

$$\mathrm{MSE}(y, \hat{y}) = \frac{1}{n_{\text{detectors}}} \sum_{i=0}^{n_{\text{detectors}}-1} (y_i - \hat{y}_i)^2 \tag{5.2}$$

where:

$$n_{\text{detectors}} = \text{Total num. of detectors}$$

$$y_i = \text{num. of vehicles that pass over a detector}$$

$$\hat{y}_i = \text{num. of vehicles that pass over a detector for some } \beta$$

We do it for our solution when adopting different β values, and also for DFROUTER. Likewise, we calculate the number of unique routes and the execution

time for our solution (again varying the β value), and for DFROUTER. Finally, an analysis of the trade-off between MSE, number of unique routes, and execution time, is presented to show how much the MSE drops when increasing the execution time and the number of unique routes.

Table 5.4 shows the behaviour of the MSE when increasing β. As we can observe, there is a decreasing tendency when β is higher, but, for all the β values, the MSE obtained is nearly 50 times lower than the one obtained by DFROUTER. Due to this, none of these β values are ruled out yet. In particular, we can observe that the relative difference between $\beta = 0.01$, and $\beta = 0.75$ is of about 10%. This is not a great difference when compared to the DFROUTER values, so all reduction factors are still considered when targeting the optimal solution.

Table 5.4: MSE values for different reduction factors and DFROUTER.

Reduction Factor (β)	**MSE**
DFROUTER	19,058,648
0.01	399,329
0.05	381,701
0.10	368113
0.15	370,985
0.20	364,145
0.25	364,472
0.30	365,609
0.35	363,815
0.40	363,435
0.45	361,895
0.50	360,811
0.60	359,644
0.75	358,326

Regarding the performance in terms of execution time when increasing β, Table 5.5 shows that such time increases by a factor of 2 on average. In particular, we can observe that the difference in the amount of time from $\beta = 0.01$ to $\beta = 0.60$ is limited to 2 hours, while for $\beta = 0.75$ it increases by 2 hours more, having an

executing time of more than 4 hours. Moreover, more than half of the values achieved for our solution are higher than those for DFROUTER. This is because of the complexity of Algorithm 5.1, and our restrictive $\boldsymbol{\delta_{mid}}$ parameter.

Table 5.5: Execution time for different reduction factors and DFROUTER.

Reduction Factor (β)	**Execution Time (minutes)**
DFROUTER	23.31
0.01	0.37
0.05	1.41
0.10	3.09
0.15	5.40
0.20	10.01
0.25	18.35
0.30	26.48
0.35	37.12
0.40	52.09
0.45	67.07
0.50	85.68
0.60	139.57
0.75	253.72

When analysing the reduction factors we also need to consider the number of unique routes that are going to be repeated with the "Data expansion" algorithm (see algorithm 5.2). In this sense, we can observe that all values are lower than for DFROUTER. Among these values, we can discard the β values less than 0.20. This is because the amount of unique routes for $\beta = 0.20$ is more than half when compared to $\beta = 0.35$, and almost 3 times less when compared to $\beta = 0.50$. Likewise, we can observe that, as β increases by 0.05, the number of unique routes increases by 1,000.

In Table 5.7 we combine the results of the previous tables to observe the general performance of our solution compared to DFROUTER. It shows that there is a correlation between MSE, execution time, unique routes, and β; so, when β becomes higher, the execution time and number of unique routes are higher, but the MSE becomes lower. Thus, we need to select an optimal β that achieves an acceptable performance in terms of MSE, while avoiding excessive execution times when compared to other solutions, and avoiding a low number of unique routes. In this case, the β value we select for the experiments that follow is 0.50, because it

Table 5.6: Number of unique routes for different reduction factors and DFROUTER.

Reduction Factor (β)	**Unique routes**
DFROUTER	64,200
0.01	213
0.05	1,142
0.10	2,394
0.15	3,811
0.20	5,625
0.25	7,342
0.30	8,744
0.35	10,127
0.40	11,544
0.45	12,880
0.50	14,149
0.60	16,664
0.75	20,329

returns the highest number of unique routes, while maintaining the execution time in less than an hour and a half.

Having identified the β value with the best trade-off, we proceed to analyse the behaviour of our solution in SUMO over a simulation period of 60 minutes. To this end, we compare the use of various methods. "Default" refers to the unoptimised vehicle traffic information file generated in Algorithm 5.3. "$\boldsymbol{\epsilon} = \{\boldsymbol{\sigma_{veh}}$, -$\boldsymbol{\sigma_{veh}}$, 0, and $\boldsymbol{\epsilon}$ in {-$\boldsymbol{\sigma_{veh}}$,+$\boldsymbol{\sigma_{veh}}$}}" refer to the optimised solution (see Algorithm 5.4).

As can be observed in Figure 5.7, the unoptimised solution (Default), performs badly in terms of the number of vehicles during simulation. This is because it never reaches a steady state, and the number of vehicles keeps rising over time. Likewise, when compared to the other solutions, we notice that there are warm-up issues. While the other methods are able to achieve peak values after roughly 9.5 minutes, the "Default" procedure reaches a similar value only at the end of simulation time. Regarding optimised solutions, we observe that all methods reach the peak after 9.5 minutes. Furthermore, we observe that the steady-state lasts for a period of 40 minutes for all optimised methods. In addition, $\boldsymbol{\epsilon} = \boldsymbol{\sigma_{veh}}$; $\boldsymbol{\epsilon} = 0$; and $\boldsymbol{\epsilon} = \boldsymbol{\epsilon}$ in $\{-\boldsymbol{\sigma_{veh}}, +\boldsymbol{\sigma_{veh}}\}$ achieve a similar performance, being the number of vehicles stable, while $\boldsymbol{\epsilon} = -\boldsymbol{\sigma_{veh}}$ rises the number of vehicles over time. Finally, all optimised methods enter the terminating state at time $t = 50$ minutes, beyond which the number of vehicles decreases substantially.

Table 5.7: Trade-off between MSE and execution time.

β	**MSE**	**Exec. Time (min.)**	**Unique routes**
DFROUTER	19,058,648	23.31	64,200
0.01	399,329	0.38	213
0.05	381,701	1.41	1,142
0.10	368,114	3.10	2,394
0.15	370,985	5.41	3,811
0.20	364,146	10.02	5,625
0.25	364,473	18.36	7,342
0.30	365,610	26.49	8,744
0.35	363,816	37.12	10,127
0.40	363,435	52.09	11,544
0.45	361,895	67.08	12,880
0.50	360,812	85.69	14,149
0.60	359,644	139.58	16,664
0.75	358,326	253.72	20,329

To determine which of the methods is the most stable one during the steady-state period, we analysed the distribution of the number of vehicles during that period. Figure 5.8 shows that when $\boldsymbol{\epsilon}$ is $\boldsymbol{\sigma_{veh}}$, 0, and $\boldsymbol{\epsilon}$ in $\{-\boldsymbol{\sigma_{veh}}, +\boldsymbol{\sigma_{veh}}\}$, the number of vehicles are the more stable, while "Default" and $\boldsymbol{\epsilon} = -\boldsymbol{\sigma_{veh}}$ are not, being "Default" the least. In particular, we can see that $\boldsymbol{\epsilon} = \boldsymbol{\sigma_{veh}}$ has the smallest difference in the distribution. Therefore, we conclude that this is the best solution.

5.4.2 Traffic Distribution Analysis and Algorithm Validation

Having selected the best β value, we now proceed by observing in Figure 5.9 the ECDF that characterises our solution, along with the distribution for DFROUTER, and the induction loop data used as reference. As mentioned in Section 5.2, DFROUTER has a maximum value of 17k vehicles, and it behaves like a linear function with a big slop line until 650, a value beyond which it starts to make a parable. On the contrary, the function for our solution is very similar to the one for real data. Both behave with a similar linear function, with a slight parable close to 700, and only differ in the maximum value (2,7k for real data, and 1,4k for our solution).

Data present in Table 5.8 and Table 5.9 complement the ECDF shown in

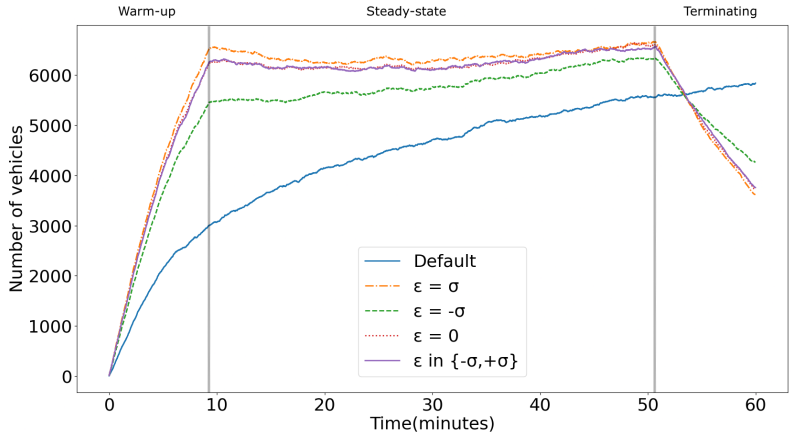

Figure 5.7: Vehicles present during simulation time using different methods.

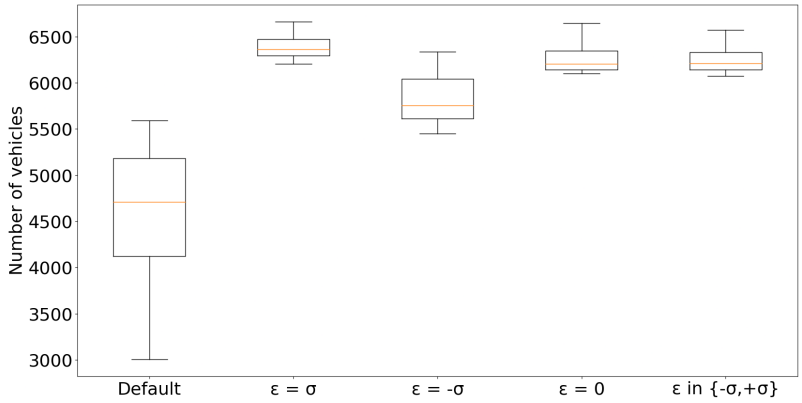

Figure 5.8: Distribution of the number of vehicles during steady-state.

Figure 5.9 by providing further details so as to gain greater insight. As we did earlier in Section 5.2, we present different statistical metrics that provide a complete overview of the differences between the real data, DFROUTER, and our proposed solution.

On one hand, in Table 5.8 we can see that, on average, our solution introduces an average decrease of 47% when compared to real data. Regarding minimum

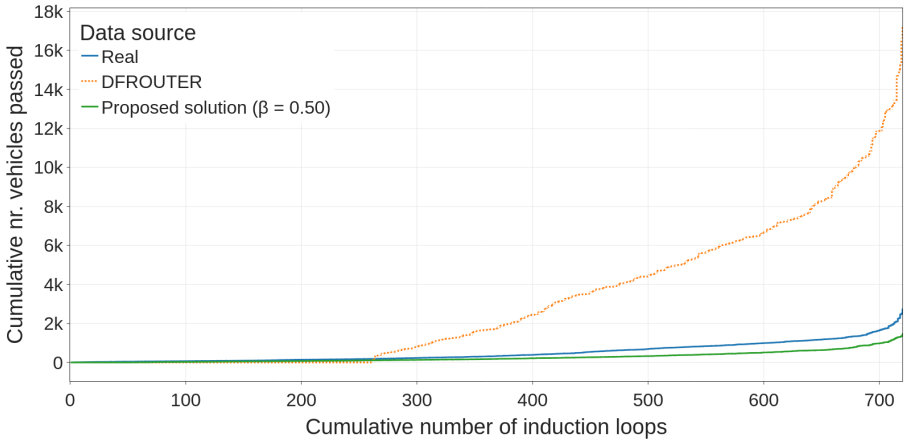

Figure 5.9: ECDF of induction loop real, DFROUTER and our solution ($\beta = 0.50$) data.

values, we observe that our solution has a minimum value of 0. This occurs when our algorithm estimates that no vehicles will pass through a given induction loop, but instead, for the actual data, we have vehicles passing over it. On the contrary, we obtain a maximum difference compared to real data of -47%, in this case for the maximum value detected. Notice that such value becomes possible despite the fact we introduce limits to the error in Algorithm 5.1, since Algorithm 5.2 does not consider this particular type of error.

On the other hand, Table 5.9 shows the relative difference for the induction loops statistics with respect to our solution, and DFROUTER. Specifically, it can be observed that, on average, we outperform DFROUTER by a 469%. Likewise, regarding standard deviation, our solution only differs from real data by 43%, outperforming DFROUTER by 689% As we can see, there is a common trend for both, and a notable difference exists in all the statistic values compared. To conclude, by observing this, we can determine that our solution provides a better fit.

As a last step, we now proceed to visualise the traffic distribution according to the induction loop data. To this end, we present three different heatmaps, as shown in Figure 5.10. In particular, three subfigures are presented (see Figure a, Figure b, Figure c), one for each dataset: real values (reference), DFROUTER, and our solution. We can observe that our solution is a better match to the real distribution than DFROUTER. This can be seen by noticing the concentration of

Table 5.8: Induction loop data difference stats (Real vs Proposed Solution).

	Real	Proposed Solution	Abs. Diff.	Rel. Diff.
Avg.	504	268	-236	-47%
Std. Dev.	481	272	-209	-43%
Q1	125	65	-60	-48%
Q2	313	174	-139	-44%
Q3	815	394	-421	-52%
Min.	4	0	-4	N.A.
Max.	2,728	1,457	-1,271	-47%

Table 5.9: Induction loop data difference stats (DFROUTER vs Proposed Solution).

	DFROUTER w.r.t. real	Proposed Solution w.r.t. real
Avg.	+516%	-47%
Std. Dev.	+732%	-43%
Q1	N.A.	-48%
Q2	+314%	-44%
Q3	+554%	-52%
Min.	N.A.	N.A.
Max.	+530%	-47%

vehicles that pass over the induction loop at the edges of the city for our solution (and the reference map), while for DFROUTER a much higher maximum value for detectors in reached, reason why most of the map is red.

5.4.3 Routes Characterisation

As we discussed previously in Section 5.2, one of the problems associated with DFROUTER, in the context of a city, is the length of the generated routes. This is the reason why we analyse different statistics for the selected β versus the DFROUTER solution. Specifically, we analyse the mean value, the standard deviation, and the maximum and minimum values associated to the route length.

As we can observe, Table 5.10 shows in detail the routes' characterisation in terms of length for both approaches. In particular, the minimum and maximum

values achieved by our proposal are 1,251 m and 25,602 m, respectively. In contrast, as seen earlier in Section 5.2, minimum and maximum values for DFROUTER are 734 m and 17,401 m. In this regard, our solution outperforms DFROUTER by 3,581% and 47%, respectively. In fact, it is very important that our minimum route value has such a length because that is one of the main disadvantages of DFROUTER. It does not seem realistic that a vehicle is going to travel a route of 34 m, or even 500 m, in a city like Valencia, where finding a parking stop is quite problematic, and where several areas have parking restrictions, requiring citizens to park far away so as to promote public & green transportation (bikes, electric scooters, etc.). Regarding quartiles, we observe that our solution improves DFROUTER by 63%, being half of our routes longer than 3,656 m, while for DFROUTER this value is at 1,897 m. Our solution achieves a route length of 4,672 m on average, while DFROUTER stays at 2,035 m; hence, our improvement is 78%.

Table 5.10: Route length statistics (DFROUTER vs. Proposed solution).

Metrics	**DFROUTER**	**Prop. Sol.**	**Abs. Diff.**	**Rel. Diff.**
Unique routes	64,200	14,149		
Avg.	2,035 m	4,672 m	+2,637 m	+78%
Std. Dev.	1,068 m	3,123 m	+2,055 m	+98%
Q1	1,448 m	2,434 m	+986 m	+50%
Q2	1,897 m	3,656 m	+1,759 m	+63%
Q3	2,385 m	5,871 m	+3,486 m	+84%
Min.	34 m	1,251 m	+1,217 m	+3,581%
Max.	17,401 m	25,602 m	+8,201 m	+47%

With respect to the distribution of the origin of the routes, Figure 5.11 shows the distribution of the vehicles for DFROUTER and our solution. In particular, this distribution is for two specific consecutive avenues (inside the red lines): *Gran Vía Marqués del Turia*, and *Gran Vía de Ramón y Cajal*. As it can be seen, our solution achieves a better spatial distribution of route origin points than DFROUTER. Specifically, while DFROUTER only has 17 points along these avenues, our solution multiplies by more than 5 such results, having 88 points.

To conclude, Figure 5.12 displays 10 random sample routes of each approach. Through this geographical example, we can better understand the data previously presented in Table 5.10. As shown, DFROUTER generates routes with a small length. In this case, these routes are distributed through various parts of the

city, but their length is too short for them to be representative. On the contrary, having a closer look at the routes of our solution, we observe that their length is significantly longer. More importantly, all of our routes are representative, since they represent a significant distance being covered in the city, and it seemed more natural and adequate for someone to actually use their car to take these routes.

5.5 Summary

In this chapter, we have made clear that the process of generating representative traffic demand is not a simple task. In particular, we have analysed the generation of this demand with the data from induction loops. For this purpose, we have assessed a widely adopted tool, DFROUTER. With it, we have demonstrated that the data obtained in terms of traffic volume and route length is not representative of the case of a city.

For this reason, we have proposed a novel approach to perform reverse engineering by generating traffic demand based on induction loop data in the context of a city. Specifically, we have demonstrated that our solution improves DFROUTER in various aspects.

Firstly, we have achieved an improvement in terms of traffic volume. In particular, DFROUTER had 516% more traffic (on average) than the real measured values that were used as reference. With our solution, we were able to reduce that percentage by 469%, only introducing an average decrease of 47% compared to the real data. Likewise, the MSE obtained for the selected reduction factor has improved the MSE of DFROUTER by 50 times.

Secondly, a better spatial distribution of the origin points of the routes has been obtained. In particular, we have discussed an example of a representative street. In this case, we have obtained 418% more origin points than DFROUTER. So, with our solution, we are able to achieve a much better distribution for the actual departure areas.

Finally, we have obtained larger routes than those generated by DFROUTER. In particular, we have increased the average length of the routes by 78%. This means that, with our solution, we are able to obtain routes with an average length of 4,672 m, while with DFROUTER it remains at 2,035 m.

To sum up, we have demonstrated in this paper that our solution outperforms DFROUTER in three key aspects: traffic volume, route spatial distribution, and route length, providing more realistic and accurate values for further experimentation and traffic analysis.

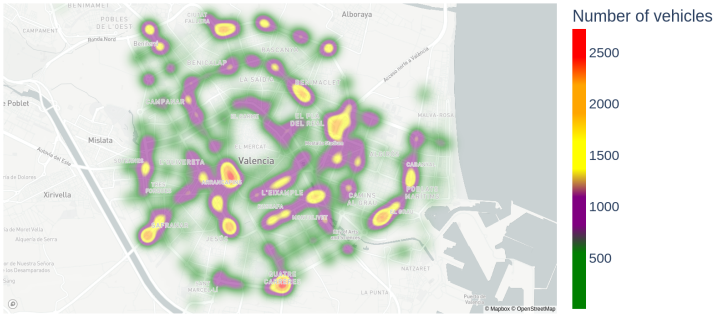

(a) Real data.

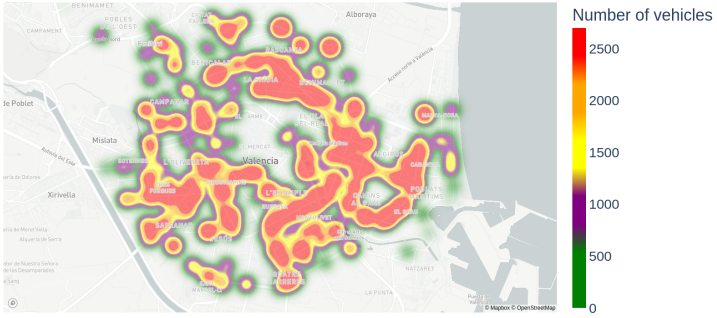

(b) DFROUTER.

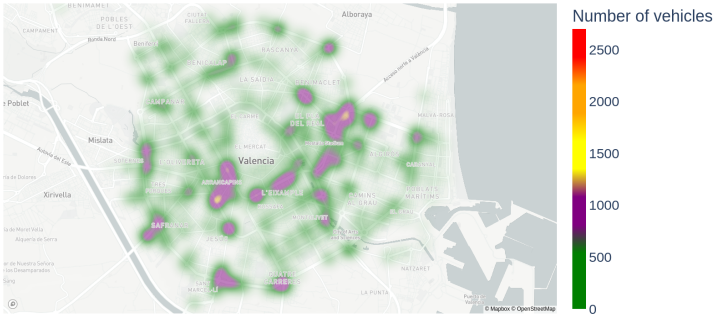

(c) Proposed solution.

Figure 5.10: Heatmap of the induction loop data distribution.

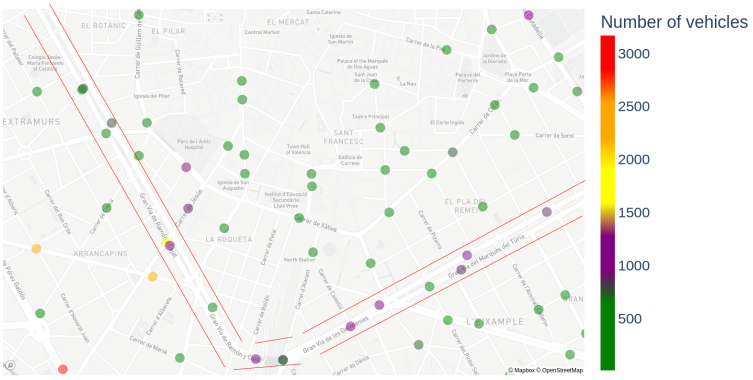

(a) DFROUTER

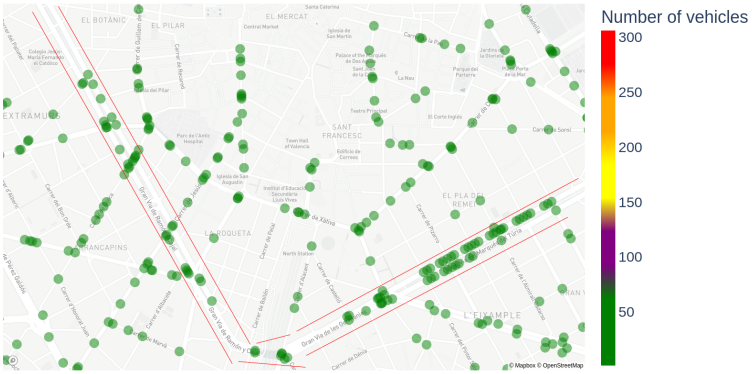

(b) Proposed solution

Figure 5.11: Route origin points distribution for two selected roads (*Gran Vía Marqués del Turia*, and *Gran Vía de Ramón y Cajal*).

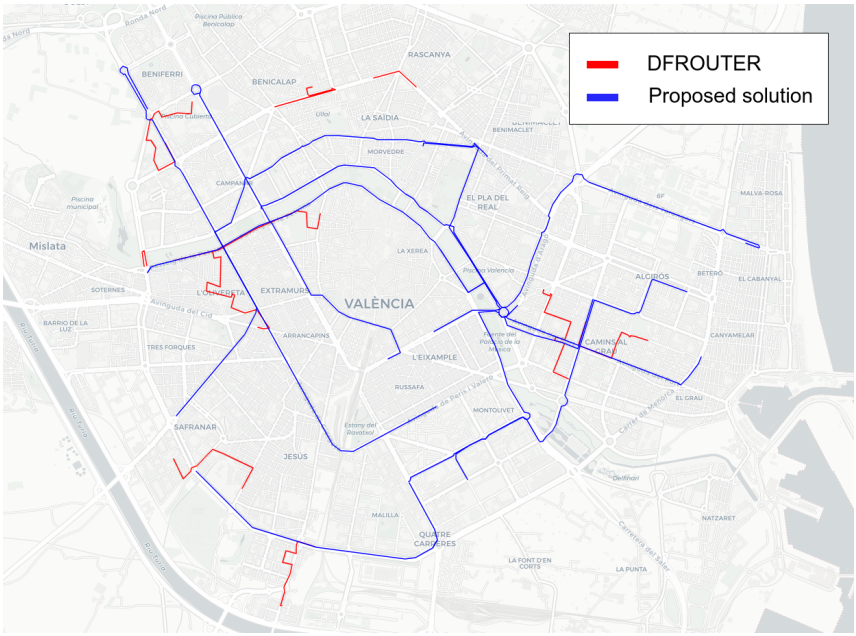

Figure 5.12: Length of 10 sample routes (DFROUTER vs. Proposed solution).

Chapter 6

Traffic Re-routing Based on Air Pollution: a Static Approach

In the previous chapter we discussed the challenges of generating accurate traffic demand using induction loop detectors and other methods to represent real-world traffic patterns. We highlighted the limitations of existing approaches, and we introduced a new method to address these issues. Building upon this, the current chapter focuses on managing and optimising traffic flow to reduce environmental impact, specifically air pollution in urban areas. Instead of traditional traffic management practices, such as closing streets or altering routes based on administrative decisions, our approach uses a static environmental parameter, the α value, to regulate traffic flow. This fixed parameter adjusts traffic weights on street segments, providing a straightforward yet effective way to control traffic distribution and manage pollution levels. By integrating this method with SUMO's DUAROUTER tool, and using Valencia as a case study, we simulate various traffic management scenarios, and assess their impact on urban air quality. Through an analysis of two models, full and partial traffic isolation, we determine which strategy is more effective at reducing pollution while maintaining a balanced traffic flow. This demonstrates that an approach based on static parameters is an effective and powerful tool for sustainable urban traffic management.

6.1 Proposed Solution

Our proposed solution uses a static approach to manage urban traffic flow and to reduce environmental impact through predefined constraints. Unlike conventional methods that rely on administrative decisions to close streets or change routes, our approach uses a fixed environmental parameter (α) to adjust traffic weights on street segments. By artificially modifying the maximum allowed speed for specific streets, this parameter helps control traffic flow and reduce pollution in targeted areas. Such method enables urban planners to implement effective traffic strategies without complex monitoring.

The re-routing algorithm integrates with SUMO through its routing component, DUAROUTER. The algorithm generates a weights file with adjusted costs for each street segment, based on the user-defined α value. This value serves as a scaling factor to modify the original speed of each lane. By applying this factor, the algorithm artificially reduces speed on selected segments, increasing their travel costs so as to discourage traffic. These adjusted costs directly affect DUAROUTER's route-finding logic, redistributing traffic according to predefined environmental constraints.

Algorithm 6.1: Proposed static algorithm to enforce traffic restrictions.

```
   Input: Traffic Demand, Network, α value
   Output: Rerouted Traffic Demand
 1 routes ← getAllRoutes(Traffic Demand);
 2 allEdges ← getAllEdges(Network);
 3 newEdgesWeights ← {} ;
 4 for Edge in allEdges do
 5 |   originalSpeed ← getOriginalSpeed(Edge);
 6 |   newSpeed ← orginalSpeed / α value;
 7 |   newEdgesWeights[Edge] = newSpeed ;
 8 end
 9 for routeId in Routes do
10 |   newRoute = requestNewRouteToDUAROUTER(routeId,
   |     newEdgesWeights);
11 |   updateRouteInTrafficDemand(newRoute);
12 end
13 return Rerouted Traffic Demand;
```

As shown in Algorithm 6.1, the proposed static traffic management strategy involves several key steps. First, the process begins by retrieving all existing routes

and edges from the traffic demand data and the network (lines 1–3). Then, the algorithm iterates over each street segment (edge) in the network to compute a new speed value using the chosen α parameter (lines 4–7). The new speed is calculated by dividing the original speed by the α value, effectively adjusting the weight of the street segment to deter traffic flow. These adjusted weights are stored in a dictionary, newEdgesWeights, which is later used to generate the weights file for DUAROUTER.

Next, after computing the new weights, the algorithm proceeds to update the routes in the traffic demand. For each route, it requests a new route from DUAROUTER based on the modified weights, thereby ensuring that the new routes reflect the adjusted traffic costs (lines 8–11). The traffic demand is then updated with the newly computed routes, resulting in a rerouted traffic demand that conforms to the desired environmental constraints.

Moreover, the integration of the algorithm with DUAROUTER, which employs the Multi-Level Dijsktra (MLD) algorithm, ensures compatibility between the computed new routes and the modified weights. As a result, traffic flow is effectively redistributed, diverting vehicles away from areas with increased weights due to the static α parameter.

The core of the re-routing strategy lies in Equation (6.1), which defines the formula used to adjust the speed of each street segment. Here, the original speed (V) of a street segment is statically modified by dividing it by the α parameter. This controlled reduction in speed increases the travel cost of the segment, guiding traffic flow away from environmentally sensitive areas.

$$f(\alpha) = \frac{V}{\alpha} \tag{6.1}$$

In summary, the use of a static α value simplifies the traffic management process while maintaining the flexibility to address various environmental constraints. By integrating with DUAROUTER, the proposed approach is demonstrated to be both effective and adaptable, making it applicable to other routing tools that use Dijkstra-based algorithms.

6.2 Experiments & Results

To evaluate the effectiveness of our proposed solution in reducing pollution levels and improving air quality, we focus on the main green area of Valencia, the old riverbed (see Figure 6.1). This area spans 1,110,000 m^2, and attracts approximately 7,000,000 visitors annually. Given its significance as a central urban green space, minimising pollutant concentrations there is essential for enhancing public health and the environment.

Figure 6.1: Old riverbed of Valencia (highlighted in red).

To conduct this study, we designed a simulation involving a set of vehicles departing from various points across the city, aiming to generate data that reflects real-world conditions. The traffic source points, shown in Figure 6.2, are strategically distributed throughout the city to capture diverse traffic patterns. Based on the traffic flow model discussed in chapter 5, which represents typical working day conditions between 8 and 9 a.m., our experiment simulates the circulation of approximately 22,500 vehicles over a 1-hour period. Additionally, as outlined in the previous chapter, the vehicle data is sourced from the DGT. Using this data, and in line with the HBEFA vehicle classes defined in chapter 4, Table 6.1 presents the vehicle distribution according to engine type and EURO norm.

Regarding the calculation of air quality levels, we employ the "Fixed Box Model" previously detailed in chapter 2. For the old riverbed, the model uses its total area (1,100,100 m^2) as the XY dimension of the box, while the height of the box is set to 20 m.

The experiments are designed to evaluate two distinct traffic management models. First, we analyse the full traffic isolation model by examining the average variation of pollutants for different α values, the AQI levels for each pollutant,

Figure 6.2: Simulation traffic sources marked in blue, and target area (old riverbed) highlighted in red.

Table 6.1: Estimation of the vehicle's distribution in Valencia according to their profile.

Engine type	**EURO norm**	**Volume (%)**
Petrol	Euro 3	23
Petrol	Euro 6	22
Diesel	Euro 4	28
Diesel	Euro 6	27

and the overall changes in pollutant distribution across the city, comparing the optimal result to the default scenario. Next, we perform a similar analysis for the partial traffic isolation model, focusing on the same parameters. Finally, we compare the best results from both models to determine which approach offers better performance in terms of pollution reduction and air quality improvement.

6.2.1 Full Traffic Isolation

To evaluate the full traffic isolation model, we gradually increase the α parameter from 1 (representing the default situation) to 3.5, and we do this for all streets and bridges near the old riverbed. Such approach allows us to analyse how pollutant levels vary with different α values, and to identify the optimal setting for reducing emissions.

The results showing the variation in terms of average pollutant emissions in the old riverbed relative to normal levels (in percentage terms) are presented in Figure 6.3. Specifically, in Figure 6.3a, it can be observed that α values of 2, 2.8, and 3.5 achieve the best results, with a decrease in PM_x emissions of approximately 8%. Conversely, for α values of 1.1 and 1.8, there is an increase in PM_x emissions of about 5%. In terms of NO_x emissions, Figure 6.3b shows a reduction of about 10% for α values of 2.2 and 2.7, while for $\alpha = 2.1$, there is a 6% increase.

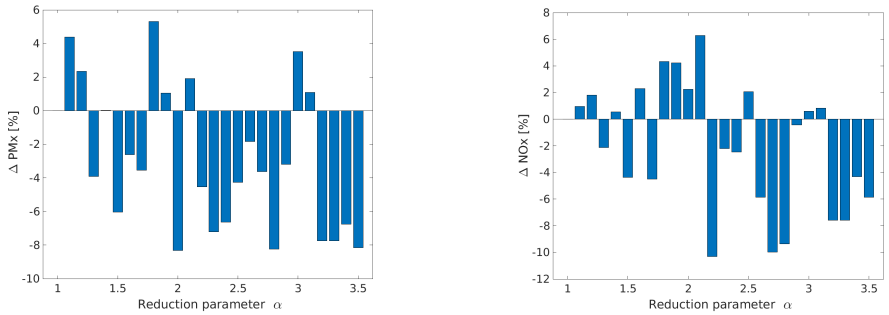

(a) PM_x (b) NO_x

Figure 6.3: Difference in pollutants in the old riverbed with respect to the default case for various α values (full traffic isolation).

Since the average variation in pollution levels alone is not sufficient to determine the optimal α value, we apply the "Fixed Box Model" to calculate the AQI for the selected area. For this purpose, we consider a time frame of $t = 1$ hour for NO_x, and $t = 24$ hours for PM_x. Based on these parameters and the assumptions mentioned earlier, we derive pollutant concentrations for each α value, as shown in Figures 6.4a, and 6.4b. As expected, the best and worst α values for PM_x concentration are consistent with those for the average variation. Similar results are observed for NO_x. Given these observations, we proceed to analyse the results in terms of AQI, which provides a more comprehensive measure of air quality.

To calculate the AQI for each pollutant and α value, we use the concentration

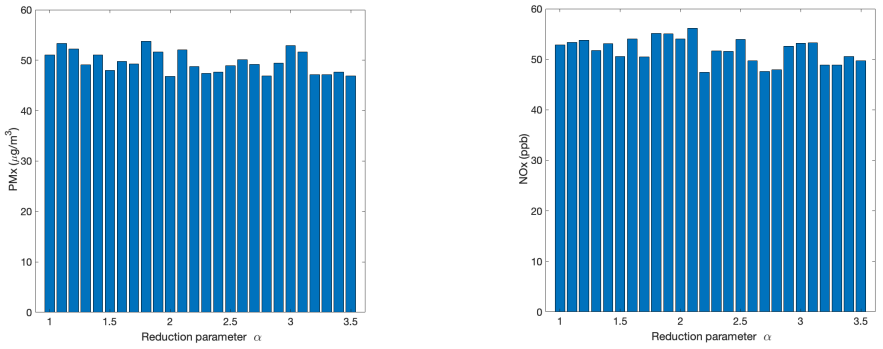

(a) PM_x (b) NO_x

Figure 6.4: Concentration of pollutants for each α in the old riverbed (full traffic isolation model).

values, the AQI Equation, and the AQI table described in chapter 2. After performing the necessary calculations, Figures 6.5a, and 6.5b are obtained. As shown, the optimal AQI values for the old riverbed area are achieved for certain α values of PM_x and NO_x, while the worst AQIs correspond to other α values of NO_x. From these individual pollutant AQIs, we compute the overall AQI for the target area, considering that the overall AQI is the average of the different pollutant AQIs.

Figure 6.6 presents the overall AQI for the old riverbed for each α value. The results indicate that several α values (3.2, 3.3, 3.4, and 3.5) yield better AQI outcomes than the default scenario ($\alpha = 1$), with AQIs of 66 and 74, respectively. Conversely, the worst α value (3) results in an AQI of 98, an increase of 24 compared to the default case. Thus, we focus on the α with the best AQI in the old riverbed to achieve the lowest pollutant levels. Specifically, $\alpha = 3.3$ emerges as the optimal solution, showing a minimal increase in city-wide pollutant levels, while significantly reducing pollutants in our target area.

After identifying $\alpha = 3.3$ as the optimal solution in terms of AQI, we proceed to analyse how pollutants are distributed throughout the city compared to the default case. Figure 6.7 shows the distribution of pollutants for PM_x and NO_x. Green areas indicate a reduction in pollutant levels relative to the default scenario, while red areas indicate an increase. Notably, there is a decrease in pollutants in the target area, but also an increase in other parts of the city, likely because most vehicles are redirected through those areas.

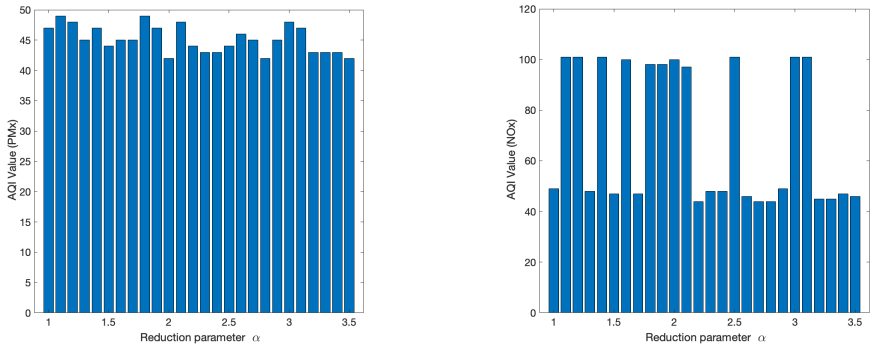

(a) PM_x (b) NO_x

Figure 6.5: AQI for each pollutant and α value in the old riverbed (full traffic isolation model).

In terms of drawbacks, we find that the red area on the right side of Figure 6.7, experiences an average increase in pollutants of 44.18%. Specifically, the increases are 48.98% for PM_x and 39.39% for NO_x. This outcome is expected because most vehicles that previously traversed the old riverbed are now diverted to this area. Despite this, the city's overall AQI does not increase, and the pollutant levels in the old riverbed decrease, indicating that the new emission distribution is satisfactory.

Regarding traffic behaviour throughout the city, Table 6.2 provides average values for speed, distance, and travel time for the various routes taken by vehicles. The results show minimal changes compared to the default situation. In terms of traffic volume along the old riverbed, Table 6.3 shows a 15.55% decrease in the number of vehicles compared to the default scenario. Overall, the restrictive solution not only improves pollutant emissions in the old riverbed, but also maintains similar values for average traffic flow parameters across the city.

Table 6.2: Average traffic performance values in the city for the default and least pollutant situation (full traffic isolation).

Metrics	**Default Situation**	$\boldsymbol{\alpha = 3.3}$	$\boldsymbol{\Delta}$ [%]
Speed	33.8 km/h	34 km/h	0.59
Distance	5006 m	5015 m	~ 0
Time	613 s	612 s	~ 0

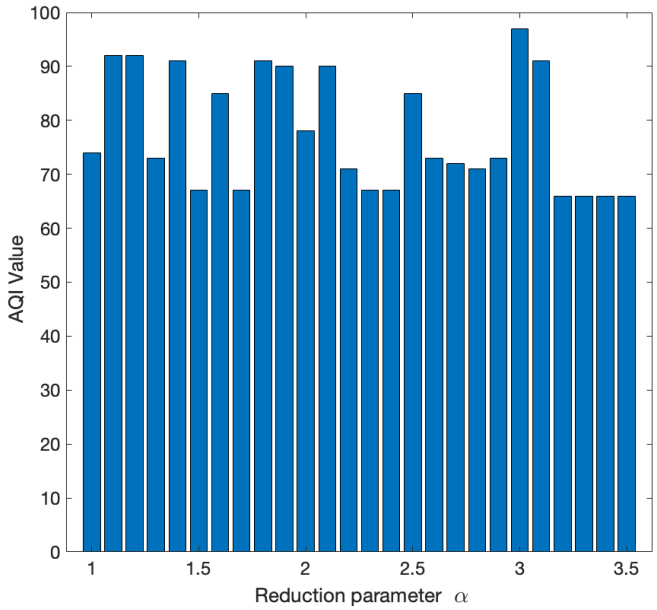

Figure 6.6: Global AQI in the old riverbed for each α (full traffic isolation).

Table 6.3: Volume of traffic in the old riverbed for default and least pollutant situations (full traffic isolation).

Metrics	**Default Situation**	$\boldsymbol{\alpha = 3.3}$	**Δ** [%]
Nº of Vehicles	6162	5204	-15.55

6.2.2 Partial Traffic Isolation

In this experiment, we once again vary the α parameter from 1 to 3.5, where $\alpha = 1$ represents the default scenario. Unlike the previous experiment, restrictions are applied only to streets near the old riverbed, and not to the bridges that cross it. This approach allows us to analyse how emissions change for different α values, and to identify the optimal configuration for the target area.

Figure 6.8 shows the average percentage variation of pollutants for each α value compared to the default case along the streets near the old riverbed. Two subfigures are presented: Figure 6.8a for PM_x, and Figure 6.8b for NO_x. For PM_x,

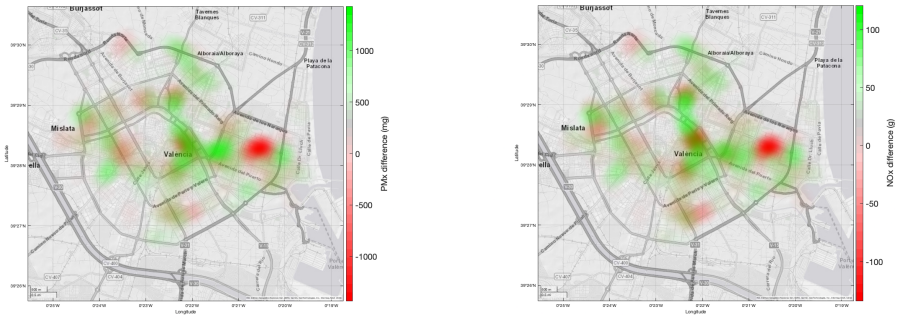

(a) PM_x (b) NO_x

Figure 6.7: Difference in pollutants throughout the city with respect to the default case for $\alpha = 3.3$ (full traffic isolation).

a significant decrease occurs for $\alpha = 2.2$ and $\alpha = 2.7$, with a reduction of about 20%. Conversely, other α values, such as 1.6, result in a 15% increase in PM_x emissions. For NO_x, the emissions behave differently; while $\alpha = 2.2$ causes a 7% increase, the best reductions, close to 7-8%, are achieved with $\alpha = 2.7$ and $\alpha = 2.9$.

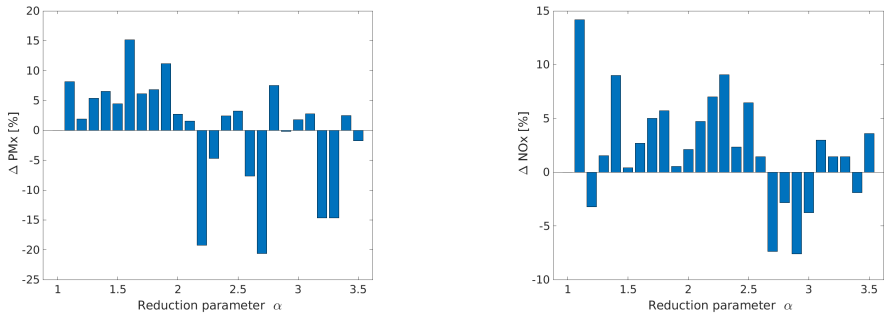

(a) PM_x (b) NO_x

Figure 6.8: Difference in pollutants with respect to the default case for various α values in the old riverbed (partial traffic isolation).

While the percentage difference in emissions provides an initial understanding, it is not sufficient to identify the optimal solution. To address this, we apply the "Fixed Box Model" to compute the AQI of the target area. Similarly to the previous

experiment, the model considers $t = 1$ hour for NO_x and $t = 24$ hours for PM_x. Based on these conditions, the pollutant concentrations for each α value are shown in Figure 6.9). Figure 6.9a displays the concentrations of PM_x, where the lowest levels are obtained for $\alpha = 2.2$ and $\alpha = 2.7$. For NO_x, the concentrations are generally consistent across different α values, except for outliers such as $\alpha = 1.1$, $\alpha = 1.4$, and $\alpha = 2.3$, which deviate from the trend.

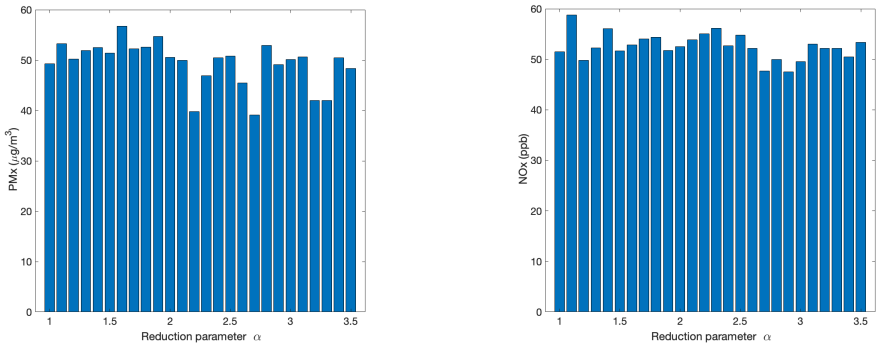

(a) PM_x (b) NO_x

Figure 6.9: Concentration of pollutants in the old riverbed for each α value (partial traffic isolation).

Figure 6.10 presents the AQI values for each pollutant across different α values. Figure 6.10a shows the AQI values for PM_x, where the lowest AQI, 36, is achieved for $\alpha = 2.7$. Regarding NO_x, the AQI values are shown in Figure 6.10b. Here, most α values result in an AQI around 50, except for certain outliers such as $\alpha = 1.1$, $\alpha = 1.4$, $\alpha = 1.7$, $\alpha = 1.8$, $\alpha = 2.1$, $\alpha = 2.5$, and $\alpha = 3.5$, which have AQI values around 100. After analysing the AQIs for both pollutants, we can identify the most favourable overall AQIs.

The overall AQI for the old riverbed is shown in Figure 6.11. As observed, multiple values emerge from the experiments. The best α values ($\alpha = 2.7$, $\alpha = 3.2$, and $\alpha = 3.3$) achieve AQI values between 47 and 48, which are 25–26 points lower than the default scenario ($\alpha = 1$), which has an AQI of 73. In contrast, the worst α values ($\alpha = 1.6$ and $\alpha = 1.9$) result in AQIs of 97, an increase of 24 points compared to the default case.

We now focus on the α values with the lowest pollutant concentrations in the old riverbed to identify the most effective solution. In particular, the solution with $\alpha = 2.7$ is selected. Examining its performance across the city, we find that this α

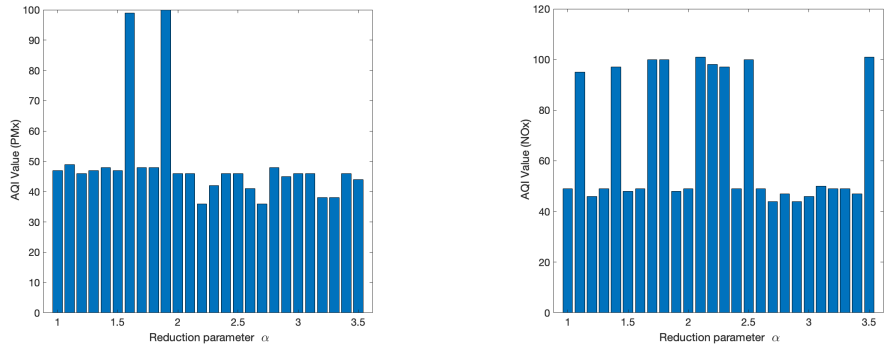

(a) PM_x (b) NO_x

Figure 6.10: AQI for each pollutant and α in the old riverbed (partial traffic isolation).

value provides favourable results, maintaining pollutant levels similar to the default approach, with a mere 1.93% increase.

Next, we examine how pollutant emissions are distributed throughout the city compared to the default situation (see Figure 6.12). Green areas indicate regions where pollutant levels are lower than the default scenario, while red areas indicate regions where levels are higher. Figure 6.12a shows the difference in PM_x distribution across the city for $\alpha = 2.7$ compared to the default case. In the target area, there is a reduction in emissions, but some parts of the city see an increase. A similar pattern is observed for NO_x in Figure 6.12b. The red areas result from diverting traffic through those streets, consequently increasing pollutant emissions.

As with any solution, there are trade-offs. In this case, the red areas indicate air quality issues, with an average increase in pollutants of 42.63% in the large red area on the right side of the map. The breakdown of this increase is 44.24% for PM_x, and 41.03% for NO_x. This outcome is expected, as most traffic is redirected to this area. Considering these results, we observe that there is a redistribution of pollutant emissions. Overall, the city's AQI does not increase because the increase in emissions in the red areas is compensated by the decrease in our target area, achieving the desired effect.

Finally, Table 6.4 shows the average traffic flow performance across the city for both the default and least pollutant situations. Overall, for the least pollutant scenario, the vehicle speed remains similar, while travel time and distance increase by 1.59% and 0.58%, respectively. Regarding the traffic volume on the streets

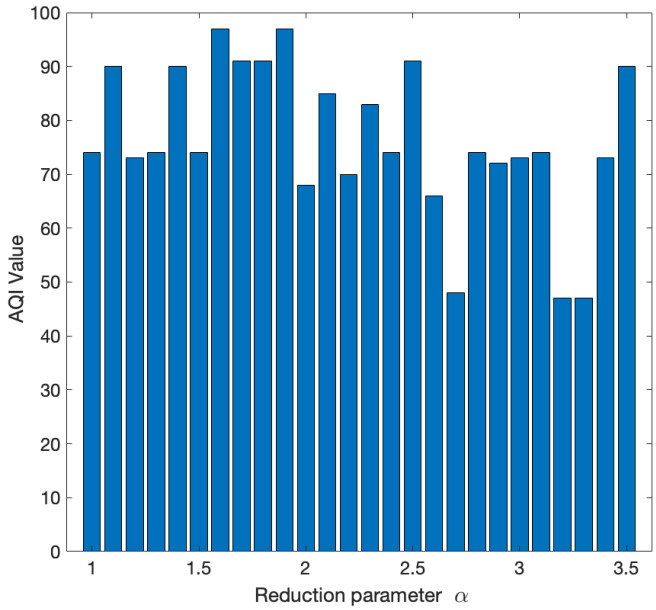

Figure 6.11: Global AQI in the old riverbed for each α (partial traffic isolation).

near the old riverbed, the results are presented in Table 6.5, showing a decrease in the number of vehicles by 14.52%. In summary, this method achieves a reduction in pollutant emissions in the target area with a negligible impact on the average traffic flow data across the city.

Table 6.4: Average traffic performance values in the city for the default and least pollutant situation (partial traffic isolation).

Metrics	**Default Situation**	$\boldsymbol{\alpha = 2.7}$	$\boldsymbol{\Delta}$ [%]
Speed	33.8 km/h	33.7 km/h	~ 0
Distance	5006 m	5034 m	0.58
Time	613 s	623 s	1.59

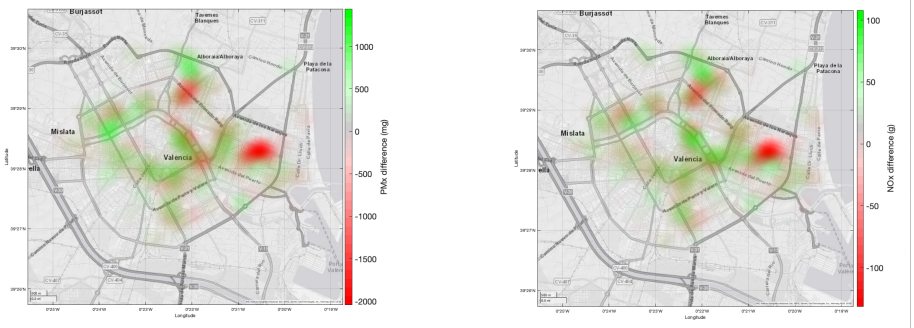

(a) PM_x (b) NO_x

Figure 6.12: Difference in pollutants throughout the city with respect to the default case for $\alpha = 2.7$ (partial traffic isolation).

Table 6.5: Volume of traffic in the old riverbed for default and least pollutant situation (partial traffic isolation).

Metrics	**Default Situation**	$\boldsymbol{\alpha = 2.7}$	**Δ** [%]
Nº of Vehicles	6162	5267	-14.52

6.2.3 Comparison Between Approaches

To determine which traffic management approach yields the best results, we compare the most effective configurations from the previous models: $\alpha = 3.3$ for full traffic isolation, and $\alpha = 2.7$ for partial traffic isolation. Table 6.6 summarises the key metrics and the differences between the results obtained for both approaches.

Table 6.6: Metrics comparison between best α values of both approaches.

Metrics	**FTI**[1] $(\boldsymbol{\alpha = 3.3})$	**PTI**[2] $(\boldsymbol{\alpha = 2.7})$	**Difference**
$\boldsymbol{\Delta PM_x}$[%]	-7.75	-20.63	-12.88 %
$\boldsymbol{\Delta NO_x}$[%]	-7.59	-7.37	0.22 %
AQI	66	47	-19
Nº of Vehicles	5204	5267	1.21 %

On one hand, when analysing the variation of pollutants in the old riverbed compared to the default case, we observe that the partial traffic isolation approach ($\alpha = 2.7$) generally provides better results. Specifically, while the full traffic isolation approach with $\alpha = 3.3$ reduces PM_x levels by 7.75%, the partial traffic isolation approach with $\alpha = 2.7$ achieves a more substantial reduction of 20.63%. In terms of NO_x, both approaches deliver similar results, with reductions of approximately 7.5% compared to the default case. In terms of the overall AQI, the partial traffic isolation approach with $\alpha = 2.7$ results in a 19-point reduction compared to the full traffic isolation scenario with $\alpha = 3.3$. This difference is noteworthy because the AQI for partial traffic isolation falls within the "good" range, whereas the AQI for full traffic isolation remains within the "moderate" range.

On the other hand, when considering the volume of traffic in the streets near the old riverbed, the differences between both approaches are minimal and mostly negligible.

To better understand the spatial distribution of pollutants across the city, we compare the two configurations using heatmaps (see Figure 6.13). In these maps, green areas indicate locations where pollutant levels are lower for the partial traffic isolation solution ($\alpha = 2.7$) compared to the full traffic isolation solution ($\alpha = 3.3$), while red areas represent locations where pollutant levels are higher. Overall, we observe that pollutant levels in the target area are reduced more effectively with the partial traffic isolation approach. Specifically, the distribution of PM_x and NO_x (Figures 6.13a and 6.13b), shows more green spots, which is consistent with the AQI results.

6.3 Summary

In this chapter, we presented a static approach to manage urban traffic flow using predefined environmental constraints. Our method relies on a static α value to adjust traffic weights on street segments. To demonstrate its effectiveness, we used SUMO's DUAROUTER and a weights file generated by our re-routing algorithm. This file contains adjusted costs for each street segment, and guides DUAROUTER's routing process. We tested this approach in Valencia, targeting the old riverbed, a key green space, to reduce air pollution.

We first examined the full traffic isolation model, applying restrictions to both streets and bridges near the old riverbed. By varying the α parameter, we significantly reduced pollutant levels in the area. The best results were achieved

[1] FTI: Full Traffic Isolation.
[2] PTI: Partial Traffic Isolation.

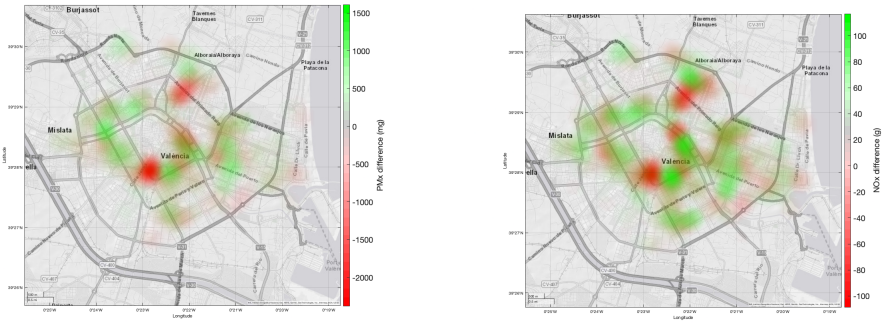

(a) PM_x (b) NO_x

Figure 6.13: Difference in pollutants with respect to $\alpha = 3.3$ (full traffic isolation) for $\alpha = 2.7$ (partial traffic isolation) throughout the city.

with $\alpha = 3.3$, which lowered the overall AQI in the target zone without substantially increasing pollutants elsewhere in the city.

Next, we explored the partial traffic isolation model, restricting only the streets around the old riverbed. This allowed for different traffic patterns and pollutant distributions. Our analysis found that $\alpha = 2.7$ was the optimal value, leading to a notable reduction in pollutants, and a better AQI than the full isolation model.

Finally, we compared both approaches to assess their effectiveness. The partial traffic isolation model with $\alpha = 2.7$ provided better overall results, achieving a greater reduction in pollutants and a lower AQI in the target area. Moreover, it had minimal impact on the overall traffic flow, showing that environmental goals can be met without major disruptions.

In summary, this chapter has demonstrated that a static traffic management approach using a predefined α value is an effective tool for reducing urban pollution. By taking advantage of SUMO's DUAROUTER and our simple method, urban planners can apply specific traffic restrictions that balance environmental and traffic management needs.

Chapter 7

Traffic Re-routing Based on Air Pollution: a Dynamic Approach

In the previous chapter, we explored a static approach to managing and optimising traffic flow to reduce air pollution in urban areas by using a fixed environmental parameter, the α value, which allowed us to adjust traffic weights on street segments. While this method provided a straightforward way to control traffic distribution and manage pollution levels, it lacked the flexibility to respond to real-time changes in traffic conditions and air quality. Building upon this, the current chapter introduces a dynamic traffic re-routing algorithm that adjusts vehicle routes based on current air quality data, while also accounting for the specific vehicle emission profiles. By integrating this dynamic method with SUMO's DUAROUTER tool, and again using the city of Valencia as our case study, we simulate various environmental crisis scenarios, such as building fires and smog episodes, to assess the impact of our approach on urban air quality. Through these simulations, we evaluate how air quality data integration enhances pollution reduction while maintaining a balanced traffic flow, demonstrating that a dynamic strategy offers a more effective and adaptive solution for sustainable urban traffic management compared to static methods.

7.1 Proposed Solution

Our proposed solution introduces a dynamic approach to mitigate urban air pollution during environmental crises. Unlike the static traffic management method discussed in the previous chapter, which relies on predefined constraints, this dynamic approach adjusts vehicle routes in real time based on current air quality data for street segments (edges), and on NO_x vehicle emission profiles. By continuously updating the traffic flow, the algorithm aims at keeping the concentrations of pollutants such as NO_x and PM_{10} at low levels, improving air quality without significantly compromising traffic efficiency.

To determine optimal routes, we use the MLD algorithm of DUAROUTER, which calculates the shortest paths based on free-flow travel times. However, our algorithm modifies these paths to incorporate air quality considerations, ensuring that vehicles are rerouted to minimise emissions in polluted areas. Although we use DUAROUTER for simulation purposes, our approach is compatible with any routing tool that bases its cost calculations on travel time, speed, or distance, and that uses a Dijkstra-based algorithm.

Additionally, vehicles are categorised according to their NO_x emissions profiles, as defined by the EEA [136]. This categorisation allows the algorithm to apply different weights to routes based on vehicle type, factoring in the specific emissions each vehicle contributes to the environment.

The steps of the dynamic traffic re-routing algorithm are formalised in Algorithm 7.1, which outlines the process of adjusting travel times based on air quality and emissions data, recalculating routes accordingly.

As shown in Algorithm 7.1, the dynamic traffic management strategy involves several key steps:

1. The algorithm starts by retrieving all existing routes and edges from the traffic demand data and network (lines 1–3). The variable *routes* contains all vehicle routes in the initial traffic demand, while *allEdges* includes all the edges present in the network. An empty dictionary *newEdgesWeights* is initialised to save the adjusted travel times for each edge and vehicle type.

2. Next, the algorithm computes the AQI weight for each edge (lines 5–8). For every edge, it calculates the free-flow travel time and retrieves the AQI value, which is then normalised relative to the maximum AQI in the network. The normalised AQI is used to compute the AQI weight (W_{AQI}) using the negative exponential function in Equation 7.1. This function assigns higher weights to highly polluted segments, making them a worse route option for the routing algorithm.

Algorithm 7.1: Proposed dynamic traffic re-routing algorithm.

Input: Traffic Demand, Network, Vehicle Emissions Profiles, AQI Data, Δ value
Output: Rerouted Traffic Demand

routes ← getAllRoutes(Traffic Demand);
allEdges ← getAllEdges(Network);
newEdgesWeights ← {};
for *Edge* ***in*** *allEdges* **do**
    freeFlowTravelTime ← getFreeFlowTravelTime(Edge);
    AQIValue ← getAQIValue(Edge);
    normalisedAQI ← normalise(AQIValue);
    W_{AQI}[Edge] ← calculateAQIWeight(normalisedAQI);
    for *vehicleType* ***in*** *Vehicle Emissions Profiles* **do**
        emissionsFactor ← getEmissionsFactor(vehicleType);
        $W_{\text{emissions}}$[vehicleType] ← normalise(emissionsFactor);
        W_{reroute}[Edge][vehicleType] ← W_{AQI}[Edge] × $W_{\text{emissions}}$[vehicleType] × Δ;
        T_{new}[Edge][vehicleType] ← freeFlowTravelTime × (1 + W_{reroute}[Edge][vehicleType]);
        newEdgesWeights[Edge][vehicleType] ← T_{new}[Edge][vehicleType];
    end
end
for *routeId* ***in*** *routes* **do**
    vehicleType ← getVehicleType(routeId);
    newRoute ← requestNewRouteToDUAROUTER(routeId, newEdgesWeights, vehicleType);
    updateRouteInTrafficDemand(newRoute);
end
return Re-routed Traffic Demand;

$$W_{\text{AQI}} = \exp\left(-\frac{1}{64} \cdot \text{Normalised AQI}^6\right) \tag{7.1}$$

3. After computing the AQI weights, the algorithm normalises the emissions factors for each vehicle type to obtain the emissions weights (lines 10–11). As stated above, the emissions factors are based on the vehicle emission profiles corresponding to different EURO standards, as defined by the EEA. The normalised emissions factors are stored as $W_{\text{emissions}}$ for each vehicle type.

4. Then, the algorithm calculates the re-routing weights and adjusts the travel times for each edge and vehicle type (lines 12–14). For every combination of edge and vehicle type, the re-routing weight W_{reroute} is calculated by multiplying the AQI weight, the emissions weight, and the "Emission Sensitivity Factor" (Δ) using Equation 7.2

$$W_{\text{reroute}} = W_{\text{AQI}} \times W_{\text{emissions}} \times \Delta \tag{7.2}$$

5. The new travel time T_{new} for each edge and vehicle type is then computed by adjusting the free-flow travel time using Equation 7.3. Then, these adjusted travel times are saved in the *newEdgesWeights* dictionary.

$$T_{\text{new}} = T_{\text{free-flow}} \times (1 + W_{\text{reroute}}) \tag{7.3}$$

6. Finally, the algorithm updates the traffic demand with new routes (lines 18–20). For each route, the algorithm identifies the vehicle type, and requests a new route from DUAROUTER based on the modified travel times. The traffic demand is then updated with these newly computed routes, resulting in a rerouted traffic flow that considers air quality and emissions data.

In summary, the dynamic traffic re-routing algorithm integrates air quality data and vehicle emission profiles into the traffic routing process. By adjusting travel times to avoid routes through highly polluted areas, especially for high-emission vehicles, the algorithm aims to reduce pollutant exposure during urban environmental crises while maintaining the traffic flow unaltered.

7.2 Experiments & Results

To evaluate the effectiveness of our proposed solution in mitigating air pollution during urban environmental crises, and similarly to the previous chapter, we

conduct simulations in the city of Valencia, Spain. This scenario provides a realistic urban environment to assess the impact of dynamic traffic re-routing strategies on both traffic flow and air quality.

Our experiments focus on two specific areas within the city that represent potential environmental crisis scenarios. In the first, the Building Fire Scenario, we simulate a building fire similar to the February 2024 incident in Valencia [137]. Here, PM_{10} concentrations are increased by ten times, and NO_x concentrations are doubled in the affected area. These assumptions are based on studies by Gupta *et al.* [138] and Yue *et al.* [139], which analyse the impact of urban fires on air quality. In the second scenario, the Smog Episode Scenario, we simulate a smog[1] event near the central train station, tripling NO_x concentrations and doubling PM10 levels, reflecting conditions observed in similar urban smog events, as documented by research in Turin [140]. Figure 7.1 shows the locations of these simulated impact areas within the city of Valencia.

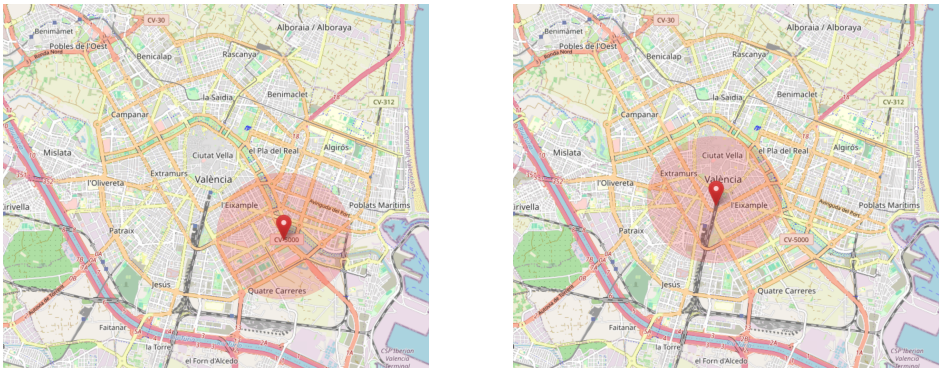

(a) Building fire scenario.

(b) Smog episode scenario near the central train station.

Figure 7.1: Simulated impact areas of environmental disasters.

As stated in the previous chapter, we generate realistic traffic conditions by designing simulations involving vehicles that depart from various points across the city during peak traffic hours, specifically between 8 a.m. and 9 a.m. on a typical weekday. This time frame captures the morning rush hour when traffic density is high, providing a robust context for evaluating our algorithm's performance. Based on the traffic flow model discussed in chapter 5, our experiment simulates the circulation of approximately 22,500 vehicles over the one-hour period.

[1]Fog or haze intensified by smoke or other atmospheric pollutants.

Regarding vehicle fleet composition, we base the vehicle type distribution on projections by Gassner *et al.* for Vienna [141], adapted to Valencia's context. Given that electric vehicles currently make up less than 1% of the fleet in Valencia, we simulate a future scenario with an increased ratio of electric vehicles. This creates a more meaningful context for evaluating our algorithm in a mixed fleet environment. Table 7.1 presents the vehicle distribution according to engine type and EURO norm, aligned with the HBEFA vehicle classes defined in chapter 4.

Table 7.1: Vehicle's distribution in the experiment according to their profile.

Engine Type	**EURO norm**	**Volume (%)**
Battery Electric	Euro 6	35
Diesel	Euro 4	5
Diesel	Euro 6	25
Petrol	Euro 3	5
Petrol	Euro 6	25
Hybrid (Petrol CNG)	Euro 6	5

For calculating air quality levels, we employ the GRAL model, described in chapter 2, to simulate pollutant dispersion in the city. As previously said, GRAL incorporates detailed building geometries and meteorological data to accurately estimate pollutant concentrations, particularly for NO_x and PM_{10}

The experiments are designed to assess the impact of our dynamic re-routing algorithm under different conditions. Specifically, we vary the Δ value from 1 to 10 to explore the trade-offs between reducing pollutants in affected areas and the potential for increased congestion elsewhere due to re-routing. By adjusting the Δ value, we aim to identify the optimal balance between improving local air quality and maintaining overall traffic efficiency.

To evaluate the performance of our algorithm, we monitor key traffic-related and pollution-related parameters. Traffic metrics include global average travel time, congestion levels, and average vehicle speed across the city, providing insight into how the algorithm impacts the overall traffic flow, and whether it introduces significant delays or congestion. Pollution metrics include the AQI within the affected areas and across the city, as well as concentrations of NO_x and PM_{10}. We track both mass emissions and pollutant concentrations to assess the algorithm's effectiveness in reducing pollution within crisis zones, and to identify any potential increases in pollution elsewhere in the city.

Having outlined the experimental setup and the parameters to be measured, we now present the results of our simulations, and discuss the implications of

our findings. We begin by evaluating how varying the Δ value affects air quality metrics such as AQI, NO_x, and PM_{10} levels in both scenarios. We then examine the effects of the optimal Δ value on traffic flow parameters to determine whether improvements in air quality are achieved without significant trade-offs in traffic efficiency.

7.2.1 Effect of Varying Δ on Air Quality

The "Emission Sensitivity Factor" (Δ) is a critical parameter in our dynamic traffic re-routing algorithm, determining how strongly the algorithm prioritises air quality considerations over travel efficiency. By adjusting Δ, we control the extent to which vehicles, particularly high-emission ones, are rerouted away from highly polluted areas. To evaluate the impact of varying Δ on air quality, we conducted simulations across a range of Δ values from 1 to 10 for both the Building Fire and Smog Episode scenarios introduced earlier.

Figures 7.2 and 7.3 present the results of these simulations, illustrating changes in NO_x and PM10 mass emissions and concentrations, both within a 1 km radius of the pollution sources, and across the entire city. While PM10 is included for completeness, our primary focus is on NO_x, as it is more directly influenced by vehicle emissions.

In the Building Fire Scenario, as shown in Figures 7.2a and 7.2c, increasing Δ leads to a significant decrease in NO_x mass emissions and concentrations within the affected area. Specifically, at $\Delta = 10$, there is a reduction of approximately 25% in NO_x mass emissions. This decline indicates that higher Δ values effectively reduce pollutant levels by re-routing traffic away from the impacted zone. However, when considering the entire city, the changes are less pronounced, with a slight increase in NO_x concentrations at higher Δ values. This suggests that, while pollution decreases locally, it may be redistributed to other parts of the city, emphasising on the need for a balanced approach.

Similarly, in the Smog Episode Scenario depicted in Figures 7.2b and 7.2d, increasing Δ results in substantial reductions in NO_x emissions and concentrations within the studied area. At $\Delta = 10$, the reduction in NO_x mass emissions exceeds 50%, showcasing the algorithm's effectiveness in mitigating pollution in critical zones. Nonetheless, fluctuations in NO_x concentrations across the city are observed, with some Δ values (e.g., $\Delta = 4$ and $\Delta = 6$) leading to slight increases in other areas due to traffic redistribution.

The PM_{10} variations mirror the trends observed for NO_x, although to a lower magnitude, as PM_{10} is less directly influenced by vehicle emissions in these scenarios.

To further assess the impact on overall air quality, we analysed the changes in the AQI. Figure 7.4 illustrates the AQI variations for both scenarios across

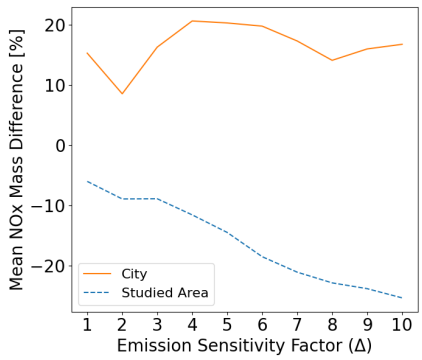

(a) NO_x Mass Difference: Building Fire Scenario.

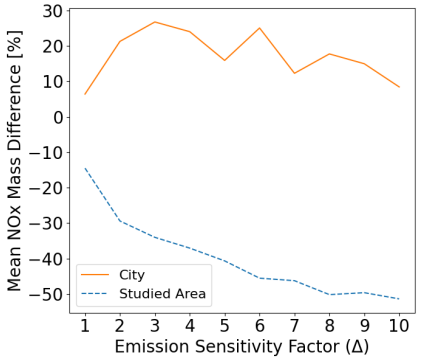

(b) NO_x Mass Difference: Smog Episode Scenario.

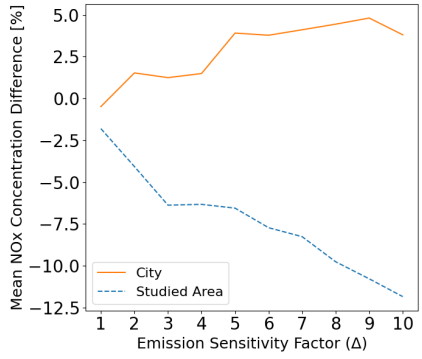

(c) NO_x Concentration Difference: Building Fire Scenario.

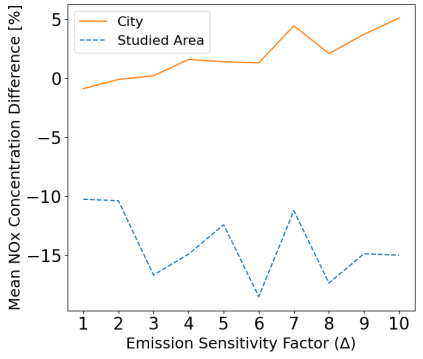

(d) NO_x Concentration Difference: Smog Episode Scenario.

Figure 7.2: Impact of varying Δ on NO_x mass emissions and concentrations for different scenarios.

different Δ values.

In the Building Fire Scenario (see Figure 7.4a), as Δ increases, the AQI in the studied area shows a slight decline, with the most significant reduction of around -6 at $\Delta = 6$. However, the AQI remains relatively stable across all Δ values. In contrast, the overall city AQI increases modestly, peaking at approximately 4 for $\Delta = 10$. This trend can be attributed to the fact that, in the city, the increased traffic congestion from re-routing leads to higher NO_x levels in other areas, thereby raising the AQI.

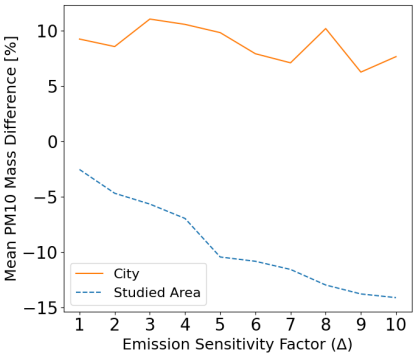

(a) PM_{10} Mass Difference: Building Fire Scenario.

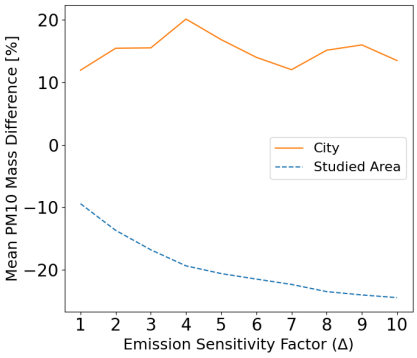

(b) PM_{10} Mass Difference: Smog Episode Scenario.

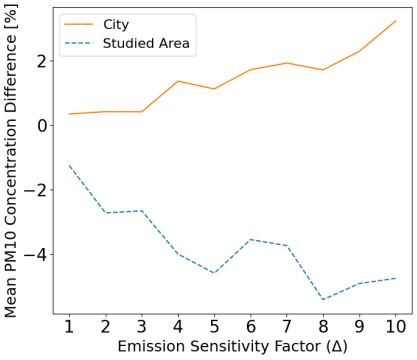

(c) PM_{10} Concentration Difference: Building Fire Scenario.

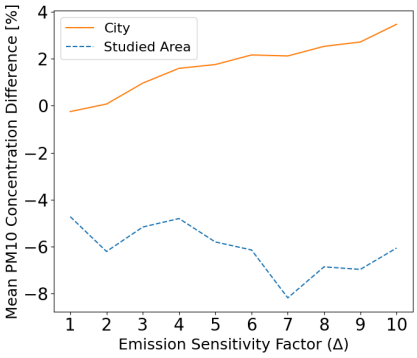

(d) PM_{10} Concentration Difference: Smog Episode Scenario.

Figure 7.3: Impact of varying Δ on PM_{10} mass emissions and concentrations for different scenarios.

For the Smog Episode Scenario (see Figure 7.4b), the optimal Δ appears to be around 6 as well. At this point, the AQI improvement is well-balanced between the city and the affected area, with the city-wide AQI increasing by approximately 3 points, while the studied area sees a significant reduction of about -7. At very high Δ values, although the AQI in the studied area is reduced further, the overall city impact shows an increase, indicating that traffic and emissions are being redistributed.

Based on these observations, $\Delta = 6$ is identified as the optimal value for this

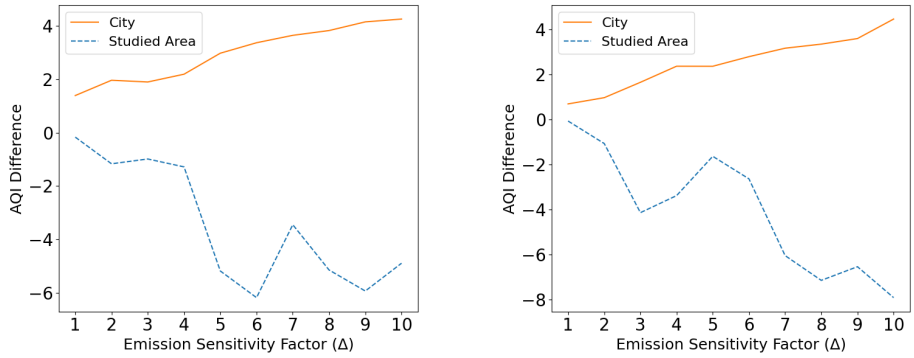

(a) AQI Variation: Building Fire Scenario.

(b) AQI Variation: Smog Episode Scenario.

Figure 7.4: Impact of varying Δ on AQI levels for different scenarios.

city. This choice provides the best trade-off between reducing AQI, and NO_x in the selected area, while controlling the increases in these metrics across the city. This selection ensures that the algorithm is effective in re-routing high-emission vehicles away from sensitive zones, while minimising negative impacts on the overall city air quality. Further research could explore more dynamic methods of adjusting Δ in real-time to respond to evolving traffic and environmental conditions.

To visualise the spatial impact of our algorithm, we present AQI heatmaps for the default scenario and the optimised $\Delta = 6$ scenario in Figure 7.5.

In the Building Fire Scenario, Figures 7.5a, 7.5c, and 7.5e depict the AQI distribution. The heatmaps reveal that, while most of the area shows minimal changes in AQI, there is a noticeable external ring where AQI levels decrease significantly, by almost 20 points. In contrast, certain parts of the northern area experience increases of up to 15 points, explaining the average AQI reduction of 6 points in the studied area.

In the Smog Episode Scenario, the corresponding heatmaps are shown in Figures 7.5b, 7.5d, and 7.5f. These figures demonstrate that our solution effectively lowers AQI levels within the targeted area, while slightly increasing them in the surrounding zones, and in a localised section of the studied area. Unlike the Building Fire Scenario, the AQI reduction in this scenario is more evenly distributed, with substantial decreases spread across the area. Comparing Figures 7.5b and 7.5d, we observe a noticeable reduction in the size of the high-pollution zone (represented by the orange circle), indicating a significant improvement in air quality within the affected area.

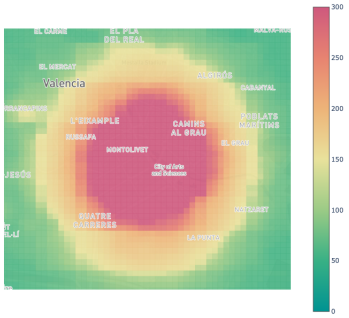

(a) Building Fire Scenario (Default).

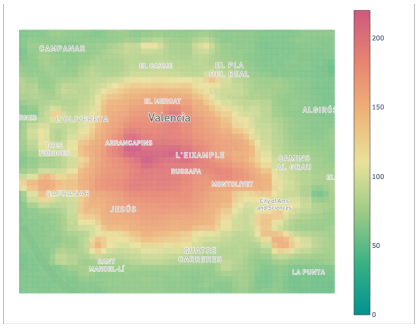

(b) Smog Episode Scenario (Default).

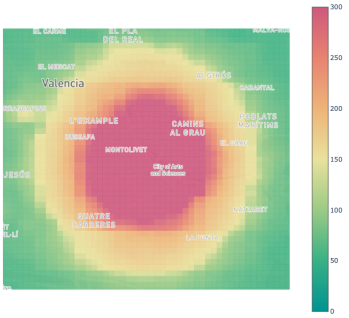

(c) Building Fire Scenario ($\Delta = 6$).

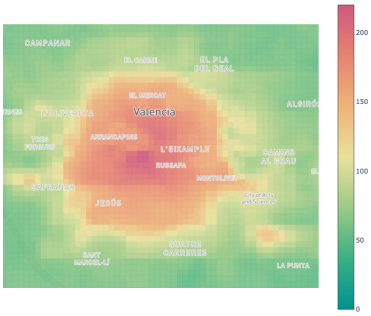

(d) Smog Episode Scenario ($\Delta = 6$).

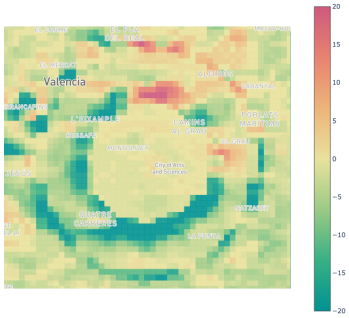

(e) Building Fire (AQI Difference).

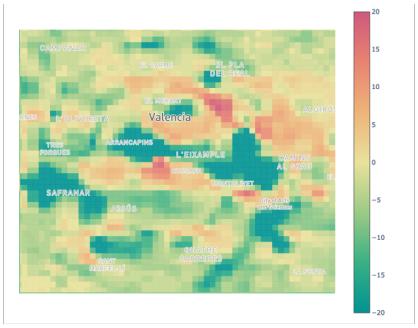

(f) Smog Episode Scenario (AQI Difference).

Figure 7.5: Comparison of AQI heatmaps for different scenarios and re-routing solutions.

Overall, these heatmaps confirm that the optimised $\Delta = 6$ re-routing strategy successfully mitigates high AQI levels in critical zones, while still maintaining acceptable air quality throughout the city. Overall, the results underscore the algorithm's capability to improve local air quality during environmental crises without causing substantial negative impacts elsewhere.

7.2.2 Traffic Flow Analysis for Optimal Δ

After identifying $\Delta = 6$ as the optimal "Emission Sensitivity Factor", we analysed the algorithm's impact on traffic flow to determine if the air quality benefits come at the expense of traffic efficiency. Key traffic metrics, including average travel time, route length, waiting time, time loss, and average speed, were evaluated for the Default scenario, and for the two environmental crisis scenarios with $\Delta = 6$. Table 7.2 summarises these metrics and the percentage differences relative to the Default scenario.

Table 7.2: Average traffic metrics across scenarios and percentage differences from the Default scenario.

Metric	**Default**	**Building Fire**	**% Diff.**	**Smog Episode**	**% Diff.**
Trip Duration (s)	625.73	631.18	+0.87%	629.55	+0.61%
Route Length (m)	5131.67	5206.08	+1.45%	5206.67	+1.46%
Waiting Time (s)	145.48	146.37	+0.61%	143.64	-1.26%
Time Loss (s)	234.37	233.97	-0.17%	233.61	-0.32%
Speed (m/s)	8.48	8.50	+0.24%	8.52	+0.47%

When analysing average trip duration and route length, we observe a marginal increase in both metrics in the Building Fire and the Smog Episode scenarios compared to the non-rerouted scenario (Default). Specifically, the average duration for vehicles to complete their routes increases by 0.87% in the Building Fire scenario, and by 0.61% in the Train Station scenario. Similarly, the average route length increases by about 1.45% in both scenarios. These small increments indicate that, while the algorithm effectively reroutes vehicles to avoid high-emission areas, it results in only a minor increase in travel times and travel distances. This demonstrates that the re-routing strategy balances air quality improvement without significantly compromising traffic efficiency.

The impact on average waiting time and time loss reveals additional insights into congestion levels. In the Building Fire scenario, the average waiting time shows a slight increase of 0.61%, indicating a small rise in congestion in some parts

of the city. Conversely, in the Smog Episode scenario, the average waiting time decreases by 1.26%, suggesting a more effective dispersion of traffic in this case. The average time loss, which measures delays due to driving below optimal speeds, shows negligible differences across all scenarios. There is a slight reduction of 0.17% in the Building Fire scenario, and 0.32% in the Smog Episode scenario, indicating that the re-routing strategy does not significantly disrupt overall traffic efficiency.

The average speed of vehicles across the network remains relatively stable, showing only minor variations between the scenarios. In the Building Fire scenario, there is a slight increase of 0.24% in the average speed, while the Smog Episode scenario sees a marginal increase of 0.47%. These small increases confirm that re-routing does not considerably impact traffic flow dynamics, and that vehicles can still maintain an efficient pace throughout the network. This demonstrates the algorithm's capability to manage re-routing effectively without causing significant slowdowns or bottlenecks.

To illustrate the practical impact of the re-routing algorithm, Figure 7.6 presents an example of a vehicle's route in the Smog Episode Scenario. The algorithm redirects the vehicle away from the high-pollution area near the train station, selecting an alternative path that maintains travel efficiency while contributing to air quality improvement.

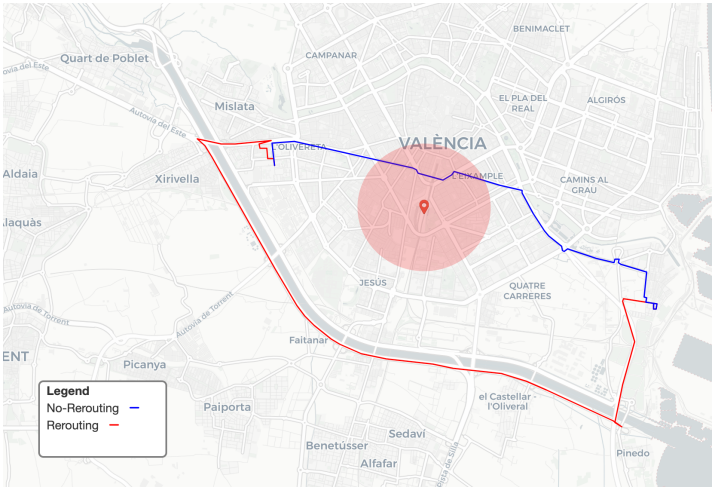

Figure 7.6: Example of a rerouted path in the Smog Episode Scenario.

Overall, the analysis indicates that the air quality benefits achieved by the re-routing algorithm with the optimal Δ value are attained without a substantial

detriment to traffic efficiency. While there are minor increases in average travel time and route length, the reductions in waiting time and time loss, particularly in the Smog Episode scenario, reflect the algorithm's ability to balance improved air quality with smooth traffic flow.

7.3 Summary

In this chapter, we presented a dynamic approach to managing urban traffic flow by integrating air quality data and vehicle emission profiles. Our method relies on adjusting vehicle routes dynamically based on the AQI and specific emissions factors for different vehicle types, controlled by an "Emission Sensitivity Factor" (Δ). To demonstrate its effectiveness, we implemented our dynamic traffic re-routing algorithm using SUMO's DUAROUTER tool, and applied it to the city of Valencia, simulating environmental crisis scenarios such as building fires and smog episodes.

We first assessed the impact of varying the Δ value on air quality metrics, specifically focusing on NO_x and PM_{10} mass emissions and concentrations. By analysing different Δ values, we found that $\Delta = 6$ provided the optimal balance we sought, significantly reducing pollutant concentrations in the affected areas without causing substantial increases elsewhere in the city. This optimal Δ effectively lowered the AQI in the target zones, demonstrating the algorithm's capability to mitigate air pollution during environmental crises.

Next, we evaluated the algorithm's effect on traffic flow parameters under the optimal Δ. We examined metrics such as average travel time, route length, waiting time, time loss, and average speed. The results indicated that the dynamic re-routing strategy led to only minimal increases in travel time and route length, with negligible impacts on waiting time and time loss. Average speeds remained stable or improved slightly, confirming that the air quality benefits were achieved without significantly compromising traffic efficiency.

In summary, this chapter has demonstrated that a dynamic traffic management approach, using air quality data and vehicle emission profiles, is an effective tool for reducing urban pollution during critical events. By leveraging SUMO's DUAROUTER and our adaptive algorithm, urban planners can implement responsive traffic strategies that balance environmental objectives with traffic efficiency, contributing to more sustainable and resilient urban environments.

Chapter 8

Predicting Air Quality for Current and Future Urban Traffic

In the previous chapters, we focused on dynamic and static traffic re-routing strategies to mitigate urban air pollution by optimising traffic flow based on environmental criteria. In this chapter, we wanted to go one step further and account for the long-term changes in vehicle technology and fleet composition, to ascertain how this significantly impacts air quality. Building upon this foundation, the current chapter examines the projected evolution of Valencia's vehicular fleet, particularly the increasing adoption of Electric Vehicles (EVs) that is expected, and its potential effects on future urban air quality. By adapting fleet evolution scenarios from a study conducted for Vienna, we simulate various future scenarios up to year 2050, considering a pessimistic outlook on public transportation uptake. Through these simulations, we assess how vehicle type shifts have an influence on the city's AQI, demonstrating that a gradual transition towards electric vehicles can substantially improve air quality over time; our analysis provides valuable insights for policymakers and urban planners aiming for sustainable urban environments.

8.1 Overview of Valencia's Traffic Fleet Evolution

Predicting future air quality in urban environments requires a comprehensive understanding of how the vehicular fleet will evolve. Changes in vehicle technology, regulatory policies, and consumer preferences significantly influence the composition of vehicles on the road, which in turn affects emission profiles and air quality outcomes. Without specific projections for Valencia, we have adapted the vehicle fleet evolution scenarios from Gassner *et al.*'s study conducted for Vienna [141].

Vienna and Valencia share several characteristics that make this adaptation reasonable. As members of the European Union, they are subject to similar environmental regulations, emission standards, and policy frameworks to reduce vehicular emissions and promote sustainable transportation. Additionally, both cities show comparable urban dynamics, including population density, economic activity, and a dependence on private vehicles for urban mobility.

In our fleet evolution scenarios for Valencia, we have taken a pessimistic view of the increasing use of public transportation. This view derives from observed trends suggesting limited investment in public transport infrastructure, and a persistent preference among residents for private vehicle use over buses or the underground metro system. Factors contributing to this preference include the convenience and flexibility offered by private vehicles and perceived shortcomings in the coverage, frequency, and reliability of public transport services.

Given these considerations, our projections highlight an increase in the adoption of hybrid and electric vehicles, driven by policy incentives, technological advancements, and initiatives by vehicle manufacturers to promote cleaner transportation options. Conversely, the share of conventional diesel and petrol vehicles is expected to decline over time, specifically older models that do not meet emission standards.

Table 8.1 summarises our proposed evolution of Valencia's vehicle fleet composition from the current state through the year 2050. The vehicle categories are defined based on engine type and Euro emission standards.

As shown in Table 8.1, the ratio of older diesel (Euro 4) and petrol (Euro 3) vehicles is projected to decrease significantly, with these categories being phased out by 2040 and 2035, respectively. Newer diesel and petrol vehicles meeting Euro 6 standards are expected to remain in the fleet, with declining shares over time. Also, hybrid vehicles see a modest increase, reflecting gradual adoption, while electric vehicles exhibit substantial growth, reaching 80% of the fleet by 2050.

In the following subsection, we plan to assess how changes in the composition of vehicle fleets affect the widespread air quality in Valencia.

Table 8.1: Proposed vehicle's fleet evolution in Valencia according to their profile.

	Diesel		Petrol		Hybrid	Electric
Year	**Euro 4**	**Euro 6**	**Euro 3**	**Euro 6**	**Euro 6**	**Euro 6**
Current	29.96%	20.21%	27.35%	18.45%	3.42%	0.61%
2030	15.00%	25.00%	15.00%	25.00%	5.00%	15.00%
2035	5.00%	25.00%	5.00%	25.00%	5.00%	35.00%
2040	0%	25.00%	0%	20.00%	10.00%	45.00%
2045	0%	20.00%	0%	12.50%	7.50%	60.00%
2050	0%	5.00%	0%	5.00%	10.00%	80.00%

8.2 Experiments & Results

To assess the potential impact of the projected evolution of Valencia's vehicle fleet on urban air quality, we performed a series of simulations modelling different future scenarios stated above. These simulations aim to evaluate how increasing the adoption of EVs, and the gradual reduction of higher-emission vehicles, affect the AQI levels across the city over time.

For our analysis, we used our customised air quality levels and the EEA associated colour codes to categorise and visualise the AQI results. Figure 8.1 presents the AQI values along with their corresponding colours, as established by the EEA guidelines.[1] This colour classification clearly explains air quality levels and facilitates comparisons between different scenarios.

We structured the results into two main subsections. The first subsection provides a detailed statistical assessment of the AQI for each scenario. This includes presenting the average AQI values, differences compared to the current situation, and the distribution of AQI values through standard distribution plots. This quantitative analysis enables us to understand the overall trends in air quality improvements over time, and to assess the effectiveness of the projected fleet evolution in reducing pollution.

The second subsection is a key part of our analysis. It focuses on the geographical representation of air quality levels across Valencia. We present AQI heatmaps for the city for all the scenarios considered, illustrating the spatial distribution of air quality, and highlighting areas of significant change. Besides, we include different heatmaps that depict the changes in AQI levels between the current scenario and each future scenario. This spatial analysis helps identify specific regions where air

[1]The colours are derived from the EEA guidelines, and the range values correspond to those presented in Table 2.4 in Chapter 2.

AQI Values	Levels of Concern
0 - 50	Good
51 - 100	Fair
101 - 150	Moderate
151 - 200	Poor
201 - 300	Very Poor
301 and higher	Extremely Poor

Figure 8.1: AQI values with their associated colours.

quality improvements are most prominent, providing valuable insights for targeted policy interventions.

By analysing these results, we aim to provide a thorough understanding of how the increasing penetration of electric vehicles, and the reduction of older, higher-emission vehicles, contribute to changes in AQI levels across Valencia. This information is essential for policymakers and urban planners in developing strategies that enhance air quality and promote sustainable urban environments.

8.2.1 Quantitative Analysis of AQI Values

As presented in Table 8.2, there is a lowered trend in average AQI values as Valencia's vehicle fleet shifts from predominantly diesel and petrol vehicles to electric ones.

In the current scenario, the average AQI is 127, placing it within the "Moderate" category according to the established thresholds. This means that, under current conditions, air quality is concerning but not severe, with potential health implications for sensitive individuals. However, the simulations show that, by 2030, the average AQI will decrease to 98, entering the "Fair" category, a 29-point improvement. This shift reflects the transition from Euro 4 diesel vehicles to the Euro 6 EVs. This improvement in air quality is expected to significantly reduce

Table 8.2: Average AQI and difference with respect to the current scenario.

Scenario	Avg. AQI	Difference w.r.t. current
Current	127	N/A
2030	98	-29
2035	71	-56
2040	58	-69
2045	53	-74
2050	51	-76

the incidence of respiratory diseases and other health issues related to poor air quality.

From 2030 to 2035, we observe a more significant reduction in AQI, dropping by 27 points, resulting in an average AQI of 71. This improvement can be attributed to a 20% increase in electric vehicle share (from 15% to 35%), as older diesel and petrol vehicles are replaced by cleaner alternatives (see Table 8.1). This marks a turning point, as the increased penetration of electric vehicles substantially affects pollutant levels, further enhancing air quality. With these data, we assume that, by 2035, most of the city will experience air quality in the "Fair" range, indicating that public health risks are significantly reduced.

The trend continues in later years, with AQI values progressively falling to 58 in 2040, 53 in 2045, and finally reaching 51 by 2050. By 2050, Valencia's air quality will consistently fall almost within the "Good" category, a drastic improvement of 76 points compared to the current situation. This outcome is driven by the near-complete transition to electric vehicles, which represent 80% of the fleet by 2050, and the absence of older diesel and petrol vehicles, which emit far more significant amounts of pollutants such as NO_x.

To complement the average AQI values, Figure 8.2 shows the normal distribution of AQI for each scenario, providing a deeper understanding of how air quality varies across different city areas.

In the current scenario (Figure 8.2a), the distribution is skewed toward higher AQI values, with many values falling into the "Moderate" or even "Poor" categories, and with no points within the "Good" category. This indicates that large portions of Valencia are exposed to harmful levels of air pollution, with significant public health risks. In addition, the long tail that gets into the "Very Poor" category highlights the variability in pollution levels across the city, where some areas face more serious pollution challenges.

As we move forward to 2030 and 2035 (see Figures 8.2b and 8.2c), the dis-

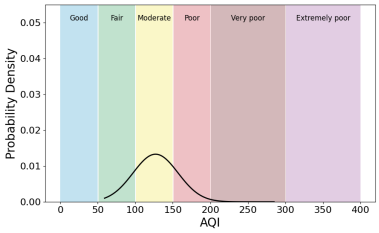

(a) Current.

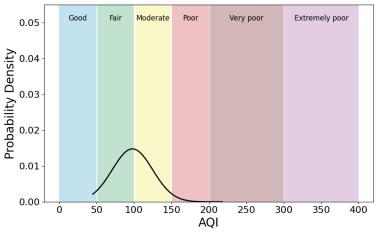

(b) Year 2030.

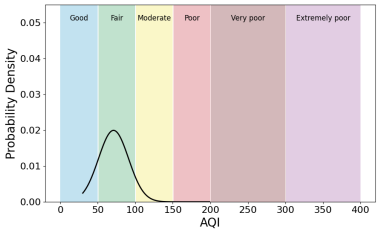

(c) Year 2035.

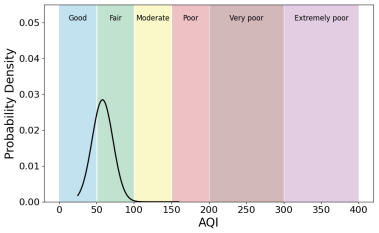

(d) Year 2040.

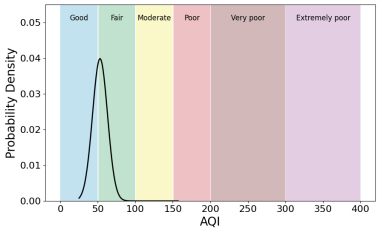

(e) Year 2045.

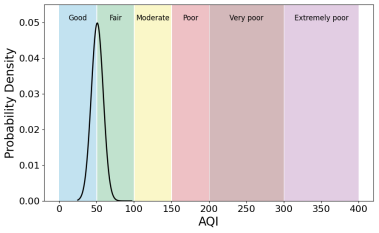

(f) Year 2050.

Figure 8.2: Air quality normal distribution in Valencia for the different years.

tribution shifts significantly leftward, reflecting the positive impact of replacing older diesel and petrol vehicles with electric alternatives. This shift is particularly pronounced in 2035 when EV adoption will increase to 35%. The more uniform distributions and shorter tails in these scenarios indicate a lower standard deviation of air quality, suggesting that pollution is becoming less concentrated in specific urban hotspots.

By 2040 (Figure 8.2d), the distribution narrows further, having a higher peak. This shows a clear trend toward lower AQI values. The average AQI drops, and

most points now fall into the "Fair" air quality range, with a low standard deviation, getting almost no points into the "Poor" category. This improvement means a more consistent reduction in air pollution across the city, driven by a continued increase in electric vehicle penetration, reducing dependence on conventional combustion engines.

Finally, the 2045 and 2050 scenarios (see Figures 8.2e and 8.2f) reveal an even tighter distribution centred around the "Good" and "Fair" categories. Their short tails suggest a narrower standard deviation, further confirming the homogenisation of air quality across the city, with most points consistently improving air conditions. By 2050, nearly all regions of Valencia will have AQI values close to 50, with a low standard deviation, showing that high-pollution areas have been almost entirely eradicated.

8.2.2 Spatial Visualisation of AQI Distributions

As the generated heatmaps show (see Figure 8.3), the spatial analysis of AQI across Valencia offers critical insights into the city's evolving pollution landscape under different vehicle fleet compositions. By analysing these changes over time, we can better understand the environmental impact of transitioning to electric vehicles and reducing reliance on traditional internal combustion engines.

In the current scenario (Figure 8.3a), the air quality across Valencia remains a significant public health concern, with all districts falling into the "Moderate" and "Poor" AQI categories. This is particularly pronounced in central areas with a concentration of vehicle congestion and, consequently, emissions. We can observe a big red stain in the middle of the city, which indicates that these areas are subjected to harmful levels of pollutants, such as NO_x and PM_x, which pose serious risks to the residents' health.

However, as we move to the 2030 scenario (Figure 8.3b), a notable improvement in air quality is observed, with much of the city transitioning into the Fair AQI category. This shift can be attributed to the gradual adoption of EVs, which comprise 15% of the vehicle fleet, replacing older diesel and petrol vehicles. Despite these improvements, certain areas, such as the city centre and some peripheral areas close to the highway, continue to show "Moderate" levels of air pollution. This underscores the urgent need for continued interventions in these zones, ensuring that no area is left behind in the transition to cleaner air.

The 2035 scenario (Figure 8.3c) brings a more pronounced improvement, with all the districts now displaying AQI values within the Fair category. By 2035, 35% of the vehicle fleet has shifted to electric alternatives, which significantly reduces emissions. As a result, pollution levels in central areas that previously fell within the "Poor" air quality category have significantly decreased.

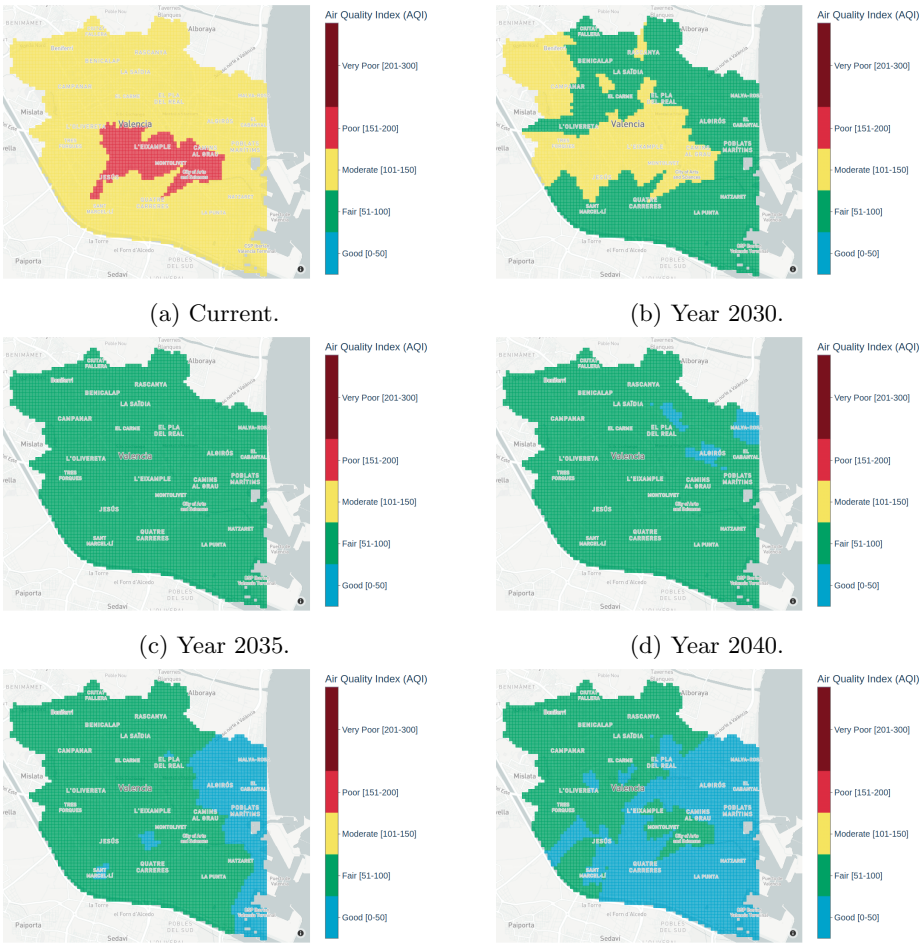

(a) Current.

(b) Year 2030.

(c) Year 2035.

(d) Year 2040.

(e) Year 2045.

(f) Year 2050.

Figure 8.3: Evolution of air quality in Valencia for the different years.

In the 2040 scenario (Figure 8.3d), Valencia significantly improves air quality, with 45% of vehicles being electric. This transition has resulted in a few areas having the “Good ” air quality category, leaving most areas with the “Fair” category. Progressing to the 2045 scenario (Figure 8.3e), the situation looks even more optimistic, with 60% of the vehicle fleet including electric vehicles. At this point,

the city has more areas falling within the "Good" category.

Finally, half of Valencia's districts achieve the "Good" air quality category in the 2050 scenario (Figure 8.3f). The scenario predicts that 80% of the city's vehicles will be electric, significantly reducing NO_x and PM_x emissions. The complete phase-out of older diesel and petrol vehicles has resulted in consistently low AQI values throughout the city. The improvement in air quality in this scenario is particularly significant in areas that previously suffered from poor air quality.

Regarding the difference heatmaps, these are shown in Figure 8.4. This figure illustrates the AQI changes between the current scenario and future vehicle fleet compositions across different years.

Firstly, we observe significant reductions in AQI across various districts by comparing the current scenario and 2030 (Figure 8.4a). Notably, areas near the centre show moderate improvements, reflecting a reduction in emissions as the fleet composition shifts toward electric vehicles. However, the overall difference is moderate, suggesting that this initial phase of vehicle replacement is insufficient to bring about dramatic reductions in air pollution.

Moving forward to 2035 (Figure 8.4b), the AQI reduction becomes more pronounced, especially in districts near the centre and close to the port. These regions experience reductions of up to 50 AQI points. This improvement coincides with a substantial rise in the share of electric vehicles in the fleet (20% increase), which replaces a large portion of older diesel and petrol vehicles.

Thirdly, the heatmaps for 2040 and 2045 (Figures 8.4c and 8.4d) show even more significant changes. Most areas now experience AQI reductions exceeding 50 points, with several districts in the eastern and centre parts of Valencia achieving reductions approaching 100 points. By this time, the city's vehicle fleet consists primarily of Euro 6 petrol, hybrid, and electric vehicles, with nearly half of the fleet comprising electric vehicles. The impact on AQI is evident, as most city areas shift from "Moderate" to "Fair" or "Good".

Finally, the 2050 scenario (Figure 8.4e) presents the most dramatic reduction in AQI levels across the city, with most of the map having bright colours. With an 80% electric vehicle share, AQI reductions of up to 100 points are common, especially in central districts. As seen earlier, almost all areas of Valencia now fall into the "Good" or "Fair" categories, showing a significant improvement in air quality, and a corresponding reduction in public health risks associated with air pollution.

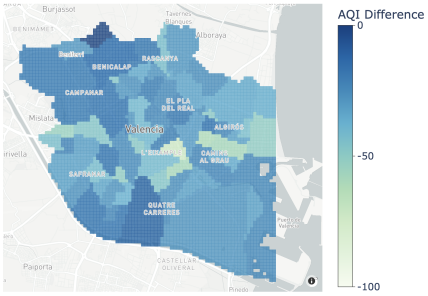

(a) Year 2030.

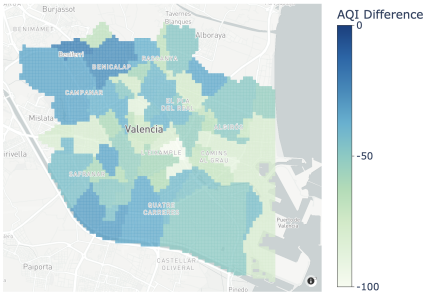

(b) Year 2035.

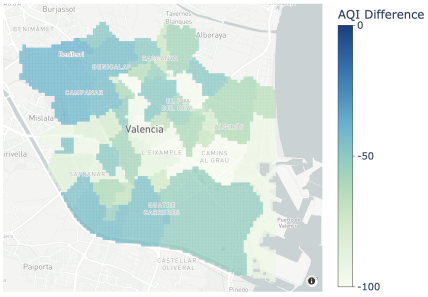

(c) Year 2040.

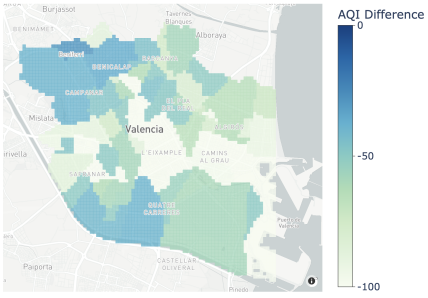

(d) Year 2045.

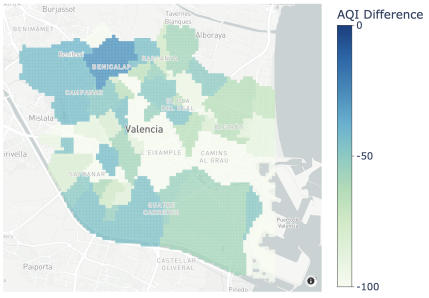

(e) Year 2050.

Figure 8.4: Difference in AQI levels in Valencia for the different years with respect to the current situation.

8.3 Summary

In this chapter, we have analysed the potential impact of Valencia's projected vehicular fleet evolution on urban air quality. Acknowledging the absence of specific local projections, we adapted fleet evolution scenarios from Gassner *et al.*'s study [141] for Vienna, given the similarities between the two European cities in terms of regulations and urban characteristics. In particular, we assumed a pessimistic scenario regarding public transportation growth, focusing on the increasing adoption of electric vehicles due to policy incentives and technological advancements.

We presented our proposed fleet composition from the current state to 2050, showing a significant decrease in older diesel and petrol vehicles, and a substantial increase in electric vehicles, being that the latter reach 80% of the fleet by 2050. Using these data projections, we conducted simulations to assess how these changes affect the AQI across Valencia.

Our quantitative analysis revealed a consistent downward trend in average AQI values as the fleet transitions towards electric vehicles. The average AQI decreased from 127 in the current scenario, to 51 by 2050, moving from the "Moderate" and "Poor" towards the "Good" air quality category. The standard distribution plots of AQI for each scenario showed a significant shift towards lower AQI values over time, indicating widespread improvements in air quality across the city.

Spatial visualisation through AQI heatmaps highlighted substantial reductions in pollutant concentrations, particularly in urban areas that previously experienced high pollution levels. Difference heatmaps between current and future scenarios underscored the areas with the most significant improvements, correlating with regions of dense traffic and high initial emissions.

In summary, this chapter demonstrated that the projected evolution of Valencia's vehicle fleet towards a greater electric vehicle adoption can lead to significant improvements in urban air quality over time. The findings emphasise the importance of promoting cleaner vehicle technologies and provide crucial insights for policymakers and urban planners. Specifically, our research suggests that policies promoting electric vehicle adoption and improving public transportation can significantly enhance air quality, public health, and the sustainability of urban environments.

Chapter 9

Conclusions, Future Work and Publications

Urban air pollution remains a critical challenge, significantly affecting public health and environmental sustainability. With the rapid growth of urban populations and increasing vehicular traffic, cities worldwide struggle to manage congestion while minimising air pollution. Traditional traffic management strategies have focused on improving traffic flow, often ignoring the environmental impacts of vehicular emissions. However, addressing urban air pollution is essential given its direct link to health problems and reduced quality of life.

Recent advancements in ITS and vehicular communication offer new opportunities to attack these issues. By employing real-time data, advanced traffic modelling, and adaptive algorithms, traffic management solutions can be developed to optimise traffic flow while prioritising environmental considerations. This requires a comprehensive framework that integrates realistic traffic simulation, accurate emission modelling, dynamic re-routing based on environmental data, and an exhaustive assessment of the environmental impacts of traffic restrictions. Throughout this thesis we addressed several key challenges: (i) creating realistic traffic models; (ii) accurately characterising vehicle emissions and air quality data; (iii) developing context-aware routing algorithms; (iv) evaluating the environmental effects of traffic restrictions; and (v) predicting future air quality with evolving vehicle fleets. We now summarise our findings, discuss potential directions for

future work, and showcase the publications derived from this research.

9.1 Conclusions

We began by establishing a robust vehicular traffic management framework. This framework integrated traffic data collection from induction loop detectors, traffic simulation using SUMO, emission modelling with the HBEFA model, and pollutant dispersion analysis using both the "Fixed Box Model" and GRAL. By combining these components, we provided a solid foundation for evaluating the impact of traffic management strategies on urban air quality. Integrating SUMO with GRAL through our SUMO2GRAL tool enabled detailed and accurate pollutant dispersion modelling in urban environments, accounting for building geometries and meteorological conditions.

Once our framework was created, we started by addressing the challenge of generating realistic traffic demand based on induction loop data. We analysed the limitations of existing tools like DFROUTER, which produced unrealistic traffic volumes and route lengths in urban contexts. To overcome these limitations, we proposed a novel reverse-engineering approach that significantly improved the accuracy of traffic volume, spatial distribution of origin points, and route lengths. Our solution reduced the discrepancy between simulated and real traffic volumes, achieving a more realistic representation of traffic flows. Specifically, we decreased the average traffic volume deviation from 516% to a much lower percentage compared to real measurements. Additionally, we improved the distribution of departure areas by increasing the number of origin points by 418% over DFROUTER, and increased the average route length by 78%, resulting in more realistic travel distances within the simulation.

After creating the traffic demand, we focused on a static approach to traffic re-routing to reduce air pollution in specific urban areas. We developed a method that adjusts traffic weights on street segments using a static α value, influencing routing decisions to minimise pollution in targeted zones. Applying this method to Valencia, we tested two models: full and partial traffic isolation around the old riverbed. Our experiments demonstrated that the partial isolation model, with an optimal α value of 2.7, achieved better results, reducing pollutant concentrations and improving the AQI in the target area by 19 points with a minimal impact on the overall traffic flow. This approach showed that environmental goals could be met without significant disruptions, highlighting the effectiveness of static traffic management using predefined environmental constraints.

Building upon the static approach, we introduced a dynamic traffic re-routing algorithm that adjusts vehicle routes based on real-time air quality data and vehicle

emission profiles. By incorporating an "Emission Sensitivity Factor" (Δ), we controlled the algorithm's responsiveness to environmental conditions. Simulating environmental crisis scenarios in Valencia, such as building fires and smog episodes, we found that an optimal Δ value of 6 significantly reduced pollutant concentrations by 15% in affected areas without causing substantial increases elsewhere in the city. The dynamic re-routing strategy demonstrated minimal impact on traffic efficiency, with only minor increases in average travel time and route length, and minor changes in waiting time and time loss. Likewise, average speeds remained stable, confirming that air quality benefits were achieved without significantly compromising traffic flow.

Finally, we examined the impact of increasing the share of EVs in the urban fleet on future air quality. Our simulations showed that, as the proportion of EVs increases, the AQI levels in the city decrease correspondingly. This finding suggests that encouraging the adoption of electric vehicles can be an effective long-term strategy for improving urban air quality. The results provide valuable insights for policymakers and urban planners considering initiatives to encourage electric vehicle use, highlighting the potential for significant air quality improvements as the vehicle fleet evolves.

With the contributions mentioned above, the original goals of this thesis have been achieved, so this dissertation can now be concluded.

9.2 Future Work

This thesis has laid a solid foundation for integrating air quality considerations into urban traffic management systems, but several research opportunities remain to extend and enhance the framework proposed here. Below are some potential future works derived from the findings of this thesis.

One of the most promising directions for future research involves enhancing the dynamic re-routing algorithm. The current study has shown the potential of dynamic traffic management strategies to reduce pollution during environmental crises, such as building fires or smog episodes. However, future research should explore further optimisation of the "Emission Sensitivity Factor" (Δ) by incorporating more pollutants beyond NO_x and PM_x, such as O_3 and SO_2. Additionally, integrating machine learning models to predict air quality and traffic patterns could improve the precision of the re-routing algorithm, enabling it to adapt more intelligently to real-time environmental data. This would enhance the algorithm's capability to mitigate pollution under various urban conditions, such as industrial accidents or heavy traffic congestion.

Similarly, SUMO2GRAL presents another area with potential for future development. While the tool has proven effective in combining traffic simulations with pollutant dispersion modelling, future enhancements could focus on adding more features based on feedback from the research community. Testing SUMO2GRAL across various urban settings and under various traffic policies would help solidify its utility.

Another important direction for future work is implementing and testing our proposed traffic management solutions in real controlled environments to demonstrate their effectiveness. While our simulations have shown promising results, validating these approaches in real-world scenarios is essential for assessing their practical applicability. By conducting pilot studies within controlled urban areas, we can evaluate the operational feasibility, identify potential implementation challenges, and gather empirical data to refine our models and algorithms. This would provide valuable insights into the interaction between traffic systems and environmental factors.

Finally, we could explore extending the applicability of traffic re-routing beyond pollution reduction. For example, optimising traffic flows during holidays, major city events, or emergency evacuations represents an opportunity for further exploration. By developing algorithms that adapt to daily traffic conditions and exceptional events, we could make traffic management more flexible, efficient, and capable of serving various urban needs.

In conclusion, while this thesis has significantly improved urban traffic management from an environmental perspective, the field has room for further research and innovation. Integrating more pollutants, enhanced simulation tools, optimised algorithms, and real-world testing will enable the development of even more robust and adaptive traffic management solutions, ultimately helping to create healthier, more sustainable urban environments.

9.3 Publications

This section lists the publications that are a result of this thesis. It also covers other collaborations and related publications published during this time.

International Journals

1. Padrón, J. D., Soler, D., Calafate, C. T., Cano, J. C., & Manzoni, P. (2022). Improving air quality in urban recreational areas through smart traffic management, Sustainability 2022. **I.F. 2022: 3.9; JCR: Q2 Category.**

2. Padrón, J. D., Hernández-Orallo, E., Calafate, C. T., Soler, D., Cano, J. C., & Manzoni, P. (2023). Realistic traffic model for urban environments based on induction loop data, Simulation modelling practice and theory 2023. **I.F. 2023: 3.5; JCR: Q1 Category.**

3. Padrón, J. D., Calafate, C. T., Cano, J. C., & Manzoni, P. (2024). Dynamic Traffic Routing for Air Quality Enhancement During Urban Environmental Crises, Transportation research part d: transport and environment 2024. **I.F. 2023: 7.4; JCR: Q1 Category.** (Under review)

International Conferences

1. Padrón, J. D., Terol, M., Zambrano-Martinez, J. L., Calafate, C. T., Cano, J. C., & Manzoni, P. (2021, September). Assessing the impact of road traffic constraints on pollution. In 2021 IEEE 94th Vehicular Technology Conference (VTC2021-Fall) (pp. 1-5). IEEE. **Core B / GGS class 2.**

2. Riviere, M., Padrón, J. D., Calafate, C. T., Cano, J. C., & Razafindralambo, T. (2023, June). Improving emergency vehicles flow in urban environments through SDN-based V2X communications. In 2023 IEEE 97th Vehicular Technology Conference (VTC2023-Spring) (pp. 1-6). IEEE. **Core B / GGS class 2.**

3. Martínez, A., Padrón, J. D., Zambrano-Martinez, J. L., & Calafate, C. T. (2023, December). Adaptive Sharing of IoT Resources Through SDN-Based Microsegmentation of Services Using Mininet. In International Conference on Simulation Tools and Techniques (pp. 229-242). Cham: Springer Nature Switzerland.

4. Padrón, J. D., Behrisch, M., & Calafate, C. T. (2024, October). SUMO2GRAL: A tool to simplify the workflow of estimating pollutant concentrations in urban areas. In 2024 IEEE/ACM 28th International Symposium on Distributed Simulation and Real Time Applications (DS-RT 2024) (pp.42-47). IEEE. **Core C.**

National Conferences (Spain)

1. Padrón, J. D., Terol, M., Zambrano-Martinez, J. L., Calafate, C. T., Cano, J. C., & Manzoni, P (2021, September). Evaluación del impacto de las restricciones de tráfico en los niveles de contaminación. In V Jornadas de Computación Empotrada y Reconfigurable.

2. Baidez, S., Zambrano-Martinez, J. L., Padrón, J. D., Aksenova, T., & Calafate, C. T. (2022, September). Cactus Pi: gestión remota de un mini-invernadero usando Telegram. In VI Jornadas de Computación Empotrada y Reconfigurable.

3. Tarazona-Gala, J., Padrón, J. D., & Calafate, C. T. (2024, June). Sistema móvil para la medición de PM2.5: estudio en el área de Valencia. In VIII Jornadas de Computación Empotrada y Reconfigurable.

Acronyms

A

API	Application Programming Interface
AQI	Air Quality Index
ATIS	Advanced Traveller Information Systems

B

BAM	Beta Attenuation Monitor

C

CDR	Call Detail Records
CFD	Computational Fluid Dynamics
CO_2	Carbon Dioxide
CO	Carbon Monoxide
CORINAIR	Coordination Information AIR
COPERT	Computer Programme to Calculate Emissions from Road Transport
CMEM	Comprehensive Modal Emissions Model
CSV	Comma Separated Values

D

DLR	German Aerospace Centre
DGT	Spanish Department of Traffic

E

ECDF	Empirical Cumulative Distribution Function
EEA	European Environmental Agency
EV	Electric Vehicle

F

FCD	Floating Car Data

G

GPS	Global Positioning System
GRAL	Graz Lagrangian Model
GIS	Geographic Information System

H

HBEFA	Handbook Emission Factors for Road Transport
HC	Hydrocarbon

I

ITS	Intelligent Transportation System

L

LTE	Long Term Evolution
LEZ	Low Emission Zones
LiDAR	Light Detection and Ranging

M

MSE	Mean Squared Error
MLD	Multi-Level Dijsktra

MOVES	Motor Vehicle Emission Simulator

N

NO_x	Nitrogen Oxides
NO	Nitric Oxide
NO_2	Nitrogen Dioxide

O

OD	Origin-Destination
OSM	OpenStreetMap
O_3	Ozone

P

PHEM	Passenger Car and Heavy-duty Emission Model
PM_x	Particulate Matter

R

RSU	Road Side Unit

S

SUMO	Simulation of Urban MObility
SNA	Social Network Analysis
SO_2	Sulphur Dioxide
SEPAR	Spanish Society of Pneumology and Thoracic Surgery

T

TRANSYT	TRAffic Network StudY Tool
TEE	Traffic Energy and Emissions Model
TEOM	Tapered Element Oscillating Microbalance

U

USEPA	United States Environmental Protection Agency

V

VANET	Vehicular Ad-Hoc Network
VSN	Vehicular Social Networks
V2I	Vehicle to Infrastructure
V2X	Vehicle to Everything
V2V	Vehicle to Vehicle
VeTESS	Vehicle Transient Emissions Simulation Software
VOC	Volatile Organic Compound

X

XML	eXtensible Markup Language

Bibliography

[1] A. M. Anwar and A. T. Oakil. "Smart Transportation Systems in Smart Cities: Practices, Challenges, and Opportunities for Saudi Cities". In: *Smart Cities: Social and Environmental Challenges and Opportunities for Local Authorities* (2023), pp. 315–337 (cited on p. 1).

[2] K. K. Yim, S. Wong, A. Chen, C. K. Wong, and W. H. Lam. "A reliability-based land use and transportation optimization model". In: *Transportation Research Part C: Emerging Technologies* 19.2 (2011), pp. 351–362 (cited on p. 1).

[3] Intel. *Urban Mobility and the Future of Smart Transportation*. `https://www.intel.com/content/www/us/en/transportation/urban-mobility.html`. Last accessed 26th September 2024. 2020 (cited on p. 1).

[4] J.-P. Rodrigue. *The geography of transport systems*. Routledge, 2020 (cited on p. 1).

[5] S. De Luca, R. Di Pace, S. Memoli, and L. Pariota. "Sustainable traffic management in an urban area: An integrated framework for real-time traffic control and route guidance design". In: *Sustainability* 12.2 (2020), p. 726 (cited on p. 2).

[6] H Boogaard, A. Patton, R. Atkinson, et al. "Long-term exposure to traffic-related air pollution and selected health outcomes: A systematic review and

meta-analysis". In: *Environment international* 164 (2022), p. 107262 (cited on p. 2).

[7] European Environmental Agency (EEA). *The costs to health and the environment from industrial air pollution in Europe – 2024 update*. https://www.eea.europa.eu/publications/the-cost-to-health-and-the. Last accessed 4th November 2024. 2024 (cited on p. 2).

[8] SEPAR. *Air pollution causes 10,000 deaths a year in Spain, many more than the 1,700 caused by traffic accidents*. https://www.separ.es/sites/default/files/SEPAR%20NP%20medio%20ambiente%20y%20salud%20%284%20jun%2019%29.pdf. Last accessed 25th September 2024. June 2019 (cited on p. 2).

[9] D. Schrank, B. Eisele, T. Lomax, J. Bak, et al. "2015 urban mobility scorecard". In: *Texas Transportation Institute* (2015) (cited on p. 2).

[10] T. Yigitcanlar, M. Wilson, and M. Kamruzzaman. "Disruptive impacts of automated driving systems on the built environment and land use: An urban planner's perspective". In: *Journal of open innovation: Technology, market, and complexity* 5.2 (2019), p. 24 (cited on p. 2).

[11] Union of Concerned Scientists. *Cars, Trucks, Buses and Air Pollution*. https://www.ucsusa.org/resources/cars-trucks-buses-and-air-pollution. Last accessed 19th September 2024. 2023 (cited on p. 8).

[12] United States Environmental Protection Agency (USEPA). *Air Pollution from Mobile Sources*. https://www.epa.gov/mobile-source-pollution. Last accessed 19th September 2024. 2024 (cited on p. 8).

[13] European Environment Agency (EEA). *Explaining Road Transport Emissions*. https://www.eea.europa.eu/publications/explaining-road-transport-emissions. Last accessed 19th September 2024. 2016 (cited on p. 8).

[14] United States Environmental Protection Agency (USEPA). *Nitrogen Dioxide (NO2) Pollution*. https://www.epa.gov/no2-pollution. Last accessed 19th September 2024. 2024 (cited on p. 8).

[15] J. Heywood. *Internal Combustion Engine Fundamentals*. New York, NY, USA: McGraw-Hill, 1988 (cited on p. 8).

[16] United States Environmental Protection Agency (USEPA). *Health Effects of Nitrogen Dioxide*. https://www.epa.gov/no2-pollution/basic-information-about-no2#Effects. Last accessed 19th September 2024. 2024 (cited on p. 8).

[17] K.-H. Kim, E. Kabir, and S. Kabir. "A review on the human health impact of airborne particulate matter". In: *Environ. Int.* 74 (2015), pp. 136–143 (cited on p. 8).

[18] United States Environmental Protection Agency (USEPA). *What is Acid Rain?* https://www.epa.gov/acidrain/what-acid-rain. Last accessed 19th September 2024. 2024 (cited on p. 8).

[19] Office for National Statistics (ONS). *Road Transport and Air Emissions*. https://www.ons.gov.uk/economy/environmentalaccounts/articles/roadtransportandairemissions/2019-09-16. Last accessed 19th September 2024. 2018 (cited on p. 9).

[20] United States Environmental Protection Agency (USEPA). *Health and Environmental Effects of Particulate Matter (PM)*. https://www.epa.gov/pm-pollution/health-and-environmental-effects-particulate-matter-pm. Last accessed 19th September 2024. 2024 (cited on p. 9).

[21] United States Environmental Protection Agency (USEPA). *Particulate Matter (PM) Basics*. https://www.epa.gov/pm-pollution/particulate-matter-pm-basics. Last accessed 19th September 2024. 2024 (cited on p. 9).

[22] Intergovernmental Panel on Climate Change (IPCC). *Climate Change 2013: The Physical Science Basis*. Cambridge, UK: Cambridge University Press, 2013 (cited on p. 9).

[23] United States Environmental Protection Agency (USEPA). *Carbon Monoxide (CO) Pollution in Outdoor Air*. https://www.epa.gov/co-pollution. Last accessed 19th September 2024. 2024 (cited on p. 9).

[24] United States Environmental Protection Agency (USEPA). *Basic Information about Carbon Monoxide (CO) Outdoor Air Pollution*. https://www.epa.gov/co-pollution/basic-information-about-carbon-monoxide-co-outdoor-air-pollution#Effects. Last accessed 19th September 2024. 2024 (cited on p. 9).

[25] United States Environmental Protection Agency (USEPA). *Sulfur Dioxide (SO2) Pollution*. https://www.epa.gov/so2-pollution. Last accessed 19th September 2024. 2024 (cited on p. 10).

[26] United States Environmental Protection Agency (USEPA). *Inventory of U.S. Greenhouse Gas Emissions and Sinks*. https://www.epa.gov/ghgemissions/inventory-us-greenhouse-gas-emissions-and-sinks. Last accessed 19th September 2024. 2024 (cited on p. 10).

[27] United States Environmental Protection Agency (USEPA). *Technical Overview of Volatile Organic Compounds*. https://www.epa.gov/indoor-air-quality-iaq/technical-overview-volatile-organic-compounds. Last accessed 19th September 2024. 2024 (cited on p. 10).

[28] United States Environmental Protection Agency (USEPA). *Volatile Organic Compounds' Impact on Indoor Air Quality*. https://www.epa.gov/indoor-air-quality-iaq/volatile-organic-compounds-impact-indoor-air-quality. Last accessed 19th September 2024. 2024 (cited on p. 10).

[29] United States Environmental Protection Agency (USEPA). *Health Effects of Ozone Pollution*. https://www.epa.gov/ground-level-ozone-pollution/health-effects-ozone-pollution. Last accessed 19th September 2024. 2024 (cited on p. 10).

[30] W. Spangl, J Schneider, L Moosmann, and C Nagl. *Representativeness and classification of air quality monitoring stations*. Umweltbundesamt Dessau-Roßlau, Germany, 2007 (cited on p. 10).

[31] G Villena, I Bejan, R Kurtenbach, P Wiesen, and J Kleffmann. "Interferences of commercial NO 2 instruments in the urban atmosphere and in a smog chamber". In: *Atmospheric Measurement Techniques* 5.1 (2012), pp. 149–159 (cited on p. 11).

[32] Z. Wang, L. Calderón, A. P. Patton, M. Sorensen Allacci, J. Senick, R. Wener, C. J. Andrews, and G. Mainelis. "Comparison of real-time instruments and gravimetric method when measuring particulate matter in a residential building". In: *Journal of the Air & Waste Management Association* 66.11 (2016), pp. 1109–1120 (cited on p. 11).

[33] J. H. Seinfeld and S. N. Pandis. *Atmospheric chemistry and physics: from air pollution to climate change*. John Wiley & Sons, 2016 (cited on p. 11).

[34] Indiana Department of Environmental Management. *Air Samplers and Monitoring Instruments*. =https://www.in.gov/idem/airmonitoring/air-samplers-and-monitoring-instruments/. Last accessed 20th September 2024. 2024 (cited on p. 12).

[35] N. Castell, F. R. Dauge, P. Schneider, M. Vogt, U. Lerner, B. Fishbain, D. Broday, and A. Bartonova. "Can commercial low-cost sensor platforms contribute to air quality monitoring and exposure estimates?" In: *Environment international* 99 (2017), pp. 293–302 (cited on p. 12).

[36] L. Spinelle, M. Gerboles, G. Kok, S. Persijn, and T. Sauerwald. "Review of portable and low-cost sensors for the ambient air monitoring of benzene and other volatile organic compounds". In: *Sensors* 17.7 (2017), p. 1520 (cited on p. 12).

[37] F. M. Bulot, S. J. Johnston, P. J. Basford, et al. "Long-term field comparison of multiple low-cost particulate matter sensors in an outdoor urban environment". In: *Scientific reports* 9.1 (2019), p. 7497 (cited on p. 12).

[38] W. Ju, C. Lu, C. Liu, W. Jiang, Y. Zhang, and F. Hong. "Rapid Identification of Atmospheric Gaseous Pollutants Using Fourier-Transform Infrared Spectroscopy Combined with Independent Component Analysis". In: *Journal of Spectroscopy* 2020.1 (2020), p. 8920732 (cited on p. 12).

[39] A. Van Donkelaar, R. V. Martin, M. Brauer, and B. L. Boys. "Use of satellite observations for long-term exposure assessment of global concentrations of fine particulate matter". In: *Environmental health perspectives* 123.2 (2015), pp. 135–143 (cited on p. 12).

[40] R. V. Martin. “Satellite remote sensing of surface air quality”. In: *Atmospheric environment* 42.34 (2008), pp. 7823–7843 (cited on p. 13).

[41] S. Rodríguez and J. López-Darias. “Dust and tropical PMx aerosols in Cape Verde: Sources, vertical distributions and stratified transport from North Africa”. In: *Atmospheric Research* 263 (2021), p. 105793 (cited on p. 13).

[42] R. S. Sokhi, N. Moussiopoulos, A. Baklanov, et al. “Advances in air quality research–current and emerging challenges”. In: *Atmospheric Chemistry and Physics Discussions* 2021 (2021), pp. 1–133 (cited on p. 13).

[43] European-Parliament. “Directive 2008/50/EC of the European Parliament and of the Council of 21 May 2008 on ambient air quality and cleaner air for Europe”. In: *Document 02008L0050-20150918* (2015) (cited on p. 14).

[44] European Environmental Agency (EEA). *European Air Quality Index*. `https://www.eea.europa.eu/themes/air/air-quality-index`. Last accessed 21st September 2024. 2024 (cited on p. 14).

[45] United States Environmental Protection Agency. “Technical Assistance Document for the Reporting of Daily Air Quality - the Air Quality Index (AQI)”. In: *EPA 454/B-18-007* (2018) (cited on p. 14).

[46] European Environmental Agency (EEA). *Sources and emissions of air pollutants in Europe*. `https://www.eea.europa.eu/publications/air-quality-in-europe-2022/sources-and-emissions-of-air`. Last accessed 21st September 2024. 2022 (cited on p. 17).

[47] J. M. Stockie. “The mathematics of atmospheric dispersion modeling”. In: *Siam Review* 53.2 (2011), pp. 349–372 (cited on p. 17).

[48] M. Kuntner and D. Öttl. *GRAL - Graz Lagrangian Model*. `https://gral.tugraz.at/`. Last accessed 11th September 2024. 2024 (cited on p. 17).

[49] A. Baklanov, O. Hänninen, L. H. Slørdal, et al. “Integrated systems for forecasting urban meteorology, air pollution and population exposure”. In: *Atmospheric Chemistry and Physics* 7.3 (2007), pp. 855–874 (cited on p. 17).

[50] Y. Tominaga and T. Stathopoulos. “CFD modeling of pollution dispersion in building array: evaluation of turbulent scalar flux modeling in RANS model using LES results”. In: *Journal of Wind Engineering and Industrial Aerodynamics* 104 (2012), pp. 484–491 (cited on p. 18).

[51] L. Ortolano. “Estimating air quality impacts”. In: *Environmental Impact Assessment Review* 5.1 (1985), pp. 9–35 (cited on p. 18).

[52] L. Canter. “Methods for the assessment of ground water pollution potential”. In: *Ground Water Quality, John Wiley and Sons, New York NY. 1985. p 270-306, 1 fig, 22 tab, 15 ref.* (1985) (cited on p. 18).

[53] A. Berchet, K. Zink, D. Oettl, J. Brunner, L. Emmenegger, and D. Brunner. “Evaluation of high-resolution gramm–gral (v15. 12/v14. 8) no x simulations over the city of zürich, switzerland”. In: *Geoscientific Model Development* 10.9 (2017), pp. 3441–3459 (cited on p. 19).

[54] A. A. Romanov, B. A. Gusev, E. V. Leonenko, A. N. Tamarovskaya, A. S. Vasiliev, N. E. Zaytcev, and I. K. Philippov. “Graz Lagrangian Model (GRAL) for pollutants tracking and estimating sources partial contributions to atmospheric pollution in highly urbanized areas”. In: *Atmosphere* 11.12 (2020), p. 1375 (cited on p. 19).

[55] G. Leduc. “Road traffic data: Collection methods and applications”. In: *Working Papers on Energy, Transport and Climate Change* 1.55 (2008), pp. 1–55 (cited on p. 22).

[56] N. K. Jain, R. Saini, and P. Mittal. “A review on traffic monitoring system techniques”. In: *Soft Computing: Theories and Applications* (2019), pp. 569–577. DOI: 10.1007/978-981-13-0589-4_53 (cited on p. 22).

[57] J. C. Herrera, D. B. Work, R. Herring, X. J. Ban, Q. Jacobson, and A. M. Bayen. “Evaluation of traffic data obtained via GPS-enabled mobile phones: The Mobile Century field experiment”. In: *Transportation Research Part C: Emerging Technologies* 18.4 (2010), pp. 568–583. DOI: 10.1016/j.trc.2009.10.006 (cited on p. 23).

[58] Q. Ge and D. Fukuda. “Updating origin–destination matrices with aggregated data of GPS traces”. In: *Transportation Research Part C: Emerging*

Technologies 69 (2016), pp. 291–312. DOI: 10.1016/j.trc.2016.06.002 (cited on p. 23).

[59] N. Caceres, L. M. Romero, F. G. Benitez, and J. M. del Castillo. "Traffic flow estimation models using cellular phone data". In: *IEEE Transactions on Intelligent Transportation Systems* 13.3 (2012), pp. 1430–1441. DOI: 10.1109/TITS.2012.2189006 (cited on p. 23).

[60] M. S. Iqbal, C. F. Choudhury, P. Wang, and M. C. González. "Development of origin–destination matrices using mobile phone call data". In: *Transportation Research Part C: Emerging Technologies* 40 (2014), pp. 63–74. DOI: 10.1016/j.trc.2014.01.002 (cited on p. 23).

[61] C. Mallikarjuna, A Phanindra, and K. R. Rao. "Traffic data collection under mixed traffic conditions using video image processing". In: *Journal of transportation engineering* 135.4 (2009), pp. 174–182. DOI: 10.1061/(ASCE)0733-947X(2009)135:4(174) (cited on p. 23).

[62] M. Savrasovs and I. Pticina. "Methodology of OD matrix estimation based on video recordings and traffic counts". In: *Procedia Engineering* 178 (2017), pp. 289–297. DOI: 10.1016/j.proeng.2017.01.116 (cited on p. 24).

[63] City Hall of Valencia. *Intensitat transit trams / Intensidad tráfico tramos*. https://valencia.opendatasoft.com/explore/dataset/intensitat-transit-trams-intensidad-trafico-tramos/api/. Last accessed 2nd July 2024. 2024 (cited on pp. 24, 50, 57).

[64] T. V. Nguyen, D. Krajzewicz, M. Fullerton, and E. Nicolay. "DFROUTER — Estimation of vehicle routes from cross-section measurements". In: *Modeling Mobility with Open Data*. Springer, 2015, pp. 3–23. DOI: 10.1007/978-3-319-15024-6_1 (cited on pp. 24, 38).

[65] S. Krauß. *Microscopic Modeling of Traffic Flow: Investigation of Collision Free Vehicle Dynamics*. Tech. rep. German Aerospace Centre (DLR), 1998 (cited on p. 25).

[66] S. A. Boxill and L. Yu. "An evaluation of traffic simulation models for supporting its". In: *Houston, TX: Development Centre for Transportation Training and Research, Texas Southern University* (2000) (cited on p. 25).

[67] TRL. *TRANSYT*. https://trlsoftware.com/products/junction-signal-design/transyt/. Last accessed 16th September 2024. 2024 (cited on p. 26).

[68] PTV. *PTV-VISUM*. https://www.ptvgroup.com/en/products/ptv-visum. Last accessed 16th September 2024. 2024 (cited on p. 26).

[69] W. Burghout, H. N. Koutsopoulos, and I. Andreasson. "Hybrid mesoscopic–microscopic traffic simulation". In: *Transportation Research Record* 1934.1 (2005), pp. 218–225 (cited on p. 26).

[70] M. Ben-Akiva, H. N. Koutsopoulos, C. Antoniou, and R. Balakrishna. "Traffic simulation with dynamit". In: *Fundamentals of traffic simulation* (2010), pp. 363–398 (cited on p. 26).

[71] C. Corporation. *TransModeler Traffic Simulation Software*. https://www.caliper.com/transmodeler/default.htm. Last accessed 16th September 2024. 2024 (cited on p. 26).

[72] PTV. *PTV-VISSIM*. https://www.ptvgroup.com/en/products/ptv-vissim. Last accessed 16th September 2024. 2024 (cited on p. 27).

[73] P. A. Lopez, M. Behrisch, L. Bieker-Walz, et al. "Microscopic traffic simulation using sumo". In: *2018 21st international conference on intelligent transportation systems (ITSC)*. IEEE. 2018, pp. 2575–2582. DOI: 10.1109/ITSC.2018.8569938 (cited on p. 27).

[74] German Aerospace Centre (DLR). *Traffic Simulations*. https://sumo.dlr.de/docs/Theory/Traffic_Simulations.html. Last accessed 16th September 2024. 2024 (cited on p. 28).

[75] P. G. Boulter, I. S. McCrae, and S. Latham. *A review of instantaneous emission models for road vehicles*. Transport Research Laboratory, 2007 (cited on p. 27).

[76] R. Smit, A. L. Brown, and Y. C. Chan. "Do air pollution emissions and fuel consumption models for roadways include the effects of congestion in the roadway traffic flow?" In: *Environmental Modelling & Software* 23.10-11 (2008), pp. 1262–1270 (cited on p. 28).

[77] P. J. Sturm, P. Weissenbacher, and S. Hausberger. "Modelling of real world vehicle emissions with a passenger car and heavy duty vehicle model". In: *International Journal of Vehicle Design* 18.3-4 (1997), pp. 312–323 (cited on p. 28).

[78] J. Hickman, D. Hassel, R. Joumard, Z. Samaras, and S. Sorenson. *MEET (Methodologies for Estimating Air Pollutant Emissions from Transport)*. European Commission, 1999 (cited on p. 28).

[79] R. Smit, D. Tormey, and P. Boulter. "The importance of instantaneous fuel consumption and emission models in road transport emission estimations". In: *International Journal of Sustainable Transportation* 2.2 (2008), pp. 111–131 (cited on p. 29).

[80] R. Joumard, P. Jost, J. Hickman, and Z. Samaras. "Hot passenger car emissions modelling as a function of speed and acceleration". In: *Science of The Total Environment* 169.1-3 (1995), pp. 167–174 (cited on p. 29).

[81] L. Ntziachristos and Z. Samaras. *COPERT 5: Computer programme to calculate emissions from road transport*. European Environment Agency, 2018 (cited on p. 29).

[82] U.S. Environmental Protection Agency. *Motor Vehicle Emission Simulator (MOVES) User Guide*. EPA-420-B-14-055, 2014 (cited on p. 29).

[83] INFRAS. *Handbook Emission Factors for Road Transport (HBEFA)*. Version 4.2. INFRAS, 2022 (cited on p. 29).

[84] L. I. Panis, C. Beckx, S. Broekx, I. De Vlieger, L. Schrooten, and L. Int Panis. "Modeling instantaneous traffic emission and the influence of traffic speed limits". In: *Science of The Total Environment* 371.1-3 (2006), pp. 270–285 (cited on p. 29).

[85] R. Borchiellini, G. Dematteis, and F. Silvestro. "Traffic emission and fuel consumption models". In: *SAE Technical Paper* (2000), pp. 2000–01–0485 (cited on p. 29).

[86] Italian National Agency for New Technologies, Energy and Sustainable Economic Development (ENEA). *Traffic Energy and Emissions Model (TEE)*. 2001 (cited on p. 29).

[87] E. Ericsson. "Independent driving pattern factors and their influence on fuel-use and exhaust emission factors". In: *Transportation Research Part D: Transport and Environment* 6.5 (2001), pp. 325–345 (cited on p. 29).

[88] H. C. Frey, A. Unal, J. Chen, and S. W. Poppell. "Modeling mobile source emissions based upon in-use and second-by-second data: Development of conceptual approaches for EPA's new MOVES model". In: *Transportation Research Record* 1842.1 (2003), pp. 98–106 (cited on p. 29).

[89] R. Smit, L. Ntziachristos, and P. Boulter. "Validation of road vehicle and traffic emission models—A review and meta-analysis". In: *Atmospheric Environment* 44.25 (2010), pp. 2943–2953 (cited on p. 29).

[90] R. Smit, J. McBroom, and B. Quest. "VERSIT+LD-A modal model of hot passenger car emissions". In: *Atmospheric Environment* 42.35 (2008), pp. 7368–7383 (cited on p. 29).

[91] H. Rakha, K. Ahn, and A. Trani. "Development of VT-Micro model for estimating hot stabilized light duty vehicle and truck emissions". In: *Transportation Research Part D: Transport and Environment* 9.1 (2004), pp. 49–74 (cited on p. 30).

[92] K. Ahn and H. Rakha. "The effects of route choice decisions on vehicle energy consumption and emissions". In: *Transportation Research Part D: Transport and Environment* 13.3 (2008), pp. 151–167 (cited on p. 30).

[93] S. Hausberger, J. Rodler, P. Sturm, and M. Rexeis. "Emission factors for heavy-duty vehicles and validation by tunnel measurements". In: *Atmospheric Environment* 37.37 (2003), pp. 5237–5245 (cited on p. 30).

[94] PHEM User Manual. *Passenger Car and Heavy Duty Emission Model*. Graz University of Technology, 2017 (cited on p. 30).

[95] G. Scora and M. Barth. *Comprehensive modal emissions model (CMEM), version 3.01 user's guide*. Centre for Environmental Research and Technology (CE-CERT), University of California, Riverside, 2006 (cited on p. 30).

[96] B. M. Broderick and R. T. O'Donoghue. "Development and application of a vehicle emissions inventory model for Ireland". In: *Environmental Monitoring and Assessment* 127.1-3 (2007), pp. 169–179 (cited on p. 30).

[97] TU GRAZ. *PHEM*. `https://www.itna.tugraz.at/assets/files/areas/em/Phem_en.pdf`. Last accessed 17th July 2024. 2024 (cited on p. 32).

[98] R. Doolan and G.-M. Muntean. "EcoTrec—A Novel VANET-Based Approach to Reducing Vehicle Emissions". In: *IEEE Transactions on Intelligent Transportation Systems* 18.3 (2017), pp. 608–620. DOI: `10.1109/TITS.2016.2585925` (cited on p. 33).

[99] A. T. Akabane, R. Immich, E. R. M. Madeira, and L. A. Villas. "iMOB: An Intelligent Urban Mobility Management System Based on Vehicular Social Networks". In: *2018 IEEE Vehicular Networking Conference (VNC)*. 2018, pp. 1–8. DOI: `10.1109/VNC.2018.8628436` (cited on p. 33).

[100] Z. Khan and A. Koubaa. "SmartFlow: An Adaptive Congestion Avoidance Protocol for Smart Transportation Systems". In: *2020 International Wireless Communications and Mobile Computing (IWCMC)*. 2020, pp. 1535–1540. DOI: `10.1109/IWCMC48107.2020.9148366` (cited on p. 33).

[101] T. S. Gomides, R. E. De Grande, F. S. Souza, and D. L. Guidoni. "A Traffic Management System to Minimize Vehicle Congestion in Smart Cities". In: *2020 IEEE International Conference on Systems, Man, and Cybernetics (SMC)*. 2020, pp. 1439–1444. DOI: `10.1109/SMC42975.2020.9283122` (cited on p. 33).

[102] A. T. Akabane, R. Immich, L. F. Bittencourt, E. R. Madeira, and L. A. Villas. "Towards a distributed and infrastructure-less vehicular traffic management system". In: *Computer Communications* 151 (2020), pp. 306–319. DOI: `10.1016/j.comcom.2020.01.002` (cited on p. 34).

[103] C. C. Ghetu, D. Rohlman, B. W. Smith, R. P. Scott, K. A. Adams, P. D. Hoffman, and K. A. Anderson. "Wildfire impact on indoor and outdoor PAH air quality". In: *Environmental science & technology* 56.14 (2022), pp. 10042–10052 (cited on p. 34).

[104] D. Martin, M. Tomida, and B. Meacham. "Environmental impact of fire". In: *Fire Science Reviews* 5 (2016), pp. 1–21 (cited on p. 34).

[105] G. Li, D. Lu, X. Yang, et al. "Resurgence of sandstorms complicates China's air pollution situation". In: *Environmental Science & Technology* 55.17 (2021), pp. 11467–11469 (cited on p. 34).

[106] J. Zhang, Y. Liu, L.-l. Cui, S.-q. Liu, X.-x. Yin, and H.-c. Li. "Ambient air pollution, smog episodes and mortality in Jinan, China". In: *Scientific reports* 7.1 (2017), p. 11209 (cited on p. 34).

[107] C. Holman, R. Harrison, and X. Querol. "Review of the efficacy of low emission zones to improve urban air quality in European cities". In: *Atmospheric Environment* 111 (2015), pp. 161–169 (cited on p. 34).

[108] L Duque, H Relvas, C Silveira, et al. "Evaluating strategies to reduce urban air pollution". In: *Atmospheric Environment* 127 (2016), pp. 196–204 (cited on p. 34).

[109] F. Malik, H. A. Khattak, and M. A. Shah. "Evaluation of the impact of traffic congestion based on SUMO". In: *2019 25th International Conference on Automation and Computing (ICAC)*. IEEE. 2019, pp. 1–5 (cited on p. 34).

[110] A. Khan, S. Chandra, and M. C. Parameshwara. "Air quality monitoring and management system model of vehicles based on the internet of things". In: *Engineering Research Express* 4 (2022) (cited on p. 34).

[111] R. Ramadhani, M. Yuliana, and R. W. Sudibyo. "Implementation of Air Quality Monitoring for Traffic Routing". In: *2022 International Electronics Symposium (IES)* (2022), pp. 291–295 (cited on p. 34).

[112] G. Thanusree, M. V. kiran, A. M. Reddy, D. R. Premsudha, A. Parida, K. Aakanksha, and G. K. Reddy. "Air Quality Monitoring at Heavy Traffic

Zone in Hyderabad". In: *International Journal of Advanced Research in Science, Communication and Technology* (2023) (cited on p. 34).

[113] R. Shrestha, I. Oh, and S. Kim. "A survey on operation concept, advancements, and challenging issues of urban air traffic management". In: *Frontiers in Future Transportation* 2 (2021), p. 626935 (cited on p. 34).

[114] K. Meduri, G. S. Nadella, H. Gonaygunta, and S. S. Meduri. "Developing a Fog Computing-based AI Framework for Real-time Traffic Management and Optimization". In: *International Journal of Sustainable Development in Computing Science* 5.4 (2023), pp. 1–24 (cited on p. 34).

[115] M. Carreras-Sospedra, S. Zhu, M. MacKinnon, W. Lassman, J. D. Mirocha, M. Barbato, and D. Dabdub. "Air quality and health impacts of the 2020 wildfires in California". In: *Fire Ecology* 20.1 (2024), p. 6 (cited on p. 34).

[116] D. Francis, R. Fonseca, N. Nelli, D. Bozkurt, J. Cuesta, and E. Bosc. "On the Middle East's severe dust storms in spring 2022: Triggers and impacts". In: *Atmospheric Environment* 296 (2023), p. 119539 (cited on p. 34).

[117] G. S. Smith, E. E. Anjum, C. Francis, L. Deanes, and C. S. Acey. "Climate Change, Environmental Disasters, and Health Inequities: The Underlying Role of Structural Inequalities". In: *Current Environmental Health Reports* 9 (2022), pp. 80 –89 (cited on p. 34).

[118] S. I. Zandalinas, F. B. Fritschi, and R. Mittler. "Global warming, climate change, and environmental pollution: recipe for a multifactorial stress combination disaster". In: *Trends in Plant Science* 26.6 (2021), pp. 588–599 (cited on p. 34).

[119] I. A. Rana. "Disaster and climate change resilience: A bibliometric analysis". In: *International journal of disaster risk reduction* 50 (2020), p. 101839 (cited on p. 34).

[120] German Aerospace Centre (DLR). *NETCONVERT*. `https://sumo.dlr.de/docs/netconvert.html`. Last accessed 11th September 2024. 2024 (cited on pp. 37, 58).

[121] German Aerospace Centre (DLR). *NETEDIT*. https://sumo.dlr.de/docs/Netedit/index.html. Last accessed 11th September 2024. 2024 (cited on p. 37).

[122] German Aerospace Centre (DLR). *TripInfo*. https://sumo.dlr.de/docs/Simulation/Output/TripInfo.html. Last accessed 23rd September 2024. 2024 (cited on p. 41).

[123] German Aerospace Centre (DLR). *Lane- or Edge-based Traffic Measures*. https://sumo.dlr.de/docs/Simulation/Output/Lane-_or_Edge-based_Traffic_Measures.html. Last accessed 23rd September 2024. 2024 (cited on p. 41).

[124] J. D. Padrón and M. Behrisch. *SUMO2GRAL*. https://github.com/seniel98/SUMO2GRAL. Last accessed 21st September 2024. 2024 (cited on p. 44).

[125] G. Valenciana. *Datos On-line - Calidad Ambiental*. Last accessed 23rd September 2024. 2024 (cited on p. 46).

[126] C. T. Calafate, D. Soler, J.-C. Cano, and P. Manzoni. "Traffic management as a service: The traffic flow pattern classification problem". In: *Mathematical Problems in Engineering* 2015 (2015). DOI: 10.1155/2015/716598 (cited on p. 50).

[127] German Aerospace Centre (DLR). *Routes from Observation Points*. https://sumo.dlr.de/docs/Demand/Routes_from_Observation_Points.html#dfrouter. Last accessed 2nd July 2024. 2024 (cited on p. 52).

[128] J. L. Zambrano, C. T. Calafate, D. Soler, J.-C. Cano, and P. Manzoni. "Using Real Traffic Data for ITS Simulation: Procedure and Validation". In: *2016 Intl IEEE Conferences on Ubiquitous Intelligence & Computing, Advanced and Trusted Computing, Scalable Computing and Communications, Cloud and Big Data Computing, Internet of People, and Smart World Congress (UIC/ATC/ScalCom/CBDCom/IoP/SmartWorld)*. 2016, pp. 161–170. DOI: 10.1109/UIC-ATC-ScalCom-CBDCom-IoP-SmartWorld.2016.0045 (cited on p. 52).

[129] German Aerospace Centre (DLR). *sumolib - SUMO Documentation*. `https://sumo.dlr.de/pydoc/sumolib.html`. Last accessed 9th July 2024. 2024 (cited on p. 56).

[130] OpenStreetMap. *OpenStreetMap*. `https://www.openstreetmap.org`. Last accessed 2nd July 2024. 2024 (cited on p. 57).

[131] DGT. *Parque de vehículos - Tablas estadísticas 2022*. `https://www.dgt.es/menusecundario/dgt-en-cifras/dgt-en-cifras-resultados/dgt-en-cifras-detalle/Parque-de-vehiculos-Tablas-estadisticas-2022/`. Last accessed 2nd July 2024 (cited on p. 57).

[132] R. C. Hampshire and D. Shoup. "What share of traffic is cruising for parking?" In: *Journal of Transport Economics and Policy (JTEP)* 52.3 (2018), pp. 184–201 (cited on p. 58).

[133] M. Zarei and A. M. Rahmani. "Analysis of vehicular mobility in a dynamic free-flow highway". In: *Vehicular Communications* 7 (2017), pp. 51–57 (cited on p. 63).

[134] N. S. Nafi, M. Hasan, and A. H. Abdallah. "Traffic flow model for vehicular network". In: *2012 International Conference on Computer and Communication Engineering (ICCCE)*. IEEE. 2012, pp. 738–743 (cited on p. 63).

[135] D. L. Gerlough and A. Schuhl. *Use of Poisson distribution in highway traffic*. Eno Foundation for Highway Traffic Control Saugatuck, CT, 1955 (cited on p. 63).

[136] EEA. *Comparison of NOx emission standards for different Euro classes*. `https://www.eea.europa.eu/media/infographics/comparison-of-nox-emission-standards/view`. Last accessed 25th September 2024. 2019 (cited on p. 96).

[137] BBC News. *At least five killed as blaze engulfs apartment blocks in Spain's Valencia*. `https://www.bbc.com/news/world-europe-68374811`. Last accessed 17th September 2024. 2024 (cited on p. 99).

[138] P. Gupta, P Doraiswamy, R Levy, et al. “Impact of California fires on local and regional air quality: The role of a low-cost sensor network and satellite observations”. In: *GeoHealth* 2.6 (2018), pp. 172–181 (cited on p. 99).

[139] X. Yue, Y. Hu, C. Tian, R. Xu, W. Yu, and Y. Guo. “Increasing impacts of fire air pollution on public and ecosystem health”. In: *The Innovation* 5.3 (2024) (cited on p. 99).

[140] M. Ravina, G. Caramitti, D. Panepinto, and M. Zanetti. “Air quality and photochemical reactions: analysis of NOx and NO2 concentrations in the urban area of Turin, Italy”. In: *Air Quality, Atmosphere & Health* 15.3 (2022), pp. 541–558 (cited on p. 99).

[141] A. Gassner, J. Lederer, G. Kovacic, U. Mollay, C. Schremmer, and J. Fellner. “Projection of material flows and stocks in the urban transport sector until 2050–A scenario-based analysis for the city of Vienna”. In: *Journal of Cleaner Production* 311 (2021), p. 127591 (cited on pp. 100, 110, 119).